ISSN: 1847-9286
Open Access Journal
www.jese-online.org

JESE

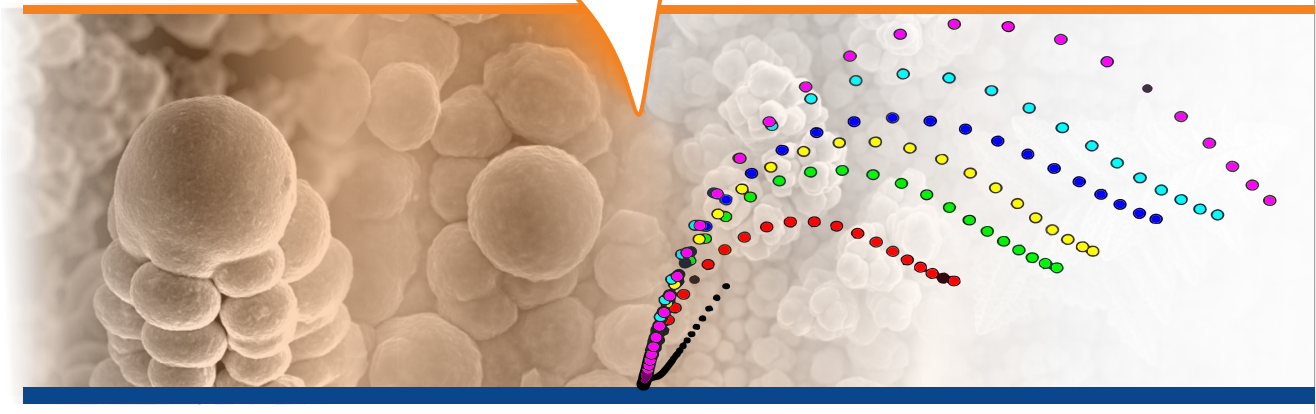

# Journal of Electrochemical Science and Engineering

*J. Electrochem. Sci. Eng.* **3**(**2**) 2013, 37-89

IAPC Publishing

*J. Electrochem. Sci. Eng.* **3(2)** (2013) 37-89
*Published:* April 19, 2013

**Open Access : : ISSN 1847-9286**
**www.jESE-online.org**

## *Contents*

*J. Electrochem. Sci. Eng*. **3(2)** (2013) 37-45; doi: **10.5599/jese.2012.0028**

Open Access : : ISSN 1847-9286
www.jESE-online.org

*Original scientific paper*

# Binder-less activated carbon electrode from gelam wood for use in supercapacitors

NIRWAN SYARIF*,**✉, IVANDINI A. TRIBIDASARI* and WIDAYANTI WIBOWO*

**Department of Chemistry, Faculty of Mathematics and Natural Sciences, University of Indonesia, Indonesia*

***Department of Chemistry, Faculty of Mathematics and Natural Sciences, Sriwijaya University, Indonesia*

✉ Corresponding Author: E-mail: E-mail: nnsyarif@gmail.com; Tel.: +62-711-580269; Fax: +62-711-580069

Received: August 8, 2012; Revised: November 30, 2012; Published: : April 19, 2013

***Abstract***

*This work focused on the relation between the porous structure of activated carbon and its capacitive properties. Three types of activated carbon monoliths were used as the electrodes in a half cell electrochemical system. One monolith was produced from activated carbon and considered to be a binder-less electrode. Two others were produced from acid and high pressure steam oxidized activated carbon. The micrographs clearly indicate that three electrodes have different porous structures. Both porosity and surface area of carbons increased due to the formation of grains during oxidation. This fact specified that an acid oxidized carbon monolith will have relatively higher capacitance compared to non-oxidized and steam oxidized monoliths. Maximum capacitance values for acid, steam oxidized and non-oxidized electrodes were 27.68, 2.23 and 1.20 F $g^{-1}$, respectively.*

**Keywords**

pyrolysis; voltammogram; surface oxidation; capacitance; micropore.

## Introduction

Supercapacitors have become the focus attention of many researchers for decades due to their potential application as energy storage devices in relation to their high energy density, great power density and long cycle life. Much effort has been done to develop advanced carbons to meet the demand for high performance supercapacitors [1]. Fossil- and organic-based carbonaceous materials are amongst the most widely used starting or precursor materials for supercapacitor electrodes because they are relatively inexpensive and easy to fabricate. These electrode materials

also have large specific surface areas, good electrical conductivity and excellent chemical stability. The carbonaceous materials extracted from biomass such as fruit peels, beans, plant shells, bamboo, woods, natural fibers and bagasse have been studied for supercapacitor carbon electrodes.

The fabrication of carbon electrodes for supercapacitors, normally requires an addition of a polymer matrix in order to bind together the carbon particles into monolithic (pellet) form. This addition blocks a part of the carbon pores [2] and additionally causes an increase in the electrical resistivity [3]. Furthermore, the use of polymer binder makes the product more expensive and environmentally less friendly. Therefore, the carbon electrode without the use of any binding agent is highly recommended in order to be potentially used in supercapacitor applications, because they might have lower resistance in the absence of a polymeric binder and they are also of lower cost [4].

In most cases, the physicochemical properties of the carbon electrode, such as its structure, electrical conductivity and porosity, was improved by an activation process. The physical activation is normally carried out by treatment of the carbonized sample using gas atmosphere (such as $CO_2$, $N_2$ and water steam) under a moderately higher temperature of 800 – 1000 °C to improve the internal porosity [5].

In this paper, we report the preparation and characterization of free binder activated carbon monolith electrodes prepared from Gelam wood, which were activated by physical process under $N_2/CO_2$ gas and followed by surface oxidation using nitric acid and high pressure steam. It should be emphasized that the use of this activated carbon for supercapacitor was not yet reported.

## Experimental

### *Activated carbon and electrode preparation*

Activated carbons were prepared from the gelam wood piles obtained from local timber industry. Non-bark wood piles sizes 10 cm length and 5 cm diameter was used in the production of activated carbon rod. Pyrolysis was conducted after preheating process and followed by second pyrolysis for activation process. Wood was preheated in the oven at 230 – 260 °C for a half hour. Wood were carbonized by heating from 40 to 700 °C at rate of 3 °C per minute under atmosphere of nitrogen flow and controlled for ½ - 1 hour at peak temperature. Nitrogen was flowed to the reactor at rate of 1 mL $min^{-1}$. The heating procedure was repeated but using $CO_2$ as the atmosphere to produce activated carbon. This activated carbon was labeled as CCP.

CCP was cut into pellets of 5 mm in thickness by using a mini-circular electric knife. CCP was subjected for surface oxidation using concentrated nitric acid and high pressure steam, both labeled as $CCPHNO_3$ and CCPWOT respectively. Activated carbons were oxidized in reflux system for 3 hours using concentrated nitric acid at 60 °C. The high pressure steam oxidation was conducted in the hydrothermal reactor for 16 hours at 200 °C. The products were washed with abundant de-mineralized water and dried. These three types of activated carbon pallets were used as electrodes.

### *Surface characterization*

The characterization of activated carbons was carried out through physical adsorption of nitrogen gas at 77 K, using a conventional volumetric system (Micromeritics ASAP 2400 instrument). The surface area based on nitrogen isotherms was calculated using the BET equation, and using the “t” method. Scanning Electron Microscopy (SEM) and Energy Dispersive X-ray analysis (EDX) were used to observe the structural morphology and composition of activated carbon, respectively. Hitachi S-4000 field emission SEM was used for this analysis, operated at 30 keV. Uncoated samples were subjected for SEM observation.

The Boehm titration method was applied to determine the acid and basic sites in the activated carbons [6]. The total acid sites were neutralized with 0.1 M NaOH solutions, and the basic sites were neutralized with a 0.1 M HCl solution. The reaction between reagents and acidic oxygenated-functional groups on the surface is based on the difference strength of the acid/base. The strength order of acidic and basic groups is as follow: carboxyl > lactone > phenol. The carboxylic and lactonic sites were titrated with a 0.1 $MNa_2CO_3$ solution, the carboxylic sites were titrated with a 0.1 M $NaHCO_3$ solution and the phenolic sites were determined by the difference. For each determination, 50 mL of the solution was added to one gram of activated carbon in a glass container. The container was inserted into vortex shaker for over one day. A 10 mL sample was titrated with 0.1 M of HCl or NaOH solutions.

*Electrochemical measurement*

Electrochemical tests of the electrodes were conducted using the cyclic voltammetry technique using a three electrode configuration on a potentiostat instrument (eDAQ Pty Ltd, model EA161). Ag/AgCl electrode was used as reference electrode and a platinum rod was used as the counter electrode. Cyclic voltammetry tests were conducted at scan rates of 2, 5, 10, 20, 50, and 100 mV $s^{-1}$ with potential windows ranging from -1 to 1 V in 1, 2, and 4 mol $L^{-1}$ KOH or $H_2SO_4$ aqueous solution as electrolytes. Considering that the anodic voltammetric charges and cathodic voltammetric charges are not the same in the shape of voltammogram curve, the average specific capacitance of the electrode was calculated using integral area approximation

$$C_{\text{avg}} = \frac{\Delta Q}{w \Delta V} = \frac{\int I dV}{s \Delta V w} \quad (1)$$

Where $\Delta Q$ is the total amount of the charge accumulated over a potential window, $\Delta V$, $w$ is the mass of active material in one electrode, $I$ is the current, and $s$ is the potential scan rate. Hence $\int I \, dV$ is integral area of voltammogram curve.

## Results and Discussion

*Pore structures and chemical characteristics*

Three carbon electrodes, namely CCP, CCPHNO3 and CCPWOT, were prepared from Gelam wood activated carbon. The pores and grains were formed during preparation affecting the properties of electrodes. Pores act as the entrance of small molecules penetrated deeper into the micro pores [7]. Penetrating water steam and gases made some cracks and led to changed porous structures [8].

The porous structure of carbon can be characterized by the adsorption isotherms and pore size distribution plot [9]. The adsorption isotherms plot for the three electrodes (Figure 1A) are type I represented by a flat curve, indicating micropores. The broadening of the knee in the very low relative pressures range in CCPHNO3 indicates that the microporosity of the carbon became wider upon acid oxidation treatment (Figure 1A (b)). Acid oxidation burst opening pore in carbon surface and increasing pore volume two times larger. In the other hand, some micro pores vanished (Figure 1A (c)) and pore size distribution became narrow (Figure 1B (c)) upon hydrothermal treatment due to fracture of the bulky network and the pore walls [10]. This fracturing blocked some pores and affected the pore structures and surface functional groups of carbon.

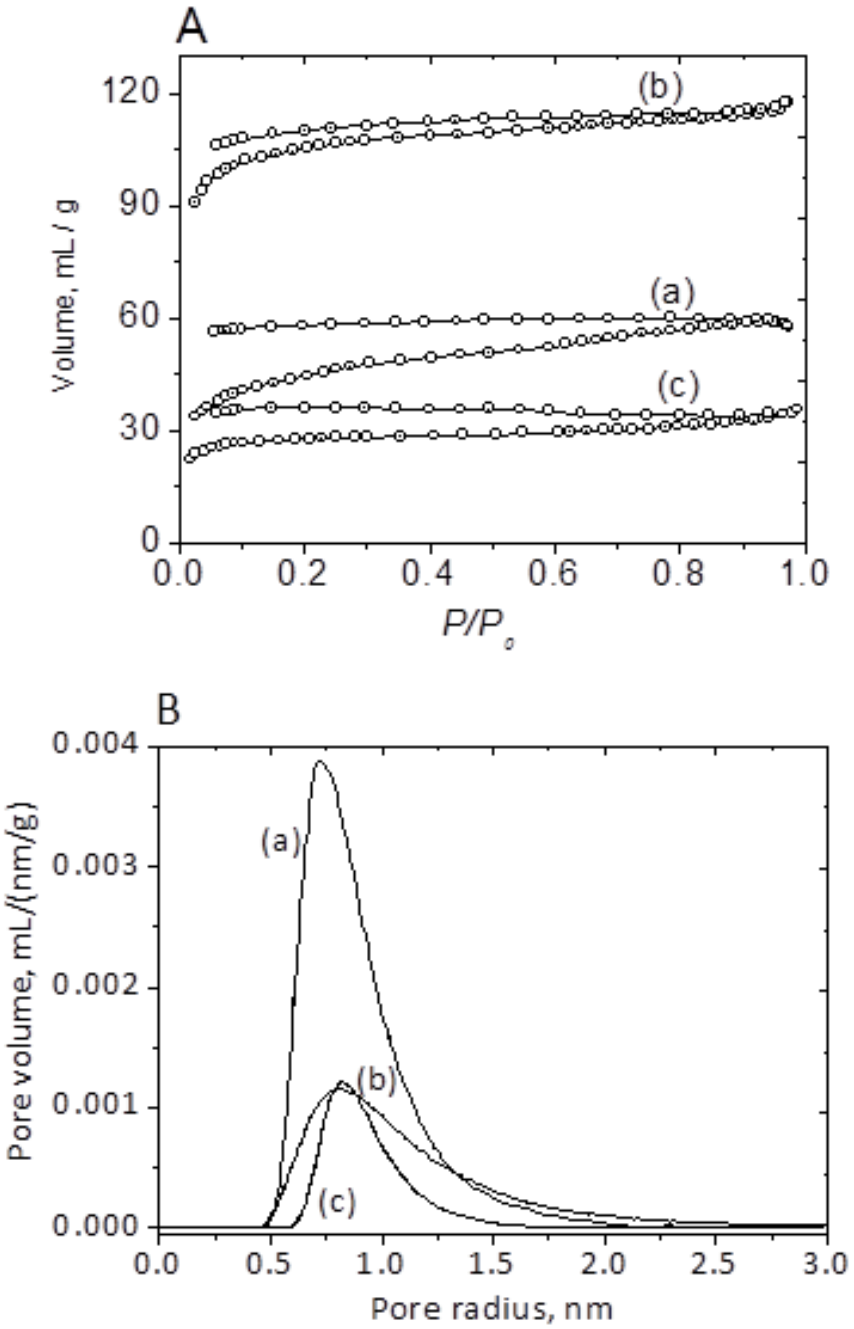


***Figure 1.*** *(A) Nitrogen adsorption-desorption on the surface of electrodes (B) Pore size distribution for* ***(a)*** *CCP,* ***(b)*** *CCPHNO3 and* ***(c)*** *CCPWOT.*

Table 1 shows the changes in surface area, pore volume, and surface functional groups as a result of oxidation treatments. CCPHNO3 had the highest BET surface (337.1 $m^2 g^{-1}$), and a total pore volume measured at $P/P_0$ = 0.95 of 0.185 $cm^3 g^{-1}$, most of the pores being micropores (81.50 %), with an average pore width of 1.1 nm. On the other hand, CCPWOT exhibited the lowest BET surface (88.800 $m^2 g^{-1}$), with a much lower total pores volume (0.014 $cm^3 g^{-1}$) and a narrower pore width (1.408 nm). A pore size distribution in the range of micropore in which larger than the size of two solvated ions, was then identified as a way of improving the energy density and the power capability [11], whereas mesopores improved the ionic mass transport inside the bulk of carbon. Therefore, it was assumed that a good balance between micro- and mesoporosity was needed to maximize capacitance [12]. Some capacitance values from the literature are

provided to clarify the relationship between pore structure and capacitance. It can also be seen from the Table 1 that the some capacitance values obtained in this study are smaller than those obtained from the literatures.

***Table 1.*** *Surface and electrochemical properties of the CCP, CCPHNO3 and CCPWOT electrodes.*

| Electrode | $S_{BET}$ / $m^2 g^{-1}$ | $V_{total}$ / $cm^3 g^{-1}$ | micro pore content, % | Functional groups concentration, mmol $g^{-1}$ | | | | $C_{sp,max}$ F $g^{-1}$ |
|---|---|---|---|---|---|---|---|---|
| | | | | fenolic | lactonic | carboxylic | base | |
| CCP | 149.848 | 0.093 | 56.249 | 0.200 | 3.85 | 0.00 | 0.24 | 1.22 |
| CCPHNO3 | 337.116 | 0.185 | 81.499 | 0.100 | 3.08 | 0.20 | 0.19 | 27.68 |
| CCPWOT | 88.800 | 0.014 | 28.306 | 0.200 | 3.40 | 0.10 | 0.22 | 2.23 |
| Carbon from sucrose [13] | 2749.0 | 2.01 | | | | | | 233 |
| Carbon from sago waste [14] | 1408.2 | 0.897 | | | | | | 64.1 |
| Carbon from coal [14] | 179.2 | 0.073 | | | | | | 16.2 |

$S_{BET}$ – specific surface area; $V_{total}$ - total pore volume, measured at $P/P_0$=0.995.

Furthermore, the specific surface area of the CCPHNO3 electrode as listed in Table 1 is 337.116 $m^2 g^{-1}$, which is higher than that of the CCP and CCPWOT electrode, *i.e.* 149.85 and 88.80 $m^2 g^{-1}$, respectively. The Boehm analysis reveals that the three electrodes have similar amounts of functional groups, except for the carboxylic and lactone groups. A computational study was undertaken on the effect of the two functional groups on the structure of graphite basal. The study found that the COOH functional groups that fill the vertical plane will bend graphite layer led to reduced effectiveness of electron transfer between layers. These functional groups improved capacitive processes of the carbon [15], and facilitated the penetration of the electrolyte ions into the interior pores. Although the CCPWOT electrode has many more functional groups, however, many more pores were vanished and the surface area was decreased, leading to a decrease in the capacitance of electrode. Furthermore, changes in the carbon pore structure can be clearly seen as surface morphology by using electron microscope.

The micrographs clearly indicate that the three electrodes have different surface morphologies. Figure 2a and 2d show the analysis of the CCP microstructure by SEM. They revealed continuous and smooth surface of the CCP with less grain boundaries wood (Figure 2a and 2d) due to the limited process of opening pore in line with the nature of the wood. The other SEM pictures show the opening pores in the surface of the carbon which occurred when CCP was treated with nitric acid (CCPHNO3), especially the oxidation of low molecular weight carbon. These SEM images of CCPHNO3 show irregular sizes and flaky grains in which the structures tend to form voids between the grains (Figure 2b and e). The number of grains and micropores of CCPHNO3 are higher than those of CCPWOT and CCP, due to the reaction between low molecular weight carbon fragments with nitrogen. The oxidation reaction generated volatile molecules that leave the pores behind after volatilization. Furthermore, SEM images of CCPWOT show more regular size and relatively uniform (Figure 2c and f). This porous structure, *i.e.* pore volume, surface area and pore size distribution along with functional groups on the surface of carbon are regarded as the important factors which determined the properties of capacitive processes, *i.e.* ionic accessibility, electrical double layer and redox reactions [16-18].

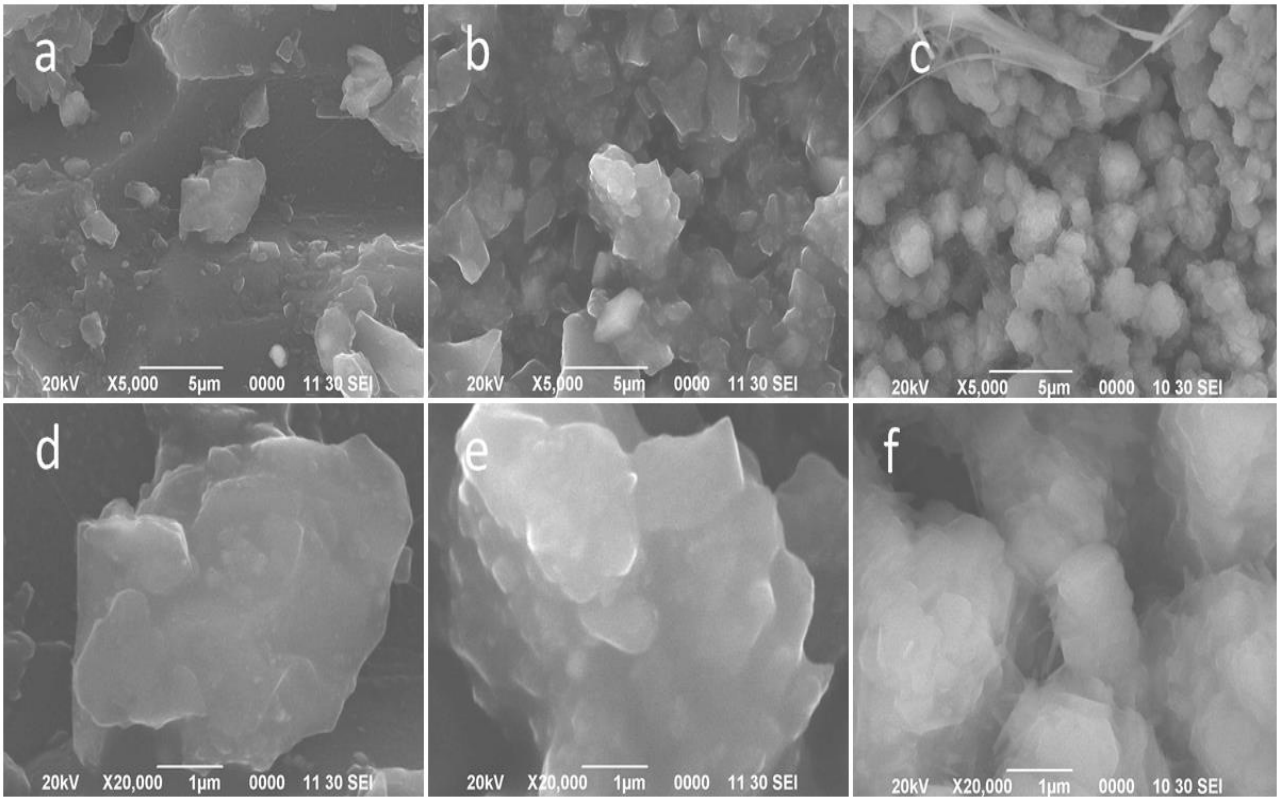


***Figure 2.*** *SEM images for CCP* ***(a and d)****, CCPHNO3* ***(b and e)****, and CCPWOT* ***(c and f)***

*Electrochemical performance*

Cyclic voltammetry tests were conducted at scan rates of 2, 5, 10, 20, 50, and 100 mV $s^{-1}$ with potential windows ranging from -1 to 1 V versus Ag/AgCl in 1, 2, and 4 mol $L^{-1}$ KOH or $H_2SO_4$ aqueous solution to quantify the electrochemical performance of CCP, $CCPHNO_3$ and CCPWOT electrodes. As shown in Figure 3 and 4, no pronounced reversible reduction oxidation peak can be observed from voltammograms for the three electrodes. The shape of the voltammograms was different from one to another.

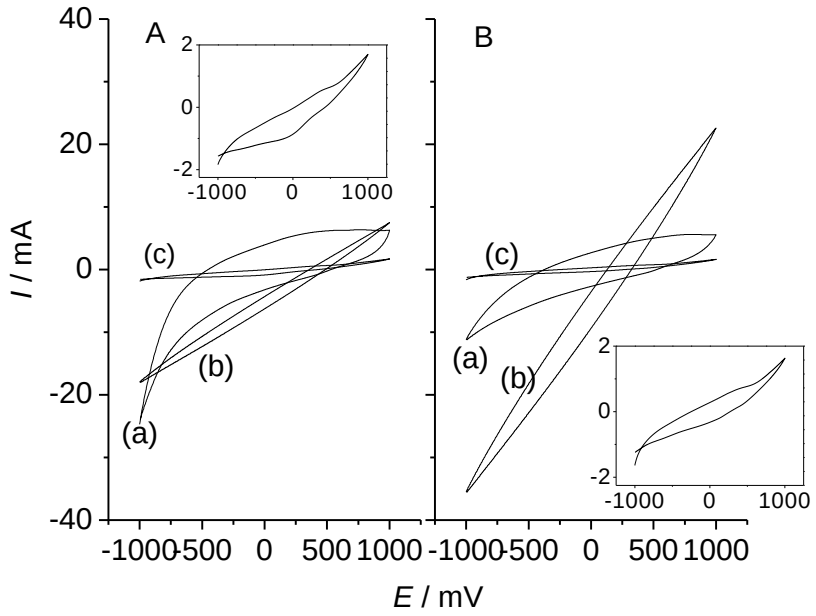


***Figure 3.*** *CV Curve of carbon electrodes* ***(a)*** *CCP,* ***(b)*** *CCPHNO3 and* ***(c)*** *CCPWOT in the $H_2SO_4$ 1M* ***(A)*** *and 4M* ***(B)****. Scan rate was 20 mV $s^{-1}$.* ***Inset****: magnification of voltammogram* ***(c)****.*

The voltammogram of the CCPWOT electrode was relativelylower compared to the other two curves. Therefore the oxidation treatment under water steam reduced the capacitance. On the other hand, the highest current of CCPHNO3 electrode points to the largest capacitance. The changes in capacitance occurred on the electrode after the oxidation process was associated with changes in pore volume of carbon, as previously described. Oxidation using strong acid clarified the existence of the Faraday process (redox reaction) that occurred at the carbon as described by other authors [19]. The voltammograms shape of CCPHNO3 in both acid and base electrolytes are much the same, which means that the tendency to establish a redox reaction was similar. The voltammogram area in Figure 3 shows the decrease in capacitance at high concentrations of $H_2SO_4$. By contrast, the capacitance of the electrodes increased at a low concentration KOH (Figure 4).

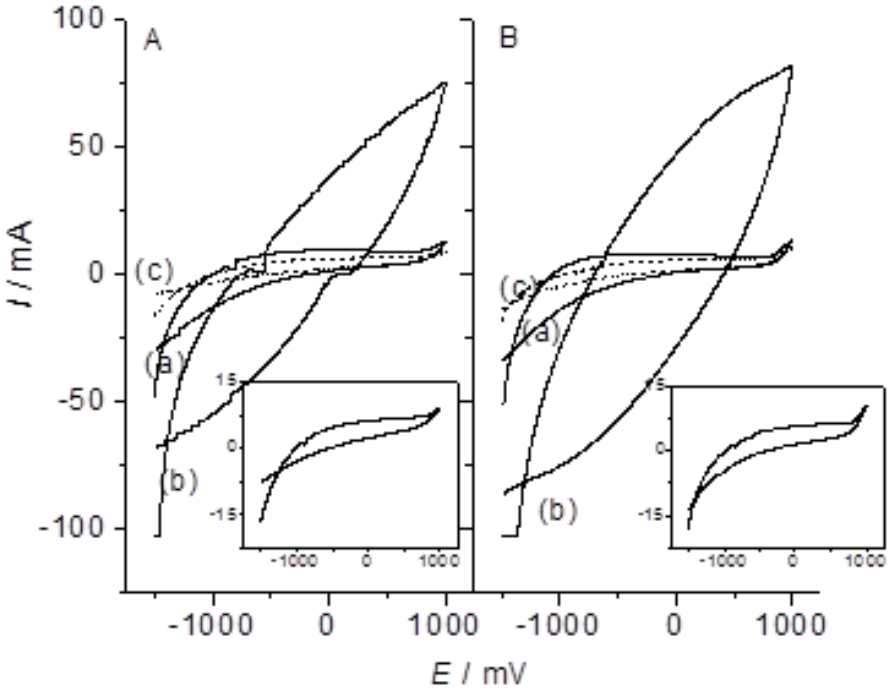


***Figure 4.*** *Voltammogram of carbon electrodes* ***(a)*** *CCP,* ***(b)*** *CCPHNO3 and* ***(c)*** *CCPWOT in the KOH 2M* ***(A)*** *and 4M* ***(B)****. Scan rate was 5mV s-1.* ***Inset****: magnification of voltammogram* ***(c)****.*

Calculations of specific capacitances for all electrodes at various scan rates in the $H_2SO_4$ solution are presented in Figure 5. At the 5 mV $s^{-1}$ scans rate in $H_2SO_4$, the CCP electrode had a specific capacitance of 1.2 F $g^{-1}$, while at a scan rate of 100 mV $s^{-1}$ this was 0.22 F $g^{-1}$. Capacitance values of the CCPWOT electrode (Figure 5 B) at 5 – 10 mV $s^{-1}$ were lower than that of CCP (Figure 5 A), but were higher at 20 – 100 mV $s^{-1}$. The capacitance values of CCP and CCPWOT electrodes were much smaller than those of the CCPHNO3 electrode (Figure 5 C). Maximum capacitance for non-oxidized, steam and acid oxidized electrodes were 1.22, 0.63 and 2.57 F $g^{-1}$, respectively. These values occurred at 5 mV $s^{-1}$.

Plots of the electrodes specific capacitances *vs*. scan rate in KOH are presented in Figure 6. Capacitances of CCP in KOH were much the same as those in $H_2SO_4$ both at low and high scan rates. Contrary to what occurred in the $H_2SO_4$, the capacitance values of the CCPWOT electrode (Figure 6B) were higher than those of CCP (Figure 6A), both at low and high scan rates. Capacitance values of CCP and CCPWOT electrodes were also much smaller than those of the CCPHNO3 electrode. Plot of specific capacitance of CCPHNO3 in KOH was discrete (Figure 6C) due to instability of the system, especially at a scan rate higher than 10 mV $s^{-1}$. A stable voltammogram

was only obtained at a scan rates higher than 40 mV $s^{-1}$ at 1M KOH. Capacitance value for acid and steam oxidized electrodes were 2.23 and 27.68 F $g^{-1}$, respectively.

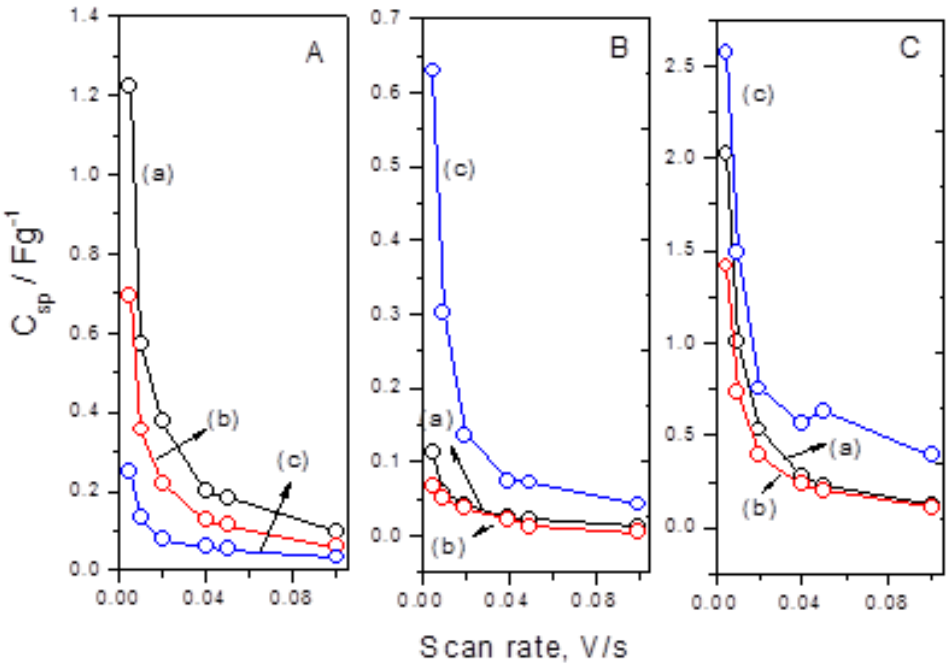


***Figure 5.*** *Plot of specific capacitance of carbon electrode* ***(A)*** *CCP,* ***(B)*** *CPPWOT and* ***(C)*** *CCPHNO3 versus scan rate in $H_2SO_4$* ***(a)*** *4M,* ***(b)*** *2M and* ***(c)*** *1M.*

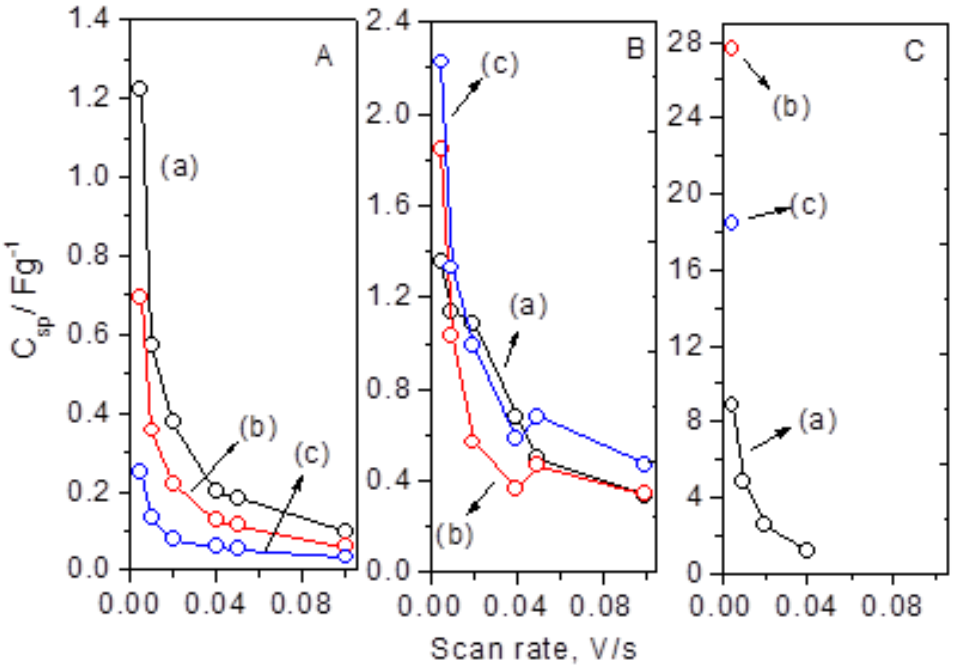


***Figure 6.*** *Plot of specific capacitance ($C_{sp}$)of carbon electrode* ***(A)*** *CCP,* ***(B)*** *CPPWOT and* ***(C)*** *CCPHNO3 versus scan rate in KOH* ***(a)*** *4M,* ***(b)*** *2M and* ***(c)*** *1M.*

The presence of the micropores in the activated carbon are unique for Gelam wood. Combining their uniqueness, simplicity of the preparation method and the abundance availability, makes these electrode materials relatively inexpensive and environmentally friendly. Thus Gelam wood activated carbon has the potential to be developed as electrodes in electrochemical capacitors.

## Conclusions

The three types of electrodes, namely CCP, CCPHNO3 and CCPWOT, prepared from Gelam wood activated carbon, have different surface morphologies which basically contained many micropores. CCP has continuous - smooth surface and contains very few grain boundaries. On the other hand CCPWOT and CCPHNO3 have rough surfaces and contain many cracks. The different oxidation methods using nitric acid and water steam gave different effects on the surface area of the carbons. Acid nitric oxidation led to a larger pore volume and surface area, while water steam oxidation led the opposite effect. In addition, CCPHNO3 had relatively large amounts of micropores. The presence of surface oxides was important factor in improving the capacitance of electrode and increased the effective utilization of the pore structure. CCPHNO3 had the highest capacitance value of 27.68 F $g^{-1}$ while the specific capacitance of the electrode CCPWOT was similar to CCP, at 2.23 and 1.22 F $g^{-1}$, respectively.

## References


[1] M. Jayalakshmi, K. Balasubramanian, *Int. J. Electrochem. Sci*. **3** (2008) 1196−1217
[2] W. Li, H. Probstle, J. Fricke, *J. Non-Cryst. Solids* **325** (2003) 1−5
[3] A.G. Pandolfo, A.F. Hollenkamp, *J. Power Sources* **157** (2006 ) 11−27
[4] E. Taer, M. Deraman, I.A. Talib, A. Awitdrus, S.A. Hashmi, A.A. Umar, *Int. J. Electrochem. Sci*. **6** (2011) 3301 – 3315
[5] C. Merino, P. Soto, E. Vilaplana-Ortego, J.M.G.d. Salazar, F. Pico, J.M. Rojo, *Carbon* **43** (2005) 551−557
[6] H.P. Boehm, Carbon 32 (1994) 759-769
[7] C. Nieto-Delgado, M. Terrones, J.R. Rangel-Mendez, *Biomass Bioenerg.* **35** (2011) 103−112
[8] S. Villar-Rodil, A. Martinez-Alonso, J.A. Pajares, J.M.D. Tascon, M. Jasienko-Hałat, E. Broniek, J. Kaczmarczyk, A. Jankowska, A. Albiniak, T. Siemieniewska, *Micropor. Mesopor. Mat.* **64** (2003) 11-19
[9] K.P. Gadkaree, M. Jaroniec, *Carbon* **38** (2000) 983−993
[10] K. Ramakrishnan, C. Namasivayam, *Sustain. Environ. Res.* **19** (2009) 173 − 178
[11] C. Du, N. Pan, *Nanotechnology* **17** (2006) 5314−5318
[12] R. Nickolov, D. Kovacheva, M. Mladenov, N.Velichkova, R. Raicheff, P. Tzvetkova, *J. Univ. Chem. Tech. Metall.* **46** (2011) 275−282
[13] K. Xia, Q. Gao, J. Jiang, J. Hu, *Carbon* **46** (2008) 1718-1726
[14] H. Aripin, L. Lestari, D. Ismail, S. Sabchevski, *Open Mat. Sci. J.* **4** (2010) 117−124
[15] M.J. Bleda-Martınez, J.A. Macia-Agullo, D. Lozano-Castello, E. Morallon, D. Cazorla-Amoros, A. Linares-Solano, *Carbon* **43** (2005) 2677−2684
[16] L.L. Zhang, X. Zhao, H. Ji, M.D. Stoller, L. Lai, S. Murali, S. Mcdonnell, B. Cleveger, R.M. Wallace, R.S. Ruoff, *Energy Environ. Sci.* **5** (2012) 9618-9625
[17] B.G. Choi, Y.S. Huh, W.H. Hong, H.J. Kim, H.S. Park, *Nanoscale* **4** (2012) 5394-5400
[18] E. Frackowiak, F. Beguin, *Carbon* **39** (2001) 937-950
[19] M. Seredych, D. Hulicova-Jurcakov, G.Q. Lu, T.J. Bandosz, *Carbon* **46** (2008) 1475-1388

*J. Electrochem. Sci. Eng*. **3(2)** (2013) 47-56; doi: **10.5599/jese.2013.0029**

Open Access : : ISSN 1847-9286
www.jESE-online.org

*Original scientific paper*

# *p*-toluene sulfonic acid doped polyaniline carbon nanotube composites: synthesis via different routes and modified properties

ASHOK K. SHARMA✉ and YASHPAL SHARMA*

*Department of Materials Science & Nanotechnology, D.C.R University of Science & Technology, Murthal-131 039 (Haryana) India*

**Department of Chemistry, G. J. University of Science & Technology, Hisar-125001, India*

✉ Corresponding Author: E-mail: aksharma210@gmail.com

Received: October 8, 2012; Revised: December 25, 2012; Published: : April 19, 2013

***Abstract***

*Composites of polyaniline and carbon nanotube (CNT) were prepared by in-situ chemical polymerization method using various aniline concentrations in the initial polymerization solution with p-toluene sulfonic acid (PTS) as secondary dopant and mechanical mixing of the PANI and CNT using different weight ratios of PANI and CNTs. The structural characterizations of the composites were done by Fourier transform infrared (FTIR) and Ultra violet visible spectroscopy (UV-Visible). Scanning electron microscopy (SEM) was used to characterize the surface morphology of the composites. It was found that the composites prepared by in-situ chemical polymerization had smoother surface morphology in comparison to the composites obtained by mechanical mixing. The capacitive studies reveal that the in-situ composite has synergistic effect and the specific capacitance of the composite calculated from cyclic voltammogram (CV) was 385.1 F/g. Thermal studies indicate that the composites are stable as compared to PANI alone showing that the CNT contributes towards thermal stability in the PANI-CNT composites.*

**Keywords**

Cyclic voltammetry; TGA; scanning electron microscopy; composites; conducting polymer; specific capacitance; chemical polymerization; doping, nanomaterials.

## Introduction

Due to exceptional electrical, electronic and mechanical properties, conducting polymers are also popular as synthetic metals. Various conducting polymers such as polyaniline, polyacetylene, polypyrrole and polythiophene have been the subject of intensive research because of their application in different fields such as optoelectronic and display devices, and as active electrode materials in primary and secondary batteries, supercapacitors, tissue engineering, drug delivery *etc* [1,2].

Carbon nanotubes after their discovery by Iijima and Ichihashi [3] have been the field of great interest because of their unique electronic, mechanical and magnetic properties [4]. Owing to their unique properties there are varieties of applications of CNT which include supercapacitors and batteries, sensors, biological applications like bone tissue engineering and many more [5]. Recently, composites of the CNT and conducting polymers were a matter of immense research because the composite from these two important materials produce the synergistic effect and produce better applications than the individual materials [6-9]. CNT acts as good filler in the polymer composite compared to other carbon materials because of their high surface area. Various conducting polymers have been investigated to be used in the composite preparation but out of these PANI acts as promising material because of its various properties like air stability, flexibility, light weight, high conductivity, ease of synthesis by chemical and electrochemical method and good processability [10,11]. Recently, PANI was investigated in the synthesis of PANI-CNT composites by using MWNT [7,9], SWNT [8] and carboxylated CNT [6,12].

The composite preparation from the PANI and CNT produces a hybrid material having great mechanical strength, high capacitance properties, electrical properties and good processability [13-16]. There are mainly two methods to prepare such composites: chemical oxidative polymerization method and the electrochemical method. The electrochemical method has limitations in terms of mass production while chemical method gives a high yield and is cheaper [17].

Doping plays an important role in the conducting polymers. Doping is the process which converts the neutral polymer backbone to a charged π conjugated system. This allows electrons to flow through π conjugated system of the conducting polymers due to the formation of conduction bands. Various dopant are used for doping of polyaniline which include *p*-toluene sulphonic acid (PTS), dodecyl benzenesulphonic acid (DBSA), camphor sulphonic acid (CSA), polyvinyl sulfonic acid (PVA) etc. [18]. However, HCl itself acts as a dopant for PANI but using a secondary dopant along with HCl enhance the electronic properties of the material and also the processability.

This study describes the synthesis of some PANI-CNT composites using *p*-toluene sulfonic acid (PTS) as secondary dopant along with HCl by means of chemical oxidative polymerization method and by mechanical mixing of the PTS doped PANI and CNT in the same proportions as used in the *in-situ* chemical oxidative polymerization. The synergistic capacitive effect of the composite was also investigated. The difference in the morphology and thermal behaviour of the composites prepared by both the methods were also investigated.

## Experimental

### *Materials*

MWNT (99 %) was purchased from Nanostructured and Amorphous Materials Inc. having outer diameter 20-40 nm and length of 1-2 μm. Aniline (S.D. Fine-Chem. Ltd, 99.5 %) was vacuum distilled prior to use. PVDF, MW Vaco Carbon and *p*-toluene sulfonic acid (PTS) sodium salt (95 %) was purchased from Sigma-Aldrich. All other chemicals like hydrochloric acid (35.4 %), ammonium peroxydisulfate (APS) (98 %), ethanol (99.9 %), sulphuric acid (98 %), activated carbon and N, N-dimethyl formamide (DMF) were obtained from S.D. Fine Chem. Ltd. and used as received without further purification. All chemicals were of analytical grade. Solutions were prepared in deionized water.

*Preparation of PANI-CNT composites by in-situ chemical polymerization*

For the preparation of PANI-CNT composites by *in-situ* chemical oxidative polymerization method 0.5 g of CNT was dissolved in 1M HCl and then ultrasonicated for 2 hours in order to disperse CNT bundles. Different amounts of aniline monomer (0.5, 1.5, 2.5, 3.5 and 4.5 ml yielding CNT: Aniline ratios of 1:1, 1:3, 1:5, 1:7 and 1:9, wt/v) was dissolved in 1 M HCl and 0.2 M PTS. This content was transferred to the flask containing ultrasonicated CNT. Again the mixture (CNT+Aniline) was put to ultrasonication for 2 hours, to incorporate aniline monomer in the CNT matrix. A freshly prepared pre-cooled ammonium peroxydisulphate (1 M) solution in 1 M HCl was added drop wise to the CNT-aniline mixture. The reaction mixture was stirred for 6 hours at 0-5 $^{o}$C. Appearance of greenish black color indicated the formation of the PANI-CNT composite. The resulting solution was filtered and washed with distilled water and methanol several times to remove the unreacted oxidant and oligomers if any. The product was dried in vacuum oven at 60 $^{o}$C overnight. PANI was also prepared as above where 2.5 ml of aniline was dissolved in the initial polymerization solution. Herein, the PANI-CNT composites with different ratios of CNT and aniline monomer will be designated as ratios of CNT: aniline monomer given in parentheses: CPC1 (1:1), CPC2 (1:3), CPC3 (1:5), CPC4 (1:7), CPC5 (1:9). Figure 1 is the schematic representation of the *in-situ* chemical oxidative polymerization method.

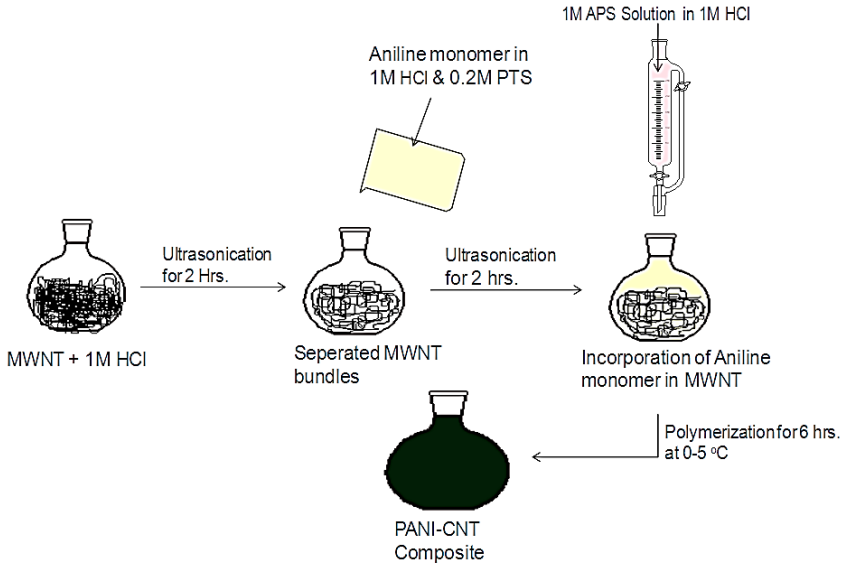


***Figure 1**. Schematic representation of the in-situ chemical oxidative polymerization method*

*Preparation of PANI-CNT composites by mechanical mixing method*

For the preparation of PANI-CNT composites by mechanical mixing method, PANI was prepared by the *in-situ* chemical route. The as such prepared PTS doped PANI was mixed with CNT in different ratios (CNT:PANI ratios were 1:1, 1:3, 1:5, 1:7 and 1:9) in DMF solvent. The mixture was ultrasonicated for 2-3 hours to disperse the CNT bundles and for better incorporation of the CNT in the polymer matrix. After sonication the mixture was magnetically stirred for 6-7 hours. Finally, the mixture was filtered and washed several times with distilled water and methanol. The PANI-CNT composites were collected by drying the powder in vacuum oven at 60 $^{o}$C. Herein, the PANI-CNT composites prepared by mechanical mixing method with different ratios of CNT and PANI will be designated as ratios of CNT: PANI given in parentheses CPM1 (1:1), CPM2 (1:3), CPM3 (1:5), CPM4 (1:7), CPM5 (1:9).

*Preparation of electrode for cyclic voltammetry*

The PANI-CNT composite prepared by *in-situ* chemical oxidative polymerization method was mixed with 10 wt. % of activated carbon and 5 wt. % of MW Vaco Carbon as conductor and 5 wt. % of binder (PVDF) in N,N-Dimethyl formamide (DMF) solvent. The mixture was ultrasonicated for 2 hours and then stirred to form slurry. The slurry was brush coated on 2×2 $cm^2$ of graphite sheet as a current collector.

*Characterization*

The chemical structure of the composite was characterized by using Fourier transform infrared spectrophotometer (Shimadzu IR Affinity-I 8000 FT-IR spectrophotometer). Interaction between PANI and CNT was investigated by means of UV-Visible spectroscopic technique (Varian Cary- 5000 spectrophotometer). The scanning electron microscopy (SEM, JEOL-JSM-5600LV) was used to examine the surface morphology and average thickness of deposited PANI over the surface of CNT. The capacitive property of the PANI-CNT composite electrodes was examined by cyclic voltammetry using three-electrode cell system with a reference electrode (saturated calomel electrode) and a counter electrode (Pt) in 1 M $H_2SO_4$ solutions as electrolyte. Cyclic voltammetry measurements were carried out by potentiostat/galvanostat (CH Instruments 600C series). The geometric surface area of the working electrode was 2×2 $cm^2$. Cyclic voltammograms were recorded in the voltage windows 0-0.8 V at a scan rate of 2 mV/s. Thermal analyses of the CNT, PANI and PANI-CNT composites was done by using thermogravimetric analyzer (Universal V4.7A TA Instruments).

## Results and Discussion

*FTIR study*

The FTIR spectrum of the PANI-CNT composite is given in Figure 2. The spectrum shows all bands of PANI. The band at 1448.58 and 1581.16 $cm^{-1}$ may be assigned to the benzoid and quinoid ring vibrations, respectively. The band at 1294.11 $cm^{-1}$ is due to the conducting form of the PANI indicating that the PANI exists in the conducting emeraldine salt form. The bands at 1100.79 and 785.68 $cm^{-1}$ may be assigned to the aromatic C-H in plane and aromatic C-H out of plane bending vibrations, respectively [19]. A broad peak at 3402.13 $cm^{-1}$ is due to the N-H stretching vibration of the aromatic amine. The bands at 1068.92 and 674.19 $cm^{-1}$ represent the symmetric stretching of the $SO_3^-$ group [18]. The bands are in agreement with the theoretical predictions and confirm the deposition of PANI over the surface of the CNT *i.e.* formation of PANI-CNT composite using PTS as secondary dopant [20,21].

*UV-Visible spectra*

UV-Visible spectra of the CNT, PANI and the PANI-CNT composite were recorded in N,N-dimethylformamide (DMF) solvent in the wavelength range from 300 to 800 nm. Figure 3 shows the UV-Visible spectra of CNT, PANI and the PANI-CNT composite. The CNT has no characteristic peak in this region. PANI has its characteristic peak at 540 nm. For the PANI-CNT composite the PANI shows its characteristic peak at 541 nm showing the protonated doped state of the polyaniline indicating the deposition of PANI over the CNT surface and formation of composite [22,23].

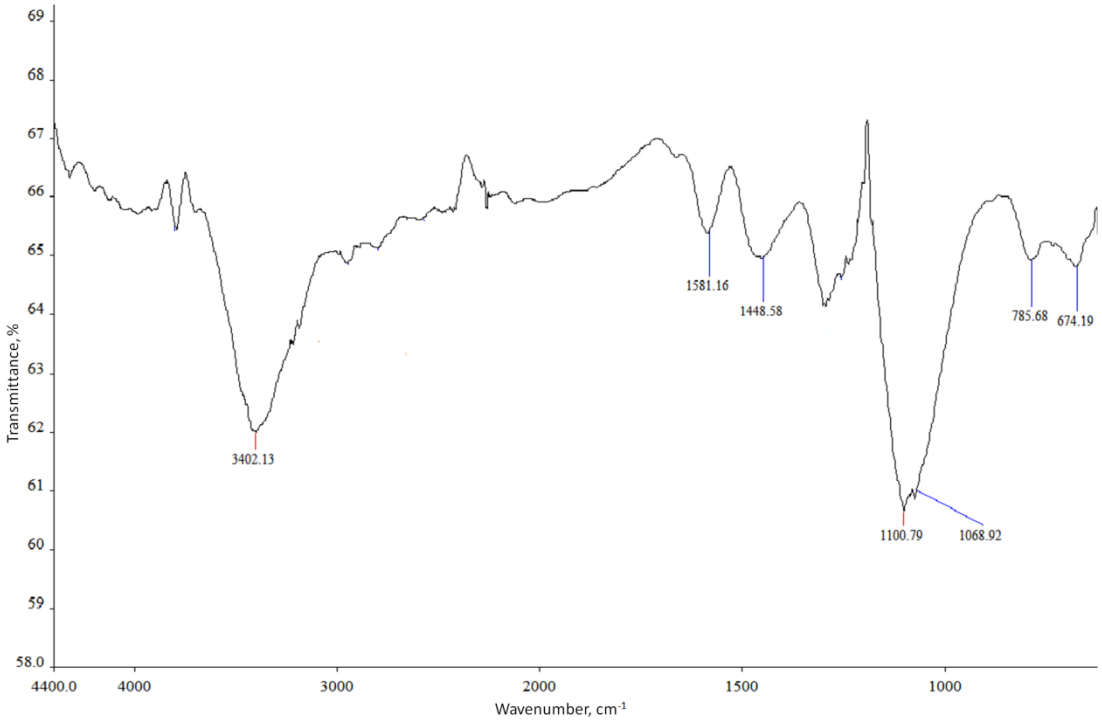


***Figure 2.*** *FTIR spectrum of the PANI-CNT composite*

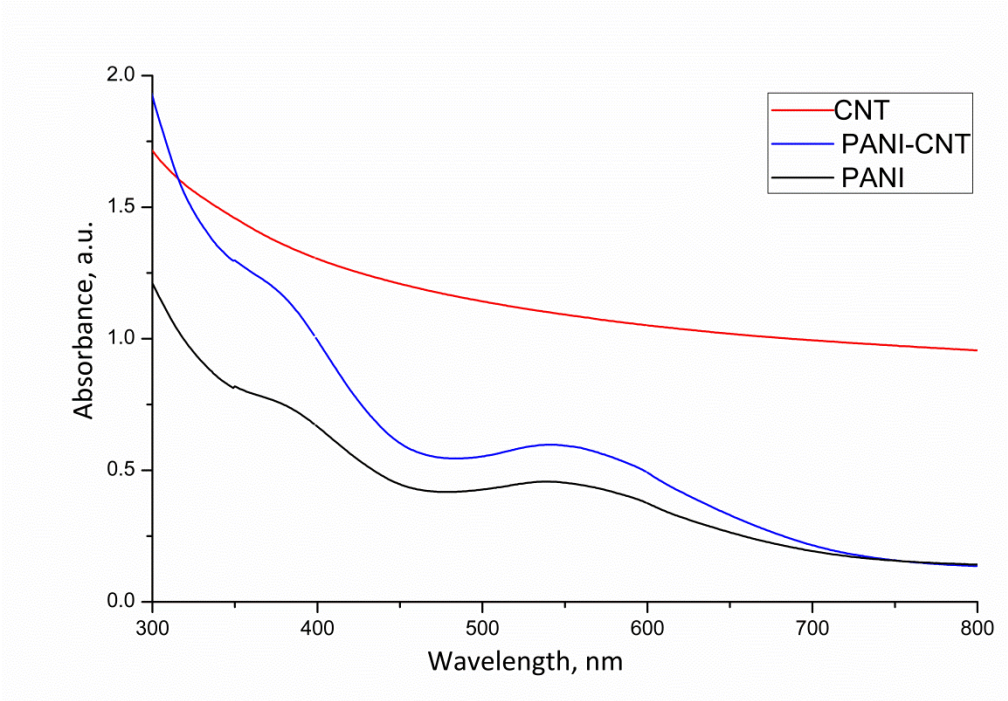


***Figure 3****. UV-Visible spectra of the CNT, PANI and PANI-CNT composite*

*Surface morphology*

Surface morphology of the composites was studied by scanning electron microscopy (SEM). Figure 4a-c shows the SEM micrographs of the CNT, CPC5 and CPM5 respectively. CNT shows smooth surface morphology with average diameter of ≈20-40 nm. Comparing Figure 4b with the SEM micrograph of CNT (Figure 4a) it could be concluded that the polyaniline becomes deposited over the surface of the CNT indicating the formation of the PANI-CNT composite. PANI-CNT composite shows that the average thickness of deposited PANI over the surface of CNT is ≈200-230 nm. Comparing Figure 4c with the SEM micrographs of CNT (Figure 4a) and the

PANI-CNT composite (Figure 4b), it can be said that the composite prepared through mechanical mixing method shows defective and irregular surface morphology which may be caused due to mixing of the two components for long period of time. However, it it is not easy to distinguish the CNT bundles in the composite which is clearly seen in case of PANI-CNT composite prepared by *in-situ* chemical oxidative polymerization method. In the case of the *in-situ* polymerization method, the PANI wrapped the CNT surface in a regular manner using each CNT bundle as can be seen in Figure 4b but in mechanical mixing method the PANI deposition takes place instead of wrapping over the CNT in irregular fashion.

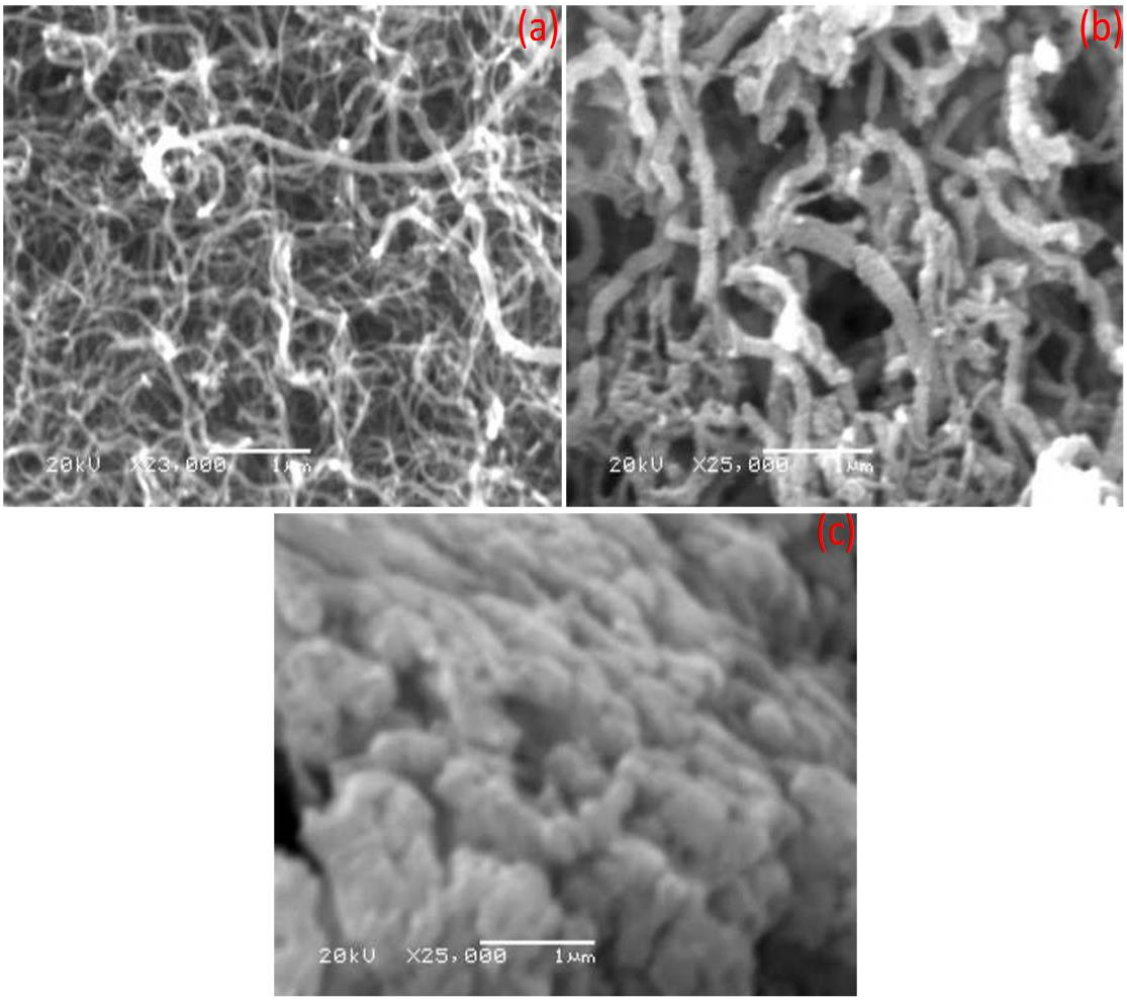


***Figure 4.*** *SEM micrographs of (**a**) CNT, (**b**) CPC5 and (**c**) CPM5 respectively*

*Capacitive study*

The capacitive characteristic of the CNT, PANI and the PANI-CNT composite prepared by *in-situ* chemical oxidative polymerization was investigated by means of cyclic voltammetry. The capacitance was calculated from the obtained cyclic voltammogram by dividing the average current with scan rate while the specific capacitance was calculated by dividing the capacitance by the weight of active material.

It can be concluded from Figure 5 that CNT behaves like an electric double layer showing almost rectangularly shaped cyclic voltammogram and is almost mirror image with respect to zero current line. For the PANI and PANI-CNT composite the redox peaks are indicative of the higher currents flowing in the PANI-CNT as compared to the PANI alone and can be attributed to the porous structure of the composite in which CNT provides a larger surface area for aniline to polymerize

upon. The specific capacitance of CNT, PANI and PANI-CNT composite calculated from cyclic voltammograms was 31.56 F/g, 314.07 F/g and 385.1 F/g, respectively. It can be explained as the synergy contribution from the PANI and the CNT because of better electrolyte access in the active material and improved contact between the current collector and the active material resulting in decreased overall internal resistance in the electrode and better capacitance value [24-27].

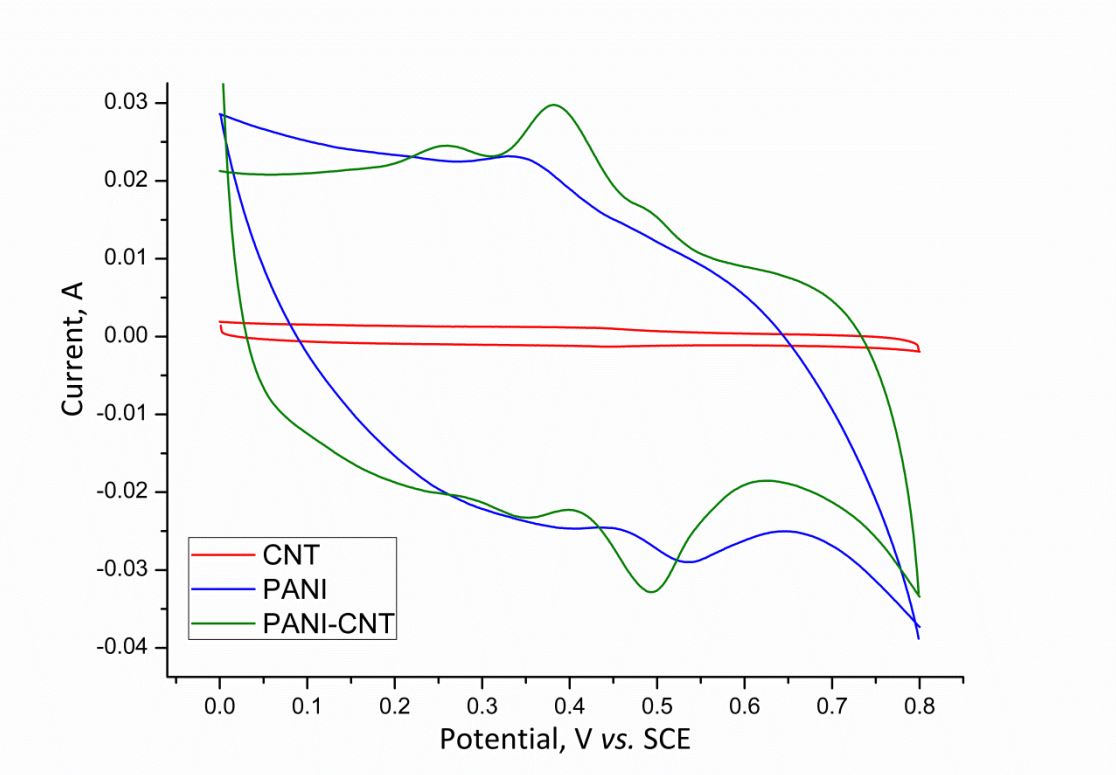


***Figure 5**. Cyclic voltammogram of CNT, PANI and the PANI-CNT composite*

*Thermal analysis*

Thermogravimetric analysis (TGA) of the CNT, PANI and the CNT-PANI composites were carried out under nitrogen atmosphere in order to investigate the % mass loss with respect to temperature. Figures 6a and 6b show the TGAs of the CNT, PANI and CNT-PANI composites prepared by chemical and mechanical mixing method, respectively. From Figure 6a it can be inferred that the composites show very good thermal stability as compared to the PANI, which can be attributed to the presence of CNT in the original polymer matrix [22]. CNT has highest thermal stability and does not show any decomposition in the temperature range of 30 to 580 $^{o}$C. The polyaniline on the other hand exhibited a slight decrease in the weight at 114 $^{o}$C which can be assigned to the loss of water [28]. Up to temperatures of 340 $^{o}$C approximately 15 % of the weight is lost. Above this temperature PANI showed regular decrease in the weight due to thermal degradation of the polymer.

The order of thermal stability of various PANI-CNT composites, prepared chemically is CPC1 > CPC5 > CPC4 > CPC3 > CPC2 indicating increased thermal stability of the composite as aniline content increases in the initial polymerization solution. Highest thermal stability of CPC1 may be assigned to 1:1 aniline to CNT ratio and hence the lesser amount of PANI. Therefore, CNT in this composite played a dominant role in promoting the thermal stability. In case of higher aniline content the thermal stability is somewhat independent to the CNT content and can be attributed to the layer by layer degradation of the deposited PANI over CNT surface.

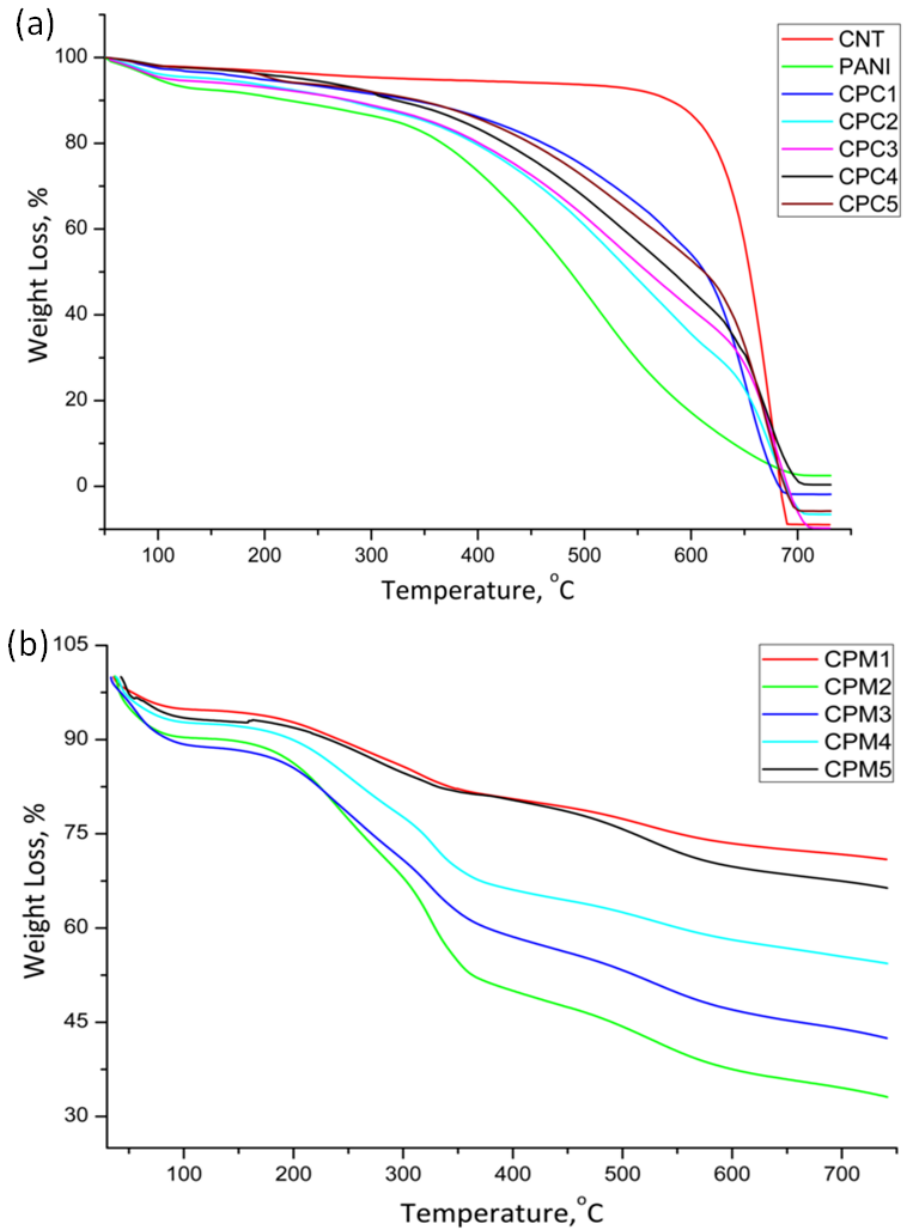


***Figure 6**. TGA Curves of **(a)** CNT, PANI and PANI-CNT composites prepared by in-situ chemical oxidative polymerization method and **(b)** PANI-CNT composites prepared by mechanical mixing method*

***Table 1.** Comparison of % weight loss of two kinds of composites at 380 and 600 °C*

| Composite | Weight loss at 380 °C, % | Weight loss at 600 °C, % |
|---|---|---|
| CPC1 | 13 | 48 |
| CPC2 | 19 | 64 |
| CPC3 | 18 | 59 |
| CPC4 | 15 | 56 |
| CPC5 | 13 | 48 |
| CPM1 | 19 | 28 |
| CPM2 | 50 | 67 |
| CPM3 | 41 | 55 |
| CPM4 | 33 | 44 |
| CPM5 | 20 | 30 |

A similar trend was obtained for the mechanically mixed composites. For comparison purpose the weight losses of the composites at temperature 380 $^{o}$C and 600 $^{o}$C are given in the table I. The results revealed that the composites prepared by chemical method have higher thermal stability compared to composites by mechanical mixing at the temperature range of 380 $^{o}$C. This can be attributed to the layer by layer deposition of the PANI over the CNT surface in case of chemically prepared composites which can also be seen in the SEM micrograph, whereas no such layered structure is obtained in the mechanically mixed composites. The other reason behind this is the smooth surface morphology of the chemically prepared composites due to separation of the CNT bundles. However, at temperature of 600 $^{o}$C the reverse order of thermal stability was seen because of presence of higher PANI content in the mechanically mixed composites [29]. Another reason is that in the case of mechanically mixed composites there is a lower chance of separation of CNT bundles and hence the PANI gets deposited over thick CNT bundles resulting in the enhanced stability at higher temperature.

## Conclusions

The composites of the PANI-CNT have been successfully synthesized chemically and by mechanical mixing of the PANI and CNT. Composites prepared by chemical polymerization have smooth surface morphology indicative of layer by layer deposition of the PANI over CNT substrate. Whereas the composites prepared by mechanical mixing appear to have irregular deposition of PANI. The thermal stability of the composite is better than the PANI indicating the contribution of CNT towards the thermal stability of the composites. The composite exhibited higher value of specific capacitance than the CNT and PANI alone and is indicative of the synergy. However, CNT did not contributed much to the capacitive value but acts as a good substrate for PANI deposition.

***Acknowledgements**: Authors are thankful to the University Grants Commission, New Delhi (INDIA) for providing financial assistance in the form of major research project.*

## References

[1] J.W. Schultze, H. Karabulut, *Electrochim. Acta* **50** (2005) 1739–1745.
[2] Y. Sharma, A. Tiwari, S. Hattori, D. Terada, A.K. Sharma, M. Ramalingam, H. Kobayashi, *Int. J. Biol. Macromol.* **51** (2012) 627-631.
[3] S. Iijima, T. Ichihashi, *Nature* **363** (1993) 603–605.
[4] J.W. Mintmire, B.I. Dunlap C.T. White, *Phys. Rev. Lett.* **68** (1992) 631-634.
[5] M. Tasviri, H.A. Rafiee-Pour, H. Ghourchian, M.R. Gholami, *Appl. Nanosci.* **1** (2011) 189–195.
[6] Y.J. Zhang, Y.W. Lin, C.C. Chang, T.M. Wu, *Synth. Met.* **161** (2011) 937–942.
[7] R. Mangu, S. Rajaputra, V.P. Singh, *Nanotechnology* **22** (2011) 215502.
[8] A.A. Mikhaylova, E.K. Tusseeva, N.A. Mayorova, A.Y. Rychagov, Y.M. Volfkovich, A.V. Krestinin, O.A. Khazova, *Electrochim*. *Acta* **56** (2011) 3656–3665.
[9] L. Zheng, X. Wang, H. An, X. Wang, L. Yi, L. Bai, *J. Solid State Electrochem.* **15** (2011) 675–681.
[10] T.A. Skotheim, R.L. Elsenbaumer, J.R. Reynolds, Handbook of conducting polymers, Marcel Dekker, New York (1997).
[11] P. Ghosh, S.K. Siddhanta, A. Chakrabarti, *Eur. Polym. J.* **35** (1999) 699-710.
[12] T.M. Wu, Y.W. Lin, C.S. Liao, *Carbon* **43** (2005) 734–740.
[13] L.S. Schadler, S.C. Giannaris, P.M. Ajayan, *Appl. Phys. Lett.* **73** (1998) 3842-3844.

[14] H.D. Wagner, O. Lourie, Y. Feldman, R. Tenne, *Appl. Phys. Lett.* **72** (1998) 188-190.
[15] D. Qian, E.C. Dickey, R. Andrews, T. Rantell, *Appl. Phys. Lett.* **76** (2000) 2868-2870.
[16] S.L. Shi, L.Z. Zhang, J.S. Li, *J. Polym. Res.* **16** (2009) 395–399.
[17] E. Frackowiak, V. Khomenko, K. Jurewicz, K. Lota, F. Béguin, *J. Power Sources* **153** (2006) 413-418.
[18] P.D. Gaikwad, D.J. Shirale, V.K. Gade, P.A. Savale, K.P. Kakde, H.J. Kharat, M.D. Shirsat, *Bull. Mat. Sci.* **29** (2006) 417–420.
[19] M.R. Karim, C.J. Lee, Y.T. Park, M.S. Lee, *Synth. Met.* **151** (2005) 131-135.
[20] S.B. Kondawar, S.A. Acharya, S.R. Dhakate, *Adv. Mat. Lett.* **2** (2011) 362-367.
[21] B.S. Kushwah, S.C. Upadhyaya, S.Shukla, A.S. Sikarwar, R.M. S. Sengar, S. Bhaduria, *Adv. Mat. Lett.* **2** (2011) 43-51.
[22] T.M. Wu, Y.W. Lin, *Polymer* **47** (2006) 3576–3582.
[23] A.K. Sharma, Y. Sharma, *Anal. Lett.* **45** (2012) 2075-2085.
[24] S.R. Sivakkumar, W.J. Kim, J.A. Choi, D.R. MacFarlane, M. Forsyth, D.W. Kim, *J. Power Sources* **171** (2007) 1062–1068.
[25] J.H. Kim, Y.S. Lee, A.K. Sharma, C.G. Liu, *Electrochim. Acta* **52** (2006) 1727-1732.
[26] J.H. Kim, A.K. Sharma, Y.S. Lee, *Mat. Lett.* **60** (2006) 1697-1701.
[27] A.K. Sharma, Y. Sharma, R. Malhotra, J.K. Sharma, *Adv. Mat. Lett.* **3** (2012) 82-86.
[28] W. Feng, , X.D. Bai, Y.Q. Lian, J. Liang, X.G. Wang, K. Yoshino, *Carbon* **41** (2003) 1551-1557.
[29] A.M. Showkat, K.P. Lee, A.I. Gopalan, S.H. Kim, S.H. Choi, S.H. Sohn, *J. Appl. Polym. Sci.* **101** (2006) 3721–3729.

*J. Electrochem. Sci. Eng.* **3(2)** (2013) 57-79; doi: **10.5599/jese.2013.0030**

**Open Access : : ISSN 1847-9286**

***www.jESE-online.org***

*Original scientific paper*

# Novel Mannich bases bearing pyrazolone moiety Synthesis, characterization and electrochemical studies

KRISHNA NAIK✉, ALURU RAGHAVENDRA GURU PRASAD*, YADATI NARASIMHA SPOORTHY and LAKSHMANA RAO KRISHNA RAO RAVINDRANATH

*Sri Krishnadevaraya University, Anantapur, A.P., India*

**ICFAI Foundation for Higher Education, Hyderabad, A.P., India*

✉ Corresponding Author: E-mail: ekrishnaiksep@yahoo.in

Received: November 23, 2012; Published: April 19, 2013

***Abstract***

*The present investigation describes a series of new {4-[3-Methyl-5-oxo-4-(4$^{l}$-substituted phenyl hydrazono)-4,5-dihydro-pyrazol-1-yl]-phenoxy}-acetic acid (2-oxo-1-piperidine-1--ylmethyl-1,2-dihydro–indol-3-ylidene)-hydrazides synthesized by the Mannich reaction of {4-[3-Methyl-5-oxo-4-(4$^{l}$-substituted phenyl hydrazono)-4,5-dihydro-pyrazol-1-yl]--phenoxy}-acetic acid (2-oxo-1,2-dihydro-indol-3-ylidene)-hydrazide with aqueous formaldehyde and a solution of piperidine in dimethylformamide. These novel Mannich bases were characterized by elemental analysis, IR, $^{1}$H NMR and mass spectral data. Electrochemical behavior of these compounds were studied by two techniques namely polarography and cyclic voltammetry. The results from both the techniques were compared and the reduction mechanism in acidic as well as basic medium was proposed.*

**Keywords**

Mannich bases, Synthesis, Polarography, Cyclic voltammetry, Comparison, Reduction mechanism.

## Introduction

Pyrazolones [1-5] and related heterocycles are widely used in medicinal chemistry as they possess wide range of biological and pharmacological properties. Further, Mannich bases exhibit pronounced biological activities. The key feature of Mannich reaction is that the amino carbonyl products are valuable synthons for synthesis [6-8] and can be readily converted to derivatives that possess useful applications in paint industry, polymer industry and particularly in medicine and the pharmaceutical industry [9-14]. Due to this reason, Mannich bases have engrossed a great deal of

attention of pharmaceutical chemists. In view of the above mentioned facts, we propose to synthesize certain novel Mannich bases containing a pyrazolone moiety.

The pharmacological properties of many compounds have been quantitatively related to their reduction process [15-18]. Structure-activity relationship studies [19,20] demonstrated that the reduction potential correlates with the antimicrobial activity of certain compounds.

Extensive work on electrochemical behavior of medicinally important compounds has been already reported from these laboratories [21,22]. In this article, the cyclic voltammetric behavior of Mannich bases on a hanging mercury drop electrode and modified carbon paste electrode is reported. A comparison of polarographic behavior of the compounds with their cyclic voltammetric behavior is also presented**.**

## Experimental

All the chemicals and reagents used in the studies were analytical reagent grade obtained from Merck. Britton-Robinson buffer solutions were prepared from the appropriate volumes of acetic acid (0.04 M), phosphoric acid (0.04 M), boric acid (0.04 M) and sodium hydroxide (0.2M). pH meter, Model LI – 10 manufactured by ELICO Private Limited, Hyderabad, India was used for pH measurements.

A CL-25 Pen Recording Polarograph manufactured by ELICO Private Limited, Hyderabad, India was used to record current-voltage curves. The capillary having the characteristics 1.80 $mg^{2/3}$ $s^{-1/2}$ at h = 80 cm was employed in the studies.

The cyclic voltammeter used consists of an X-Y recorder (Model RE 0074), a PAR 175 Potentiostat and an PAR 175 Universal Programmer. A single compartment cell Model 303 SMDE with silver wire as reference electrode and platinum wire as counter electrode was used for cyclic voltammetric studies. A stationary mercury drop electrode (SMDE 303) with a drop area 0.0096 $cm^2$ was used as the working electrode.

### *General polarographic procedures (Scheme 1)*

8.0 mL of the buffer solution of desired pH, 2.0 mL of Mannich base solution ($1.0\times10^{-2}$ M) in dimethylformamide, 6.0 mL of dimethylformamide (DMF) and 4.0 mL of distilled water were mixed thoroughly in the polarographic cell. The polarograms were recorded after the expulsion of dissolved oxygen with nitrogen gas. Geltain was used as the maximum suppressor in all the investigations except in the experiments where the effect of surfactants was studied.

### *Synthesis of Mannich bases*

{4-[3-Methyl-5-oxo-4-(4$^{|}$-substituted phenyl hydrazono)-4,5-dihydro-pyrazol-1-yl]-phenoxy}-acetic acid hydrazide I were synthesized and characterized by the procedures reported in the literature [23].

### *Synthesis of {4-[3-Methyl-5-oxo-4--(4$^{|}$-substituted phenyl hydrazono)-4,5-dihydro-pyrazol-1-yl]--phenoxy}-acetic acid (2-oxo-1,2-dihydro-indol-3-ylidene)- hydrazide IV.*

The required isatins were prepared by the procedure described by Marvel and Heirs [24].

### *Synthesis of isonitrosoacetanilide (II)*

22 g of chloral hydrate and 300 mL of water was taken into a one litre round bottom flask. 3.25 g of sodium sulphate, 12 g of aniline (in 75 mL of water), 12 mL of concentrated hydrochloric acid and 27g of hydroxyl amine hydrochloride (in 25 mL of water) were added and heated over a

wire gauge for about 45 minutes. The reaction mixture was cooled, the solid separated was filtered and dried.

*a. Synthesis of Isatin 46 (R = H). (III)*

A miture of 8 mL of concentrated $H_2SO_4$, 18 g of dry isonitrosoacetanilide taken in a round bottem flask was heated to 80 $^oC$ for about 10 minutes. The reaction mixture was cooled to room temperature and poured onto crushed ice. The precipitated isatin was filtered, washed several times with cold water and dried.

*c. Synthesis of {4-[3-Methyl-5-oxo-4-(4$^l$-substituted phenyl hydrazono)-4,5-dihydro-pyrazol-1-yl]-phenoxy}-acetic acid(2-oxo-1,2-dihydro-indol-3-ylidene)-hydrazide IV.*

A mixture of I (R = H) and III in 1 : 1 molar ratio when heated in DMF-water bath for 45 minutes, resulted in a compound with melting point 214 $^oC$. Based on spectral data, the compound was assigned structure as {4-[3-Methyl-5-oxo-4-(phenyl - hydrazono)-4,5-dihydro-pyrazol-1-yl]-phenoxy}-acetic acid (2-oxo-1,2-dihydro – indol-3-ylidene)- hydrazide IVa (R = H).

Other members of the series were prepared by similar procedures and their characterization data are given in the Table 1.

***Table 1.*** *Characterization of {4-[3-Methyl-5-oxo-4-(4$^l$-substituted phenyl hydrazono)-4,5-dihydro-pyrazol-1-yl]-phenoxy}-acetic acid (2-oxo-1,2-dihydro-indol-3-ylidene)-hydrazide.*

| Compound | R | M.P. $^oC$ | Yield, % | Molecular formula | Mass fraction found, % (Calc., %) | | | | | |
|---|---|---|---|---|---|---|---|---|---|---|
| | | | | | C | H | N | O | Cl | Br |
| IVa | H | 214 | 70 | $C_{26}H_{25}N_7O_4$ | 62.52 (62.48) | 5.01 (4.89) | 19.63 (19.50) | 12.82 (12.70) | | |
| IVb | $CH_3$ | 241 | 70 | $C_{27}H_{27}N_7O_4$ | 63.15 (63.02) | 5.26 (5.15) | 19.10 (18.95) | 12.47 (12.32) | | |
| IVc | $OCH_3$ | 234 | 70 | $C_{27}H_{27}N_7O_4$ | 61.24 (61.12) | 5.10 (4.95) | 18.52 (18.38) | 15.12 (15.00) | | |
| IVd | $OC_2H_5$ | 224 | 75 | $C_{28}H_{29}N_7O_5$ | 61.87 (61.75) | 5.34 (5.25) | 18.04 (17.88) | 14.73 (14.62) | | |
| IVe | Cl | 225 | 75 | $C_{26}H_{24}ClN_7O_4$ | 58.48 (58.35) | 4.49 (4.32) | 18.38 (18.22) | 11.99 (11.75) | 6.65 (6.52) | |
| IVf | Br | 243 | 80 | $C_{26}H_{24}BrN_7O_4$ | 53.98 (53.82) | 4.15 (3.98) | 16.95 (16.80) | 11.07 (10.95) | | 13.82 (13.65) |

*IR Spectral details*

The IR (KBr) spectrum (Figure 1) of {4-[3-Methyl-5-oxo-4-(phenyl hydrazono)-4,5-dihydro-pyrazol-1-yl]-phenoxy}-acetic acid (2-oxo-1,2-dihydro–indol-3-ylidene)- hydrazide (hydrazone) IVa showed characteristic strong absorption bands at 3205 (NH), 3170 (Indole NH), 1602 (C = N), 1656 (pyrazoline C = O), 1700 (Indole C = O) and 1618 (CONH). The spectral data and the respective assignments of IV are given in the Table 2.

*$^1$H NMR Spectral details*

The $^1$H NMR (200 MHz) spectrum (Figure 2) of {4-[3-Methyl-5-oxo-4-(phenyl hydrazono)-4,5--dihydro-pyrazol-1-yl]-phenoxy}-acetic acid (2-oxo-1,2-dihydro–indol-3-ylidene)-hydrazide (hydrazone) IVa in DMSO – $d_6$ showed the signals at δ1.1 (s, 3H, $CH_3$), δ10.93 (s, 1H, Ar – NH), δ5.78 (s, 2H, N-$CH_2$ – CO), δ12.75 (s, 1H, Indole NH) and δ7.1 – 7.3 (m, 9H, Ar – H) (Table 3).

***Table 2:*** *IR (KBr) Spectral data of {4-[3-Methyl-5-oxo-4-(4[I]-substituted phenyl hydrazono)-4,5-dihydro-pyrazol-1-yl]-phenoxy}-acetic acid (2-oxo-1,2-dihydro-indol-3-ylidene)-hydrazide.*

| Compound | $\nu_{max}$ / cm$^{-1}$ | | | | | |
|---|---|---|---|---|---|---|
| | >NH | Indole NH | >C=N- | Pyrazoloine C=O | Indole>C=O | >CO-NH- |
| IVa | 3205 | 3170 | 1602 | 1656 | 1700 | 1618 |
| IVb | 3180 | 3140 | 1600 | 1654 | 1700 | 1622 |
| IVc | 3100 | 3150 | 1505 | 1654 | 1701 | 1625 |
| IVd | 3195 | 3155 | 1604 | 1654 | 1701 | 1624 |
| IVe | 3175 | 3140 | 1605 | 1654 | 1701 | 1624 |
| IVf | 3190 | 3150 | 1604 | 1654 | 1701 | 1624 |

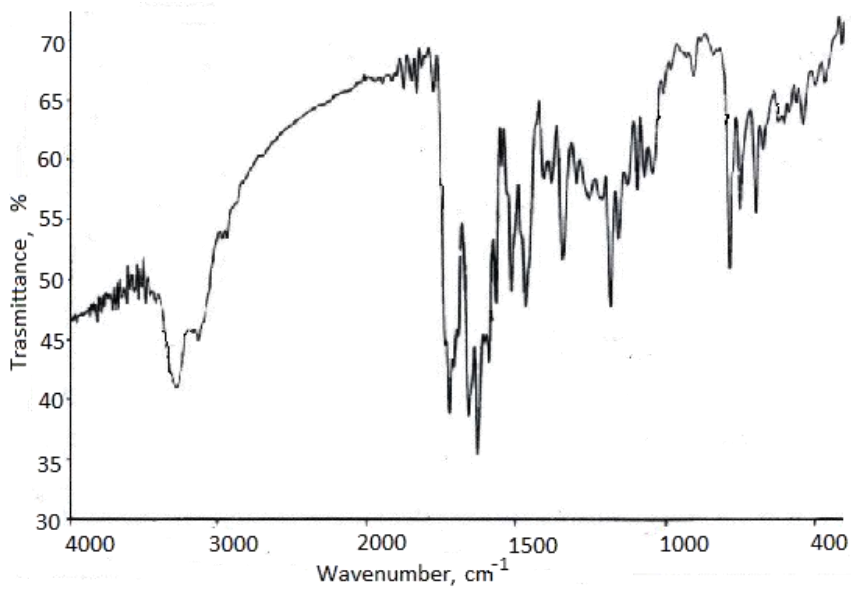


***Figure 1.*** *IR Spectrum of {4-[3-methyl-5-oxo-4-(phenyl hydrazono)-4,5-dihydro-pyrazol-1-yl]--phenoxy}-acetic acid (2-oxo-1,2-dihydro-indol-3-ylidene)-hydrazide*

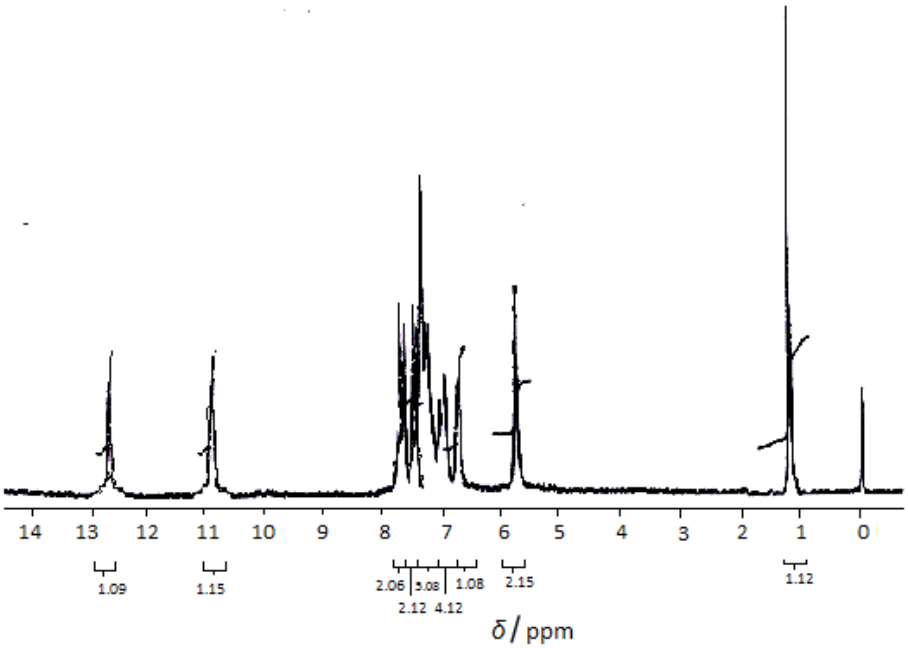


***Figure 2.*** *[1]H NMR spectrum of {4-[3-methyl-5-oxo-4-(phenyl hydrazono)-4,5-dihydro-pyrazol-1--yl]--phenoxy}-acetic acid (2-oxo-1,2-dihydro-indol-3-ylidene)-hydrazide*

***Table 3.*** *$^1$H NMR Spectral data of {4-[3-Methyl-5-oxo-4-(4$^l$-substituted phenyl hydrazono)-4,5-dihydro-pyrazol-1-yl]-phenoxy}-acetic acid (2-oxo-1,2-dihydro-indol-3-ylidene)-hydrazide.*

| Compound | $\delta$ / ppm |
|---|---|
| IVa | 1.1 (s, 3H, $CH_3$), 5.78 (s, 2H, N-$CH_2$-CO), 6.8 (s, 1H, Ar–NH), 6.9-7.0 (m, 4H, $C_6H_4$), 7.1–7.3 (m, 5H, Ar-H), 7.4 (d, 2H, $C_6H_4$), 7.7 (d, 2H, $C_6H_4$)' 10.93 (s, 1H, CONH), 12.75 (s, 1H, Indole NH) |
| IVb | 0.95 (s, 3H, $CH_3$), 1.14 (s, 3H, $CH_3$), 5.82 (s, 2H, N-$CH_2$-CO), 6.8 (s, H, Ar-NH), 6.9-7.0 (m, 4H, $C_6H_4$), 7.1-7.3 (m, 4H, Ar–H), 7.4 (d, 2H, $C_6H_4$), 7.7 (d, 2H, $C_6H_4$), 10.95 (s, 1H, CONH), 12.75 (s, 1H, Indole NH) |
| IVc | 1.12 (s, 3H, $CH_3$), 3.24 (s, 3H, $OCH_3$), 5.8 (s, 2H, N-$CH_2$CO), 6.8 (s, 1H, Ar-NH), 6.9-7.0 (m, 4H, $C_6H_4$), 7.1-7.3 (m, 4H, Ar-H), 7.4 (d, 2H, $C_6H_4$) and 7.7 (d, 2H, $C_6H_4$), 10.95 (s, 1H, CONH), 12.75 (s, 1H, Indole NH) |
| IVd | 0.95 (s, 3H, $CH_3$), 1.15 (t, 3H, $CH_3$), 3.16 (q, 2H, O-$CH_2$), 5.76 (s, 2H, N-$CH_2$CO), 6.8 (s, 1H, Ar-NH), 6.9-7.0 (m, 4H, $C_6H_4$), 7.1-7.3 (m, 4H, Ar-H), 7.4 (d, 2H, $C_6H_4$) and 7.7 (d, 2H, $C_6H_4$), 10.91 (s, H, CO-NH), 12.72 (s, 1H, Indole NH) |
| IVe | 1.05 (s, 3H, $CH_3$), 5.8 (s, 2H, N-$CH_2$CO), 6.8 (s, H, Ar-NH), 6.9-7.0 (m, 4H, $C_6H_4$), 7.1-7.3 (m, 4H, Ar-H), 7.4 (d, 2H,$C_6H_4$) and 7.7 (d, 2H, $C_6H_4$), 10.93 (s, H, CO-NH), 12.7 (s, 1H, Indole NH) |
| IVf | 1.02 (s, 3H, $CH_3$), 5.78 (s, 2H, N-$CH_2$CO), 6.8 (s, H, Ar-NH), 6.9-7.0 (m, 4H, $C_6H_4$), 7.1-7.3 (m, 4H, Ar-H), 7.4 (d, 2H, $C_6H_4$) and 7.7 (d, 2H, $C_6H_4$), 10.93 (s, H, CO-NH), 12.75 (s, H, Indole NH) |

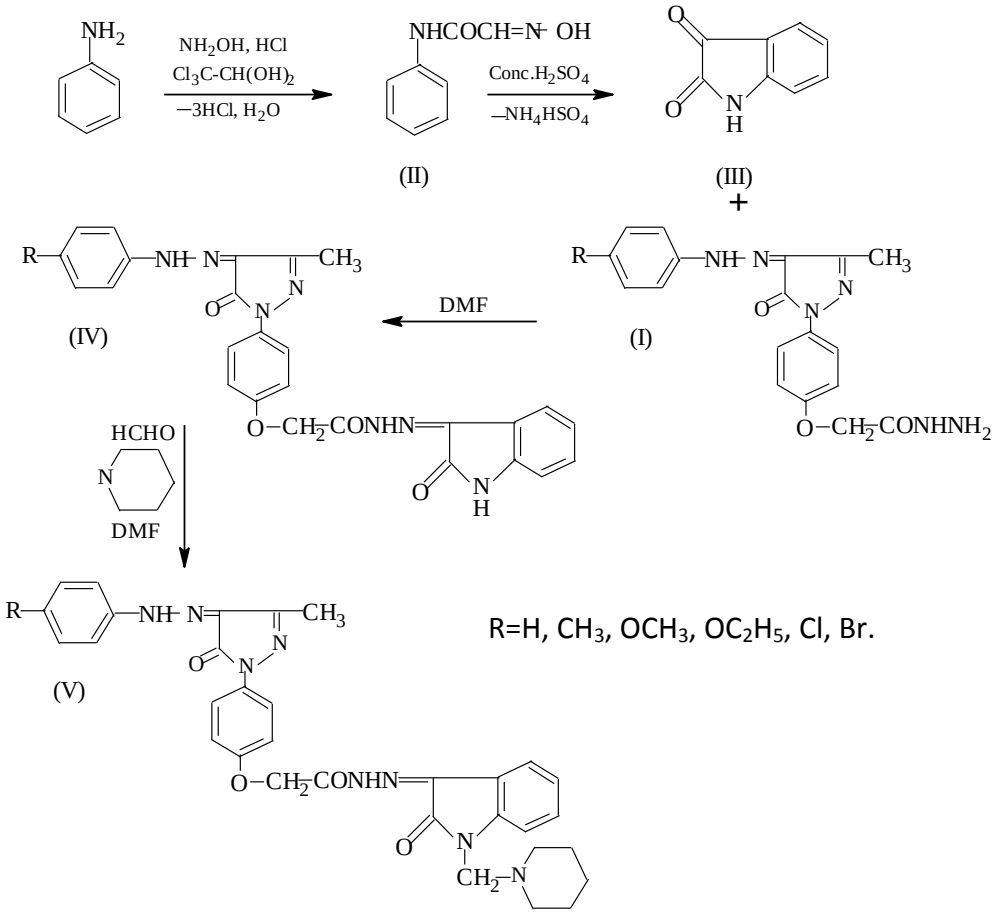


***Scheme 1.*** *Synthesis of {4-[3-Methyl-5-oxo-4-(4$^l$-{4-[3-Methyl-5-oxo-4-(4$^l$-substituted phenyl hydrazono)-4,5-dihydro-pyrazol-1-yl]-phenoxy}-acetic acid (2-oxo-1- piperidine-1-ylmethyl-1,2 –dihydro – indol-5-ylidene)- hydrazide (V)*

*d. Synthesis of {4-[3-Methyl-5-oxo-4-(4$^{l}$-substituted phenyl hydrazono)-4,5-dihydro-pyrazol-1-yl]-phenoxy}-acetic acid (2-oxo-1-piperidine-1-ylmethyl-1,2-dihydro–indol-3-ylidene)- -hydrazide (V).*

A mixture of hydrazone IVa (R = H), aqueous formaldehyde and a solution of piperidine in DMF were stirred for about six hours at room temperature to give {4-[3-Methyl-5-oxo-4-(phenyl hydrazono)-4,5-dihydro-pyrazol-1-yl]-phenoxy}-acetic acid (2-oxo-1-piperidine-1-ylmethyl-1,2-di -hydro–indol-3-ylidene)- hydrazide V a ( R = H).

Similar treatment of hydrazones IV b-f with piperidine in presence of formaldehyde in DMF at room temperature yielded respective {4-[3-Methyl-5-oxo-4-(4$^{l}$-substituted phenyl hydrazono)-4,5- -dihydro-pyrazol-1-yl]-phenoxy}-acetic acid-(2-oxo-1-piperidine-1-ylmethyl-1,2-dihydro–indol-3-yli-dene)- hydrazide V b-f (R = $CH_3$, $OC_2H_5$, -Cl, -Br).

The structures of the compounds V a- f were established on the basis of elemental analysis and spectral data (Table 4) and spectral data (Table 5 and Table 6).

*IR Spectral details*

The IR (KBr) spectrum (Figure 3) of {4-[3-Methyl-5-oxo-4-(phenyl hydrazono)-4,5-dihydro-pyra-zol-1--yl]-phenoxy}-acetic acid (2-oxo-1-piperidine-1-ylmethyl-1,2-dihydro–indol-3-ylidene)- hydra-zide V a exhibited characteristic bands at around 3195 (NH), 1610 (C = N), 1676 (pyrazoline C = O), 1720 (Indole C = O), 1654 (C – NH) and 2933 $cm^{-1}$ ($CH_2$) (Table 5).

The spectral data and the respective assignments of V are detailed below.

***Table 4.*** *Characterization data of {4-[3-Methyl-5-oxo-4-(4$^{l}$-substituted phenyl hydrazono)-4,5-dihydro-pyrazol-1-yl]-phenoxy}-acetic acid (2-oxo-1-piperidine-1-ylmethyl-1,2-dihydro-indol-3-ylidene) - hydrazide V*

| Compd | R | M.P. | Yield, % | Molecular formula | Mass fraction Found, % (Calc., %) | | | | | |
|---|---|---|---|---|---|---|---|---|---|---|
| | | | | | C | H | N | O | Cl | Br |
| Va | H | 158 | 70 | $C_{32}H_{32}N_8O_4$ | 64.86 (64.72) | 5.40 (5.28) | 19.91 (19.86) | 10.81 (10.75) | | |
| Vb | $CH_3$ | 164 | 70 | $C_{33}H_{34}N_8O_4$ | 65.34 (65.21) | 5.61 (5.45) | 18.48 (18.34) | 10.56 (10.38) | | |
| Vc | $OCH_3$ | 167 | 70 | $C_{33}H_{34}N_8O_5$ | 63.66 (63.56) | 5.46 (5.32) | 18.00 (17.85) | 12.86 (12.64) | | |
| Vd | $OC_2H_5$ | 159 | 75 | $C_{34}H_{36}N_8O_5$ | 64.15 (64.01) | 5.66 (5.45) | 17.61 (17.50) | 12.56 (12.42) | | |
| Ve | Cl | 161 | 75 | $C_{32}H_{31}ClN_8O_4$ | 61.29 (61.15) | 4.94 (4.78) | 17.87 (17.73) | 10.21 (10.8) | 5.66 (5.45) | |
| Vf | Br | 160 | 80 | $C_{32}H_{31}BrN_8O$ | 57.23 (57.08) | 4.62 (4.42) | 16.69 (16.54) | 9.53 (9.38) | | 11.90 (11.70) |

***Table 5.*** *IR (KBr) spectral data of {4-[3-Methyl-5-oxo-4-(4$^{l}$-substituted phenyl hydrazono)-4,5-dihydro-pyrazol-1-yl]-phenoxy}-acetic acid (2-oxo-1-piperidine-1-ylmethyl-1,2-dihydro-indol-3-ylidene)- hydrazide V.*

| Compound | $\nu_{max}$ / $cm^{-1}$ | | | | | |
|---|---|---|---|---|---|---|
| | >NH | >C=N- | Pyrazoloine C=O | Indole C=O | >CO-NH- | $>CH_2$- |
| Va | 3195 | 1610 | 1676 | 1720 | 1654 | 2933 |
| Vb | 3170 | 1616 | 1674 | 1715 | 1658 | 2920 |
| Vc | 3120 | 1610 | 1680 | 1712 | 1654 | 2625 |
| Vd | 3175 | 1614 | 1674 | 1711 | 1656 | 2915 |
| Ve | 3155 | 1616 | 1674 | 1714 | 1658 | 2920 |
| Vf | 3170 | 1614 | 1674 | 1716 | 1626 | 2625 |

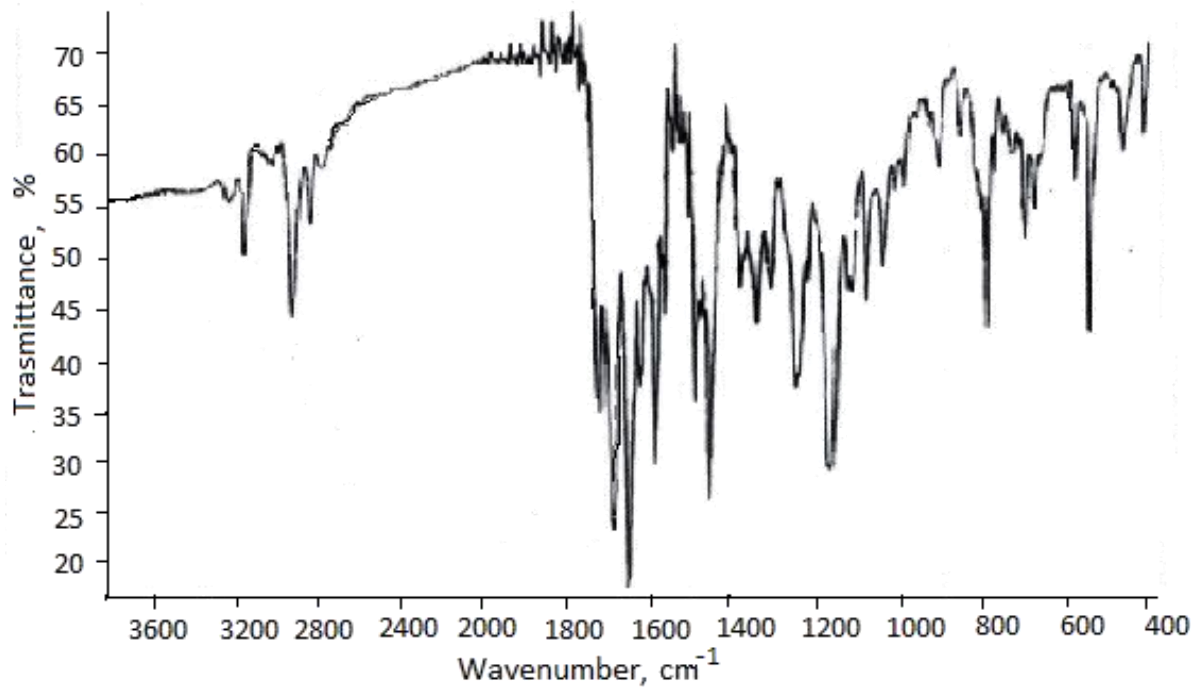


***Figure 3.*** *IR Spectrum of {4-[3-methyl-5-oxo-4-(phenyl hydrazono)-4,5-dihydro pyrazol-1-yl]-phenoxy} –acetic acid (2-oxo-1-piperidine-1-ylmethyl-1,2-dihydro-indol-3-ylidene)-hydrazide*

*$^1$H NMR Spectral details*

The $^1$H NMR (200 MHz) spectrum (Figure 4) of 3-[methyl-5-oxo-4-(4$^{|}$-*substituted* phenyl hydrazono)-4,5-dihydro-pyrazol-1-yl]-phenoxy}-acetic acid (2-oxo-1-piperidine-1-yl-methyl-1,2-dihydro–indol-3-ylidene)- hydrazide V was recorded in DMSO-$d_6$ and the data is given below. The appearance of a signal at δ 4.5 due to N–$CH_2$-N, confirmed the formation of Mannich bases (Table 6).

***Table 6.*** *$^1$H NMR Spectral data of {4-[3-Methyl-5-oxo-4-(4$^{|}$-substituted phenyl hydrazono)-4,5-dihydro-pyrazol-1-yl]-phenoxy}-acetic acid (2-oxo-1-piperidine-1-ylmethyl-1,2-dihydro-indol-3-ylidene)- hydrazide*

| Compound | *δ* / ppm |
|---|---|
| Va | 1.14 (s, 3H, $CH_3$), 1.45 (m, 6H, $(CH_2)_3$), 2.56 (t, 4H, $CH_2$-N-$CH_2$), 4.45 (s, 2H, N-$CH_2$-N), 5.9 (s, 2H, N-$CH_2$CO), 6.8 (s, 1H, Ar-NH), 6.9-7.0 (m, 4H, $C_6H_4$), 7.1-7.3 (m, 5H, Ar -H), 7.4 (d, 2H, $C_6H_4$), 7.7 (d, 2H, $C_6H_4$), 9.5 (s, H, -CONH). |
| Vb | 0.97 (s, 3H, $CH_3$), 1.12 (s, 3H, $CH_3$), 5.90 (s, 2H, N-$CH_2$-CO), 6.81 (s, H, Ar-NH), 6.9-7.0 (m, 4H, $C_6H_4$), 7.1-7.3 (m, 4H, Ar–H), 7.4 (d, 2H, $C_6H_4$), 7.7 (d, 2H, $C_6H_4$), 9.6 (s, 1H, CONH), 1.45 (m, 6H, $(CH_2)_3$), 2.54 (t, 4H, $CH_2$-N-$CH_2$), 4.48 (s, 2H, N-$CH_2$-N). |
| Vc | 1.15 (s, 3H, $CH_3$), 3.12(s, 3H, $OCH_3$), 5.91 (s, 2H, N-$CH_2$CO), 6.8 (s, 1H, Ar-NH), 6.9-7.0 (m, 4H, $C_6H_4$), 7.1-7.3 (m, 4H, Ar-H), 7.4 (d, 2H, $C_6H_4$) and 7.7 (d, 2H, $C_6H_4$), 2.51 (t, 4H, $CH_2$-N-$CH_2$), 1.41 (m, 6H, $(CH_2)_3$), 4.41(s, 2H, N-$CH_2$-N), 9.51 (s, 1H, CONH). |
| Vd | 0.98 (s, 3H, $CH_3$), 1.11 (t, 3H, $CH_3$), 3.11 (q, 2H, O-$CH_2$), 2.58 (t, 4H, $CH_2$-N-$CH_2$), 4.42 (s, 2H, N-$CH_2$-N), 5.81 (s, 2H, N-$CH_2$CO), 6.82(s, 1H, Ar-NH), 6.9-7.0 (m, 4H, $C_6H_4$), 7.1-7.3 (m, 4H, Ar-H), 1.45 (m, 6H, $(CH_2)_3$), 7.4 (d, 2H, $C_6H_4$) and 7.7 (d, 2H, $C_6H_4$), 9.41 (s, H, CO-NH). |
| Ve | 1.07 (s, 3H, $CH_3$), 2.57(t, 4H, $CH_2$-N-$CH_2$), 4.47 (s, 2H, N-$CH_2$-N), 5.92 (s, 2H, N-$CH_2$CO), 6.8 (s, H, Ar-NH), 6.9-7.0 (m, 4H, $C_6H_4$), 7.1-7.3 (m, 4H, Ar-H), 7.4 (d, 2H,$C_6H_4$) and 7.7 (d, 2H, $C_6H_4$), 1.47 (m, 6H, $(CH_2)_3$), 9.38 (s, H, CO-NH). |
| Vf | 1.06 (s, 3H, $CH_3$), 1.43 (m, 6H, $(CH_2)_3$), 5.91 (s, 2H, N-$CH_2$CO), 6.79 (s, H, Ar-NH), 6.9-7.0 (m, 4H, $C_6H_4$), 7.1-7.3 (m, 4H, Ar-H), 7.4 (d, 2H, $C_6H_4$) and 7.7 (d, 2H, $C_6H_4$), 9.51 (s, H, CO-NH), 2.52 (t, 4H, $CH_2$-N-$CH_2$), 4.49 (s, 2H, N-$CH_2$-N). |

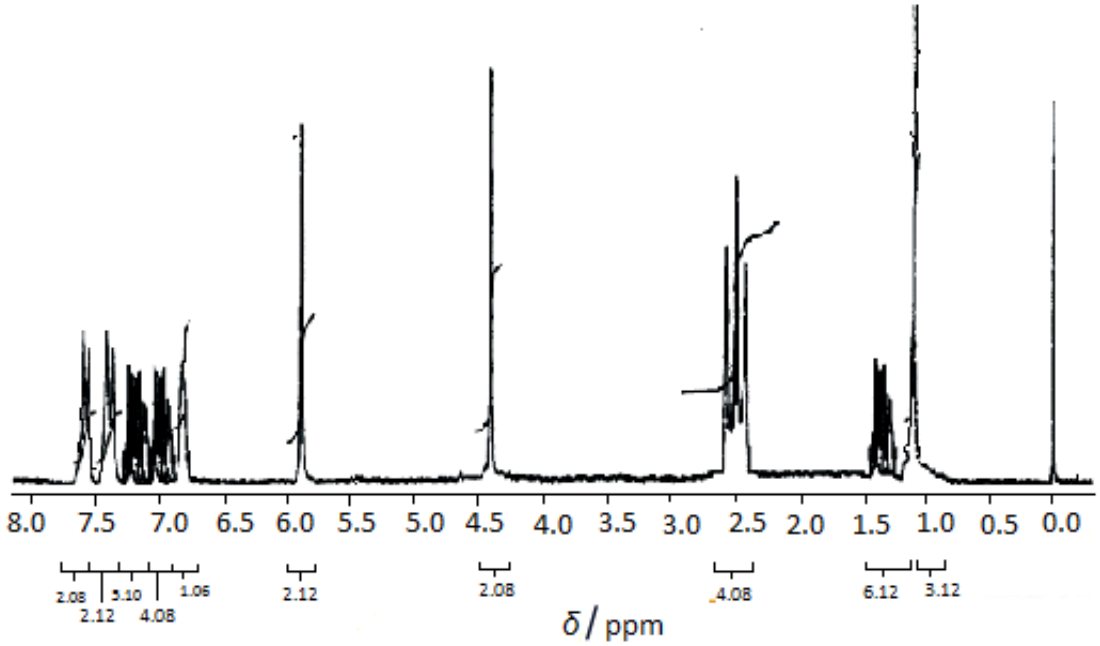


***Figure 4.*** *$^1$HNMR spectrum of {4-[3-methyl-5-oxo-4-(phenyl hydrazono)-4,5-dihydro pyrazol-1-yl]-phenoxy} – acetic acid (2-oxo-1-piperidine-1-ylmethyl-1,2-dihydro-indol-3-ylidene)-hydrazide*

*Mass spectral details*

The mass spectrum of {4-[3-Methyl-5-oxo-4-(phenyl hydrazono)-4,5-dihydro-pyrazol-1-yl]-phenoxy}-acetic acid (2-oxo-1-piperidine-1-yl methyl-1,2-dihydro-indol-3-ylidene)-hydrazide Va (R = H, X = $CH_2$) exhibited the molecular ($M^+$) ion peak at m/z 592.

The fragmentation pattern noticed in the mass spectrum of {4-[3-Methyl-5-oxo-4-(4$^|$-phenyl hydrazono)-4,5-dihydro-pyrazol-1-yl]-phenoxy}-acetic acid (2-oxo-1-piperidine-1-yl methyl-1,2-dihydro-indol-3-ylidene)-hydrazide Va (R = H, X = $CH_2$) is presented in Scheme 2.

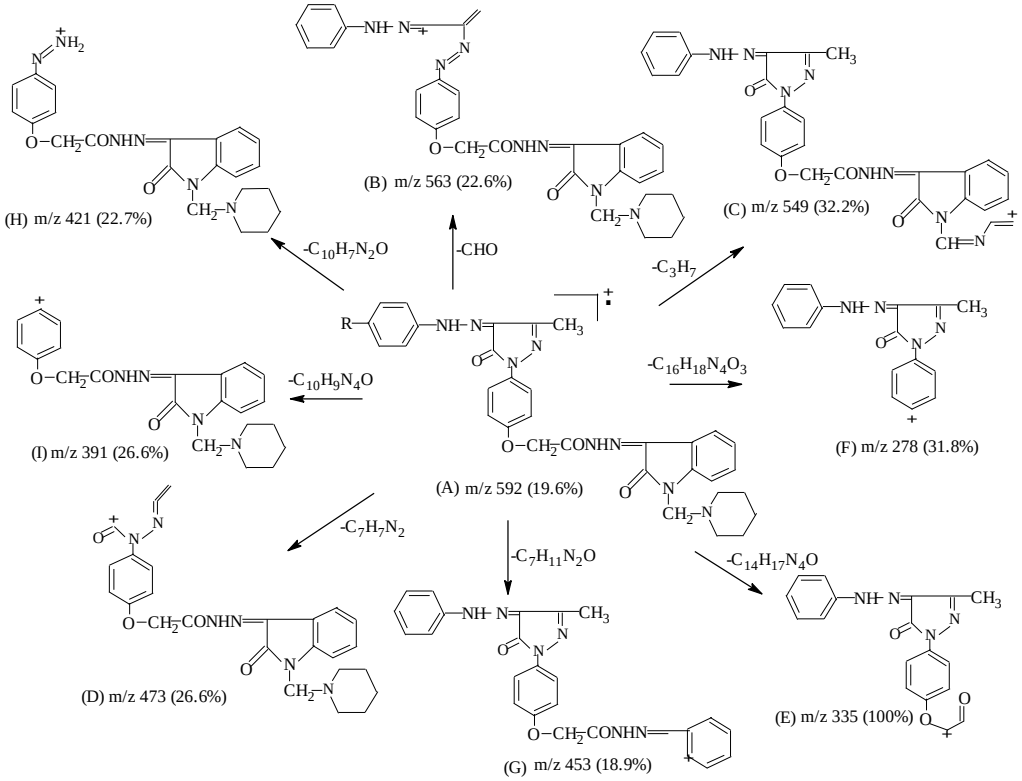


***Scheme 2.*** *Fragmentation details of {4-[3-Methyl-5-oxo-4-(phenyl hydrazono)-4,5-dihydro-pyrazol-1--yl]-phenoxy}-acetic acid (2-oxo-1-piperidine-1-ylmethyl-1,2-dihydro-indol-3-ylidene)-hydrazide*

The molecular ion A was observed at m/z 592 (19.6 %). Disintegration of molecular ion A yielded the cation B at m/z 563 (22.6 %). Elimination of $C_3H_7$ molecule from molecular ion A resulted in the formation of cation C at m/z 549 (32.2 %). Loss of $C_7H_7N_2$ radical from A resulted in the formation of cation D at m/z 473 (26.6 %). Expulsion of $C_{14}H_{17}N_4O$ radical from molecular ion yielded cation E at m/z 335 (100 %). The other important fragments noticed were 278 (31.8 %, F), 453 (18.9 %, G), 421 (22.7 %, H) and 391 (26.6 %, I).

## Results and Discussion

### *Polarographic behaviour of Mannich bases*

#### *General polarographic behaviour*

{4-[3-methyl-5-oxo-4-(4$^{I}$-substituted phenyl hydrazono)-4,5-dihydro-pyrazol-1-yl]-phenoxy}-acetic acid (2-oxo-1-piperidine-1-ylmethyl-1,2-dihydro–indol-3-ylidene)-hydrazides Va-f (Table 7) gave two cathodic waves in the pH range 1.1-7.1 and three cathodic waves in the pH range 8.1-10.1. The Polarograms of Va is shown in the Figure 5. An inspection of structure of above compounds showed that the sites susceptible for reduction at the dropping mercury electrode were exocylic >C=N, exocyclic >C=O and cyclic >C=N.

*Table 7. Details of Mannich bases synthesized*

| Compound | Substituent (-R) |
|---|---|
| Va | H |
| Vb | 4$^{I}$-$CH_3$ |
| Vc | 4$^{I}$-$OCH_3$ |
| Vd | 4$^{I}$-$OC_2H_5$ |
| Ve | 4$^{I}$-Cl |
| Vf | 4$^{I}$- Br |

Among these groups exocyclic azomethine group was more susceptible for reduction than other groups. However [3-methyl-4,5-dioxo-4,5-dihydro-pyrazol-1-yl]-acetic acid hydrazide does not give reduction wave under experimental conditions. This was probably due to stabilization [25] of the pyrazoline-5-one by ketoenol tautomerism. These observations unambiguously suggest that the waves observed in the present studies were due to reduction of two exocyclic azomethine groups.

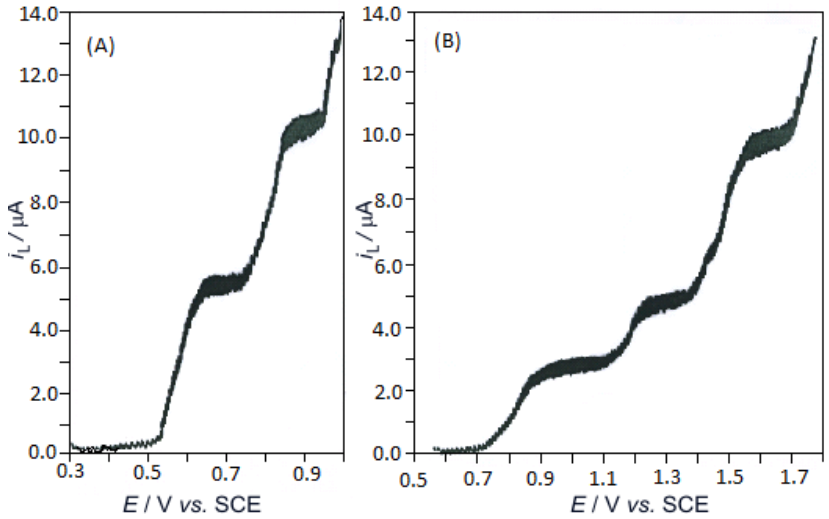


***Figure 5**. Polarograms of {4-[3-Methyl-5-oxo-4-(phenyl hydrazono)-4,5-dihydro-pyrazol-1--yl]--phenoxy}-acetic acid (2-oxo-1--piperidine-1-ylmethyl-1,2-dihydro-indol-3-ylidene)-hydrazide ; c = 1 mM; Medium : Aqueous dimethylformamide (40 % v/v). A represents the polarogram at pH 4.1 and B that at indicate 8.1 respectively.*

*Half wave potential-pH relation*

Half wave potentials of first and second waves shifted to more negative potentials with increase in pH of the medium in the range 1.1-7.1 (Table 1 in Supplementary material). The typical $E_{1/2}$ – pH graphs are shown in Figure 6. The half wave potentials of the waves were not altered in alkaline medium. The value of $\Delta E_{½}/\Delta$pH for both waves lie in the range of 0.089-0.094. The $E_{1/2}$-pH plots observed in the pH range 1.1-10.1 suggest that both the protonated form (acidic) and the deprotonated form (basic) of the depolariser were electroactive.

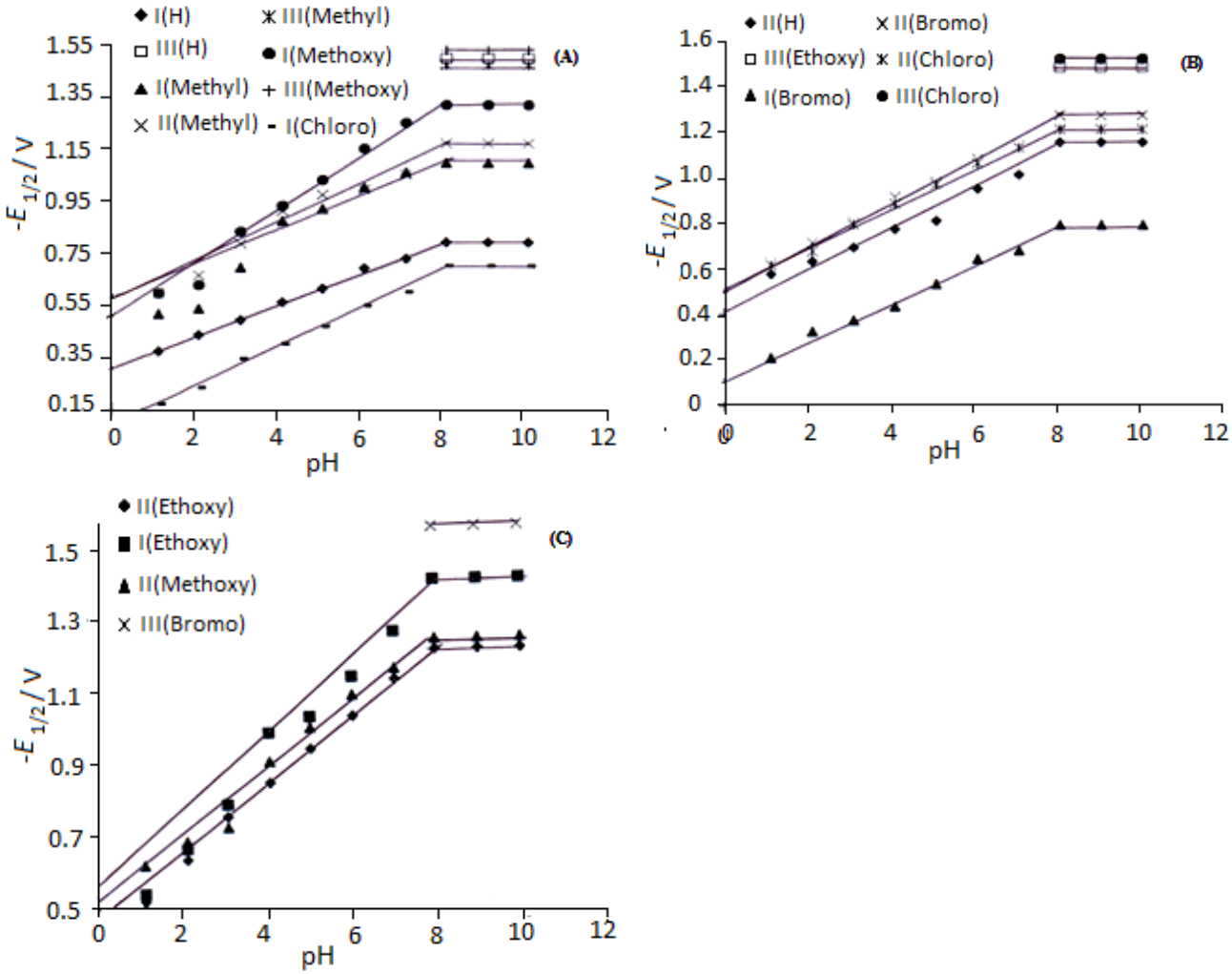


***Figure 6.*** *Plot of pH vs $-E_{1/2}$ for Mannich bases. c= 1 mM; Medium = Dimethylformamide (40 % v/v). I, II and III indicate first, second and third wave respectively of corresponding compound at indicated pH as shown in the figures (A), (B), (C), (D) and (E).*

*Effect of the height of mercury column head on the limiting current*

The limiting currents ($i_L$) recorded at different heights of the mercury column vary linearly with the square root of mercury column height ($h^{1/2}$). The constant values of $i_L/h^{1/2}$ confirm the diffusion controlled nature of first and second waves. $i_L - h^{1/2}$ plots are shown in Figure 7.

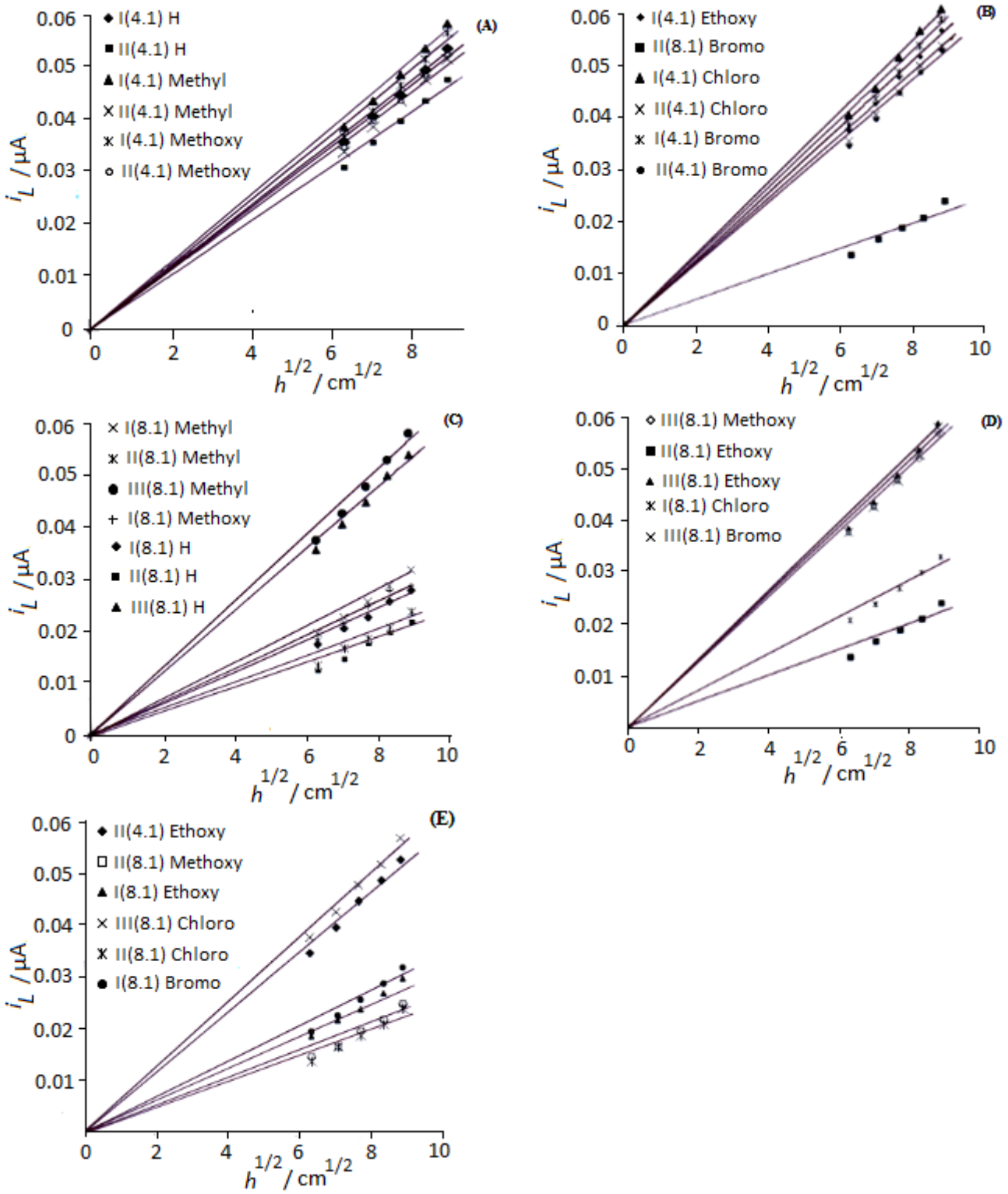


***Figure 7.*** *Effect of mercury column height (h) on limiting current ($i_L$ ). c= 1 mM Medium = Dimethylformamide (40 % v/v). I, II and III indicate first, second and third wave resp.*

*Effect of concentration on the diffusion current*

The influence of concentration on the limiting current in the range 0.5-3.5 mM was recorded in solutions of pH 4.1. The limiting current-concentration plots are presented in Figure 8. The plots were linear and passing through the origin. This observation further confirms the diffusion controlled nature of two waves. (First wave and second wave).

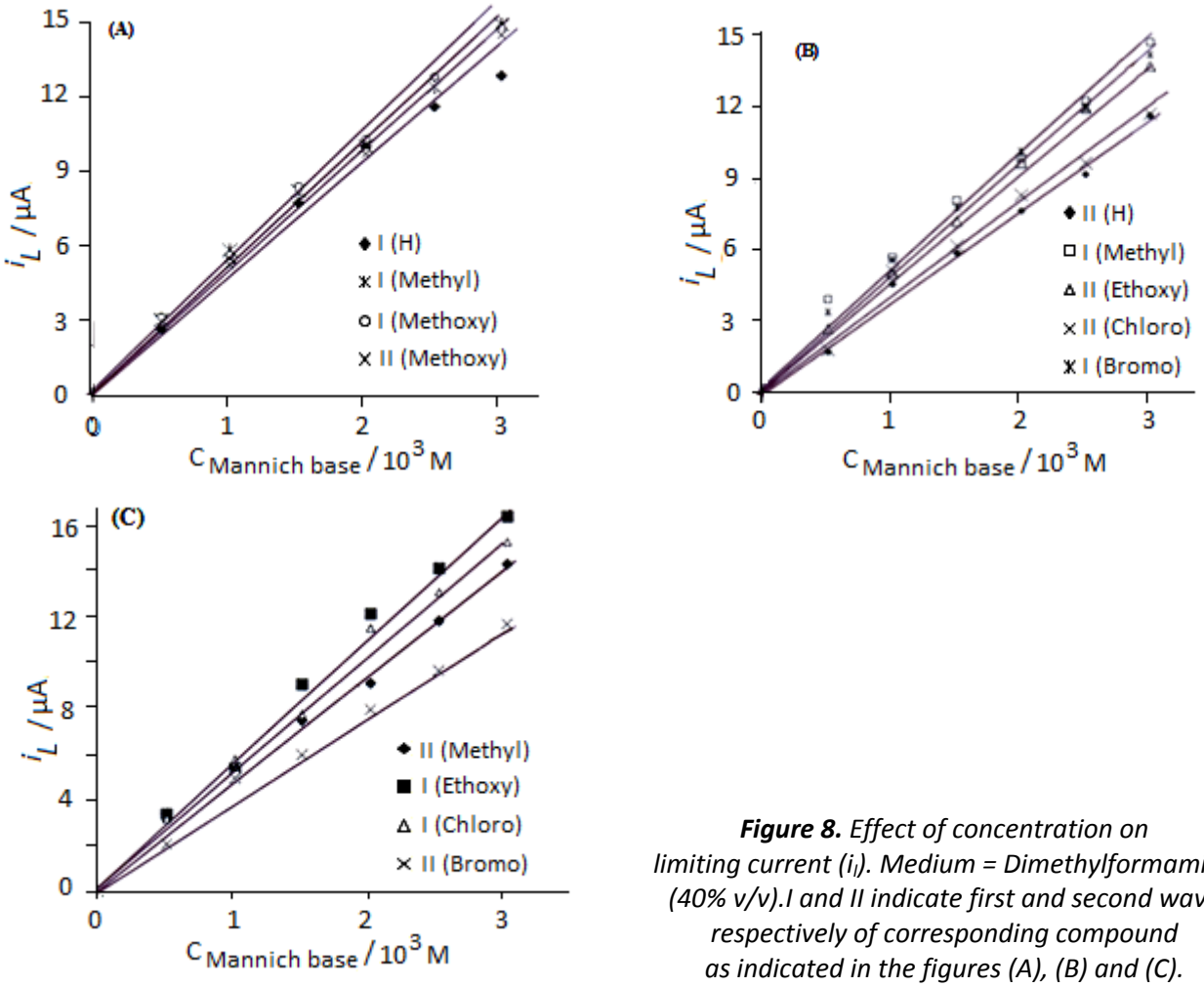


***Figure 8.*** *Effect of concentration on limiting current ($i_l$). Medium = Dimethylformamide (40% v/v).I and II indicate first and second wave respectively of corresponding compound as indicated in the figures (A), (B) and (C).*

*Nature of the electrode process*

The linear $E_{dme}$ versus log ($i/i_d$-$i$) plots at typical pH 4.1 are shown in Figure 9. The slopes were linear in the range 0.066-0.10 V and were not in agreement with the theoretical values 0.030 V and 0.015 V expected for two electron and four electron reversible reduction process respectively. This indicates the irreversible nature of reduction process. The irreversible nature of the polarographic waves was further confirmed by employing Tome's criteria [26]. The $\alpha_{na}$ values are presented in Table 1 in Supplementary material. The irreversible nature of the two waves was attributed to the bulky group present at the end of >C=N-NH-linkage [27].

*Nature of the electrode process*

The linear $E_{dme}$ versus log ($i/i_d$-$i$) plots at typical pH 4.1 are shown in Figure 9. The slopes were linear in the range 0.066-0.10 V and were not in agreement with the theoretical values 0.030 V and 0.015 V expected for two electron and four electron reversible reduction process respectively. This indicates the irreversible nature of reduction process. The irreversible nature of the polarographic waves was further confirmed by employing Tome's criteria [26]. The $\alpha_{na}$ values are presented in Table 1 in Supplementary material. The irreversible nature of the two waves was attributed to the bulky group present at the end of >C=N-NH-linkage [27].

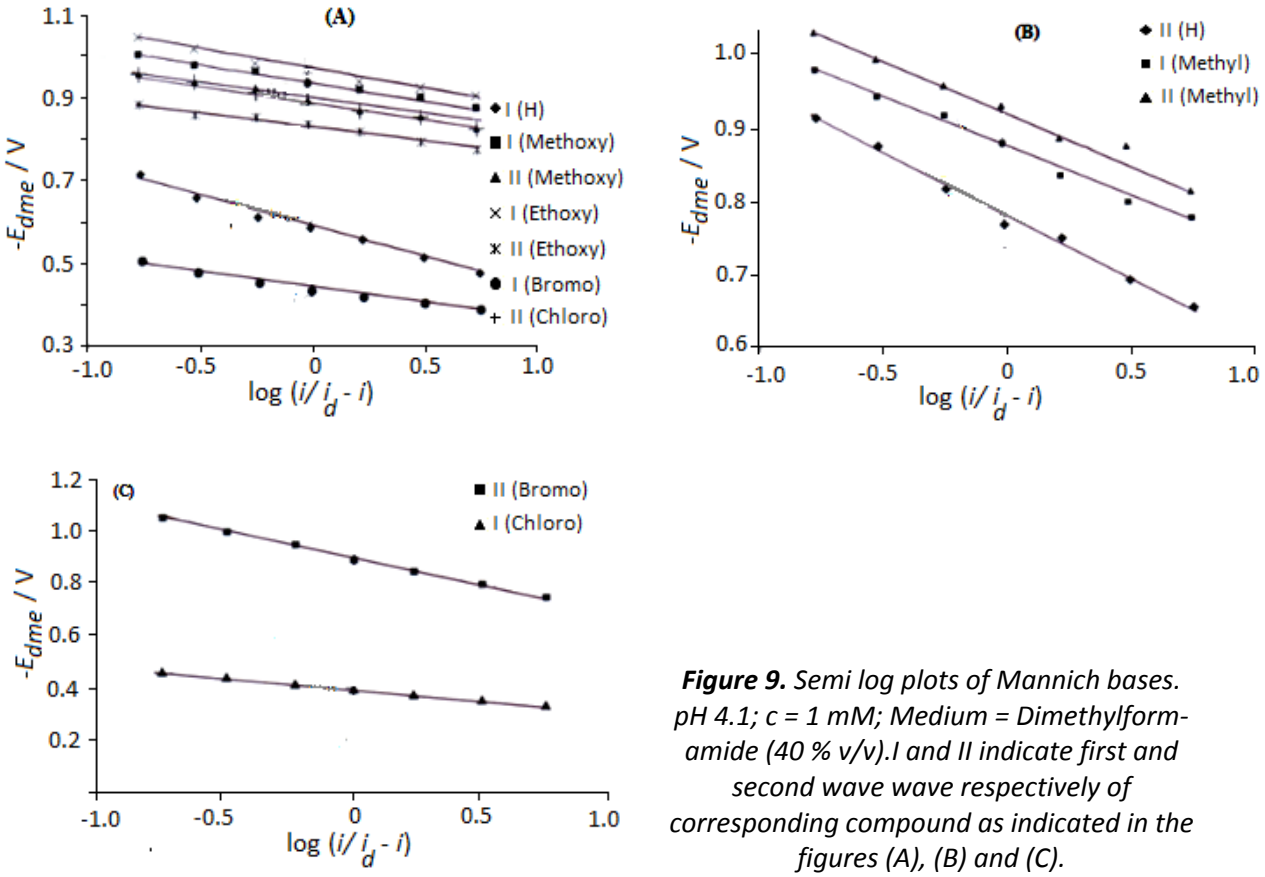


***Figure 9.*** *Semi log plots of Mannich bases. pH 4.1; c = 1 mM; Medium = Dimethylformamide (40 % v/v).I and II indicate first and second wave wave respectively of corresponding compound as indicated in the figures (A), (B) and (C).*

*Kinetic parameters of the electrode reaction*

The kinetic parameters $k^{o}_{fh}$ and $\Delta G^*$ of the electrode reaction at typical pH values evaluated for first and second waves are presented in Table 1 in Supplementary material. The magnitude of $k^{o}_{fh}$ decreases and $\Delta G^*$ increases with the increase in pH of the medium. This indicates irreversible nature of the electrode process [28].

*Controlled potential electrolysis*

The electrochemical reduction of {4-[3-methyl-5-oxo-4-(4$^{I}$-substituted phenyl hydrazono)-4,5--dihydro-pyrazol-1-yl]-phenoxy}-acetic acid (2-oxo-1-piperidine-1-ylmethyl-1,2-dihydro–indol-3--ylidene)-hydrazide (V) has been studied by the method of controlled potential electrolysis at pH 4.1.

Controlled potential electrolysis was carried out in a Lingane H-type cell. A large pool of mercury at the bottom of the large compartment was used as cathode and a similar pool of mercury at the bottom of smaller compartment served as anode. The cathode compartment contains 10 mL of V (0.01 M), 30 mL of DMF, 20 mL of KCl (1.0 M) and 40 mL of the buffer solution of required pH (4.1). A potential of -1.2 V was applied and maintained at constant potential by the manual control of output from the battery. The electrolysis was followed by recording the decrease in current with time. The number of electrons per molecule was calculated from i-t curves and was found to be 8 [29]. 1 mL of solution was withdrawn from the electrolysis cell to confirm the presence of aniline by standard spot test [30]. Part of the experimental solution was partially evaporated on water bath to half of its volume, allowed to cool to room temperature and was extracted with ether. The ether layer was evaporated under reduced pressure. The yellow crystalline solid obtained was identified to be 2-(5-thioxo- 4,5- dihydro-[1,3,4]-oxadiazole-2--ylmethyl)-2,4-dihydro-pyrazol-3-one 'A' by elemental analysis, TLC, IR, and $^{1}$H NMR spectral data.

Remaining experimental solution was made slightly alkaline and extracted with ethylacetate. The ethylacetate extract was subjected to column chromatography and three compounds were

separated by using benzene-methanol 4:1 (v/v) solvent as an eluent. The compounds B, C and D were found to be aniline, (4-Amino-3-methyl-5-oxo-4,5-dihydro-pyrazol-1-yl)-acetic acid hydrazide and 3-Amino-1--piperidin-1-ylmethyl-1,3-dihydro-indol-2-one respectively.

***Table 8****. Characterization data of 2-(5-thioxo-4,5-dihydro-[1,3,4]-oxadiazole-2-ylmethyl)-2,4-di-hydro-pyrazol-3-one*

| | |
|---|---|
| Mass fraction of element found, % (Calc., %) | C 36.34 (36.36), N 28.31 (28.27), O 16.18 (16.14), S 16.11 (16.18) |
| IR (KBr) Spectral data ($\nu_{max}$ / $cm^{-1}$) | 3126 (oxadiazole NH); 3180 (NH); 1603 (C = N); 1670 (C = O); 1134 (C = S) |
| $^1$H NMR Spectral data ($\delta$ /ppm) | 2.3(s, H, $CH_3$); 5.45 (s, 2H, N – $CH_2$), 14.7 (s, H, thiol-thione tautomeric proton NH), 3.9 & 4.1 ($NH_2$) |
| Mass spectral data: m/e (Relative abundance, %) | 172(77); 171(100); 156(10); 143(33.3); 140(40); 127(47.7); 112(57.7); 100(8.8); 84(13.3); 59(53.3); 57(34.4); 51(28.8); 29(38.8); 27(12.2) |

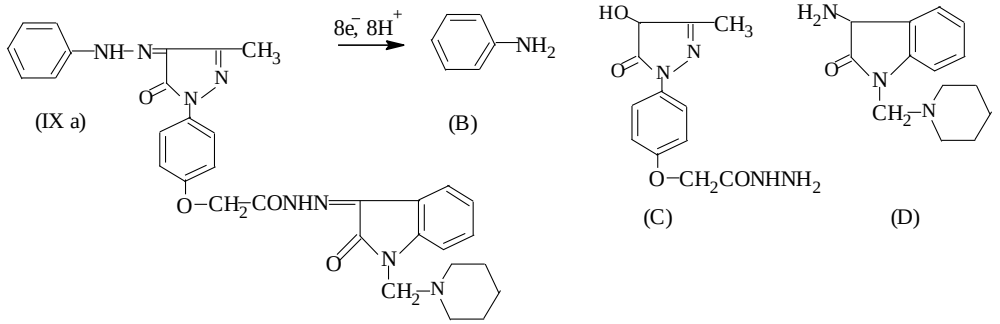


The compounds were characterized by IR and $^1$H NMR data. The compound B was further confirmed as aniline by azodye test.

***Table 9.*** *Elemental analysis and spectral data of B , C and D.*

| Comp. | Mass fraction of element found, % (Calc., %) | IR Spectral data ($\nu_{max}$ / $cm^{-1}$) | $^1$H NMR Spectral data ($\delta$/ ppm) |
|---|---|---|---|
| B | C 77. 31 (77.33), N 15. 13 (15.09) | 3180 (NH), 760 (ArH). | 4.0 (s, 2H, ArNH), 6.46 – 7.01 (m, 5H, ArH) |
| C | C 38. 90 (38.96), N 37.68 (37.78), O 17.45 (17.34) | 1676 (C=O), 1654 (CONH), 2933 ($CH_2$). | 0.9 (s, 3H, $CH_3$), 4.09 (s, 2H, N – $CH_2$), 3.9 & 4.2 (s, 2H, $NH_2$), 6.0 (s, 2H, $CONH_2$). |
| D | C 68.59 (68.51), N 17.21 (17.17), O 6.45 (6.54) | 3180 (NH), 1666 (C = O). | 4.52 (s, 2H, $NCH_2N$), 2.0 (s, 2H, $NH_2$), 2.70 (t, 4H, $NCH_2$), 6.44 (m, 4H, ArH). |

*Reduction mechanism in acidic medium*

Based on the experimental results (Table 10), it was proposed that two azomethine groups in the compounds Va-f were reduced separately involving four electrons. The reduction steps appear as two waves in solutions of pH 1.1-7.1.

It was clear that compounds Va-f were reduced at the dropping mercury electrode through a mechanism which involves the azomethine, imine intermediate and amine via usual sequence.

Hydrazone → Imine → Amine

V was protonated at azomethine group to yield protonated form II. The weak >C=N-NH undergo cleavage at >C=N-NH single bond [31,32] with the uptake of four electrons and two protons to form the unstable imine intermediates IV and V which subsequently undergo two electron reduction to form VI and VII.

It was reported [33,34] that the above mentioned steps of the reduction (formation of VI & VII) occur at the same potential. The mechanism (Scheme 3) proposed was also supported by the results obtained in cyclic voltammetry.

*Reduction mechanism in basic medium*

In alkaline medium (pH>p$K_a$), V exists in the azomethine anionic form (I). The latter in alkaline solutions, was susceptible to chemical cleavage partially into the corresponding carbonyl compounds III, IV and V as shown in the Scheme 4. The first and second waves noticed in alkaline solutions were attributed to the two 4 electron reduction processes of azomethine anionic form to the species containing amino group. The third wave was attributed to the two 2 electron reduction process of heterocyclic carbonyl compounds (IV and V) obtained during the chemical cleavage of dianion I. The heterocyclic carbonyl compounds were reduced to carbinols by two electron reduction process. The decrease in the height of the first and second waves with increase in alkali concentration was attributed to the partial chemical cleavage of dianion.

*Effect of substituents on polarographic behaviour*

It is known that the polarographic reduction of compound depends on the nature of the compound, the position of the substituent and the reaction medium. Heyrovsky [35,36] correlated the polarographic behaviour of a representative number of compounds with their structure. He opined that the the reducibility of given compound is influenced by conjugated double bonds, triple bonds and aromatic rings present in the substrate.

$E_{1/2}$-$\sigma$ plots for the compounds under investigation are presented in Figure 10. The values of specific reaction constant ($\rho$) [38] are presented in Table 11.

***Table 10.*** *Millicoulometric [37] data of {4-[3-methyl-5-oxo-4(4$^{l}$-substituted phenyl hydrazono)-4,5-di -hidro-pyrazole-1-yl)-phenoxy}-acetic acid (2-oxo-1-piperidine-1-ylmethyl-1,2-dihdro-indol-3-ylidene)- -hydrazide at pH 4.1 and 8.1.*

| pH | Current, µA | | | Time, s | | | n value | | |
|---|---|---|---|---|---|---|---|---|---|
| | First wave | Second wave | Third wave | First wave | Second wave | Third wave | First wave | Second wave | Third wave |
| 4.1 | 5.4 | 4.8 | - | - | - | - | - | - | - |
| | 4.4 | 4.0 | - | 7200 | 7200 | - | 3.2 | 3.2 | - |
| 8.1 | 3.4 | 3.2 | - | 10800 | 10800 | - | 3.0 | 3.2 | - |
| | 2.7 | 2.1 | 5.3 | - | - | - | - | - | - |
| | 2.4 | 1.9 | 3.5 | 7200 | 7200 | 7200 | 2.8 | 2.8 | 2.1 |
| | 2.1 | 1.7 | 2.5 | 10800 | 10800 | 10800 | 3.5 | 3.4 | 1.6 |

It was apparent from Table 1 in Supplementary material that the values of $D$, $E_{1/2}$/pH, $\alpha_{na}$ and $I$ (diffusion current constant) were practically in the same range for entire reaction series under study. Thus it was possible to discuss the effect of substituents quantitatively in terms of the Hammett equation [39]. The values of the Hammett substituent constants were taken from the literature [39]. $E_{1/2}$–$\sigma$ plots in media of pH 4.1 and 9.1 for all the compounds under study are shown in Figure 10. The values of specific reaction constant ($\rho$) calculated from the graphs were found to be in the range of 0.15-0.85. The specific reaction constant values are all positive [40,41] (Table 11) and low indicating that the nucleophilic reaction was taking place. This confirms that the electron uptake was the potential rate determining step [42].

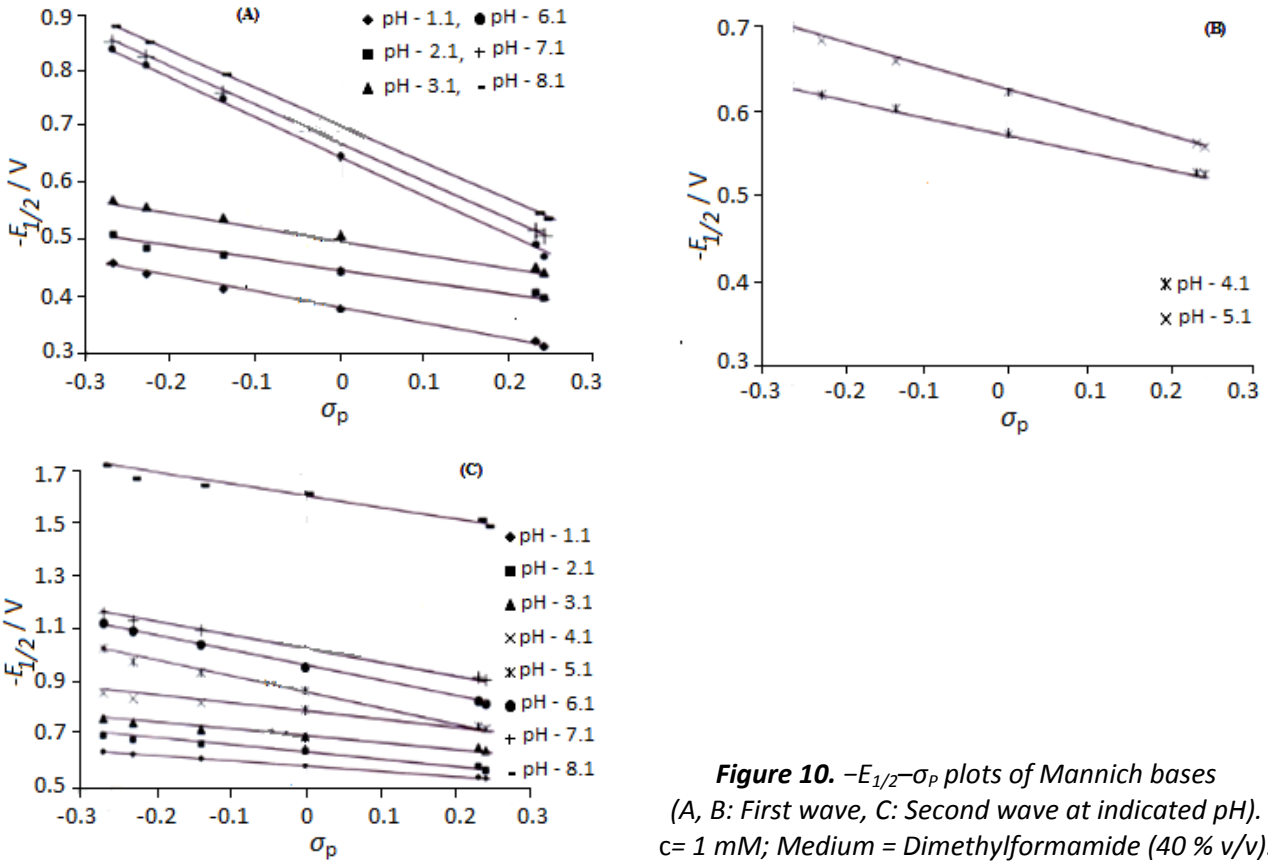


***Figure 10.*** *$-E_{1/2}$–$\sigma_P$ plots of Mannich bases (A, B: First wave, C: Second wave at indicated pH). c= 1 mM; Medium = Dimethylformamide (40 % v/v).*

*Cyclic voltammetric studies of {4-[3-methyl-5-oxo-4(4$^{l}$-substituted phenyl hyarazono)-4,5-dihydro-pyrazol-1-yl]phenoxy}-acetic acid (2-oxo-1-piperidine-1-ylmethyl-1,2-dihydro-indol-3-ylidene)-hydrazide (V a-f) at hanging mercury drop electrode*

The cyclic voltammetric data of compounds Va-f at pH 2.1, 4.1, 6.1, 8.1 and 10.1 are given in Tables 2-7 in Supplementary material. The voltammograms contain two cathodic peaks in acidic solutions and three cathodic peaks in basic solutions at all sweep rates. The cyclicvoltammograms of Va is shown in the Figure 11.

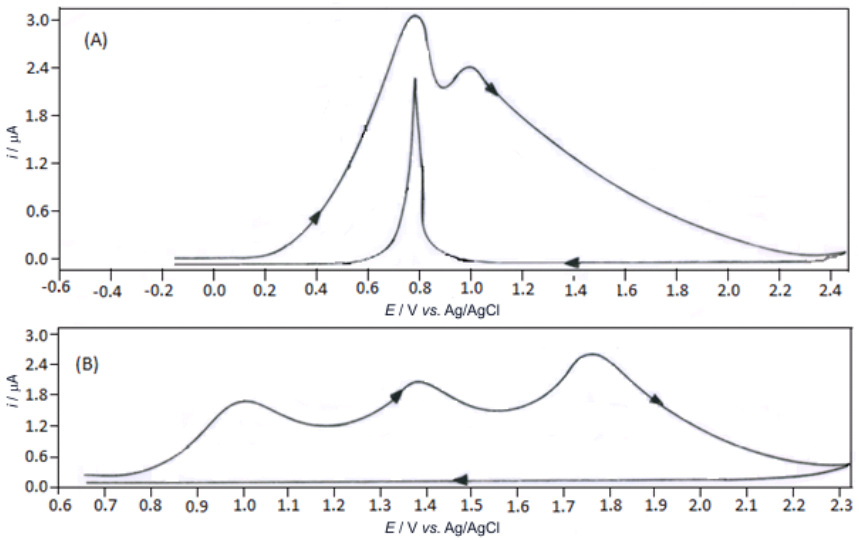


***Figure 11.*** *Cyclic Voltammograms of {4-[3-Methyl-5-oxo-4-(phenyl hydrazono)-4,5-dihydro-pyrazol-1-yl]--phenoxy}-acetic acid (2-oxo-1-piperidine-1-ylmethyl-1,2-dihydro-indol-3-ylidene)-hydrazide; A represents the cyclicvoltammogram at pH 4.1 and B that at pH 8.1.* c *= 1 mM; Medium: Aqueous dimethylformamide (40 % v/v); sweep rate 100 mv/s.*

*Influence of scan rate on peak potential and peak current*

The cathodic peak potentials were shifted to more negative values with the increase in scan rate. The cathodic peak currents increase with the increase in scan rate. The results are shown in Tables 2-7 in Supplementary material.

*Nature of the electrode process*

$i_{pc}$ *vs.* $\gamma^{1/2}$ was a linear plot passing through the origin for the cathodic peaks. This suggests the diffusion controlled nature of the reduction process. This fact was further confirmed by the increase of peak currents with the increase in the concentration of the depolarizer.

The irreversible nature of the electrode process was indicated by following observations.

1. The anodic peak was absent in the reverse scan.
2. The value of ($E_{pc/2}$ – $E_{pc}$) was greater than 56.5/$n$ mV, where $n$ represents number of electronics involved in the corresponding electrode process.
3. The $E_{pc}$ shifted towards more negative potentials with increase in the concentration of the depolarizer.
4. The current function ($i_{pc}/\gamma^{1/2}C$) was independent of scan rate and
5. ($i_{pc}/\gamma^{1/2}$) *vs.* $\upsilon$ graph was similar to the one expected for case II of Nicholson-Shain Criteria [43].

***Table 11.*** *Effect of pH (Britton-Robinson buffers) on the reaction constant for the reduction of {4-(3-methyl-5-oxo-4-(4$^{l}$-substituted phenyl hydrozono)-4,5 dihydro-1-yl]-phenoxy}-acetic acid (2-oxo-1 piperidine – 1- ylmethyl-1,2-dihydro-indol-3-ylidene)-hydrazide.*

| pH | $\rho$ value | |
|---|---|---|
| | First wave | Second wave |
| 1.1 | 0.29 | 0.20 |
| 2.1 | 0.25 | 0.25 |
| 3.1 | 0.25 | 0.25 |
| 4.1 | 0.20 | 0.20 |
| 5.1 | 0.33 | 0.58 |
| 6.1 | 0.66 | 0.66 |
| 7.1 | 0.58 | 0.58 |
| 8.1 | 0.66 | 0.50 |
| 9.1 | 0.66 | 0.50 |
| 10.1 | 0.66 | 0.50 |

*Effect of pH on the peak potential and peak current*

The results presented in ***Tables 2-7*** in Supplementary material show that the cathodic peak potential shifts towards more negative values with the increase in pH of the solution.

The first and the second cathodic peak currents decrease with increase in pH of solutions from 2.1 to 10.1, while peak current corresponding to the third wave noticed in alkaline solutions remains constant. The results were similar to those observed in polarographic studies. Hence the reduction mechanism at HMDE was assumed to be same as that noticed at DME.

Voltammograms recorded in media of pH 4.1 under repeated cycles showed that the peak height decreases with increase of repetition of cycles. However, no significant change was noticed in the shape of the voltammogram. This may be ascribed to the adsorption of the depolarizer on the mercury solution interface.

*Reduction pattern in acidic media*

From the position of the peak on potential axis, it was proposed that first and second cathodic peaks obtained in acidic solutions were due to the reduction of azomethine group to amines. The reduction mechanism is shown in Scheme 3.

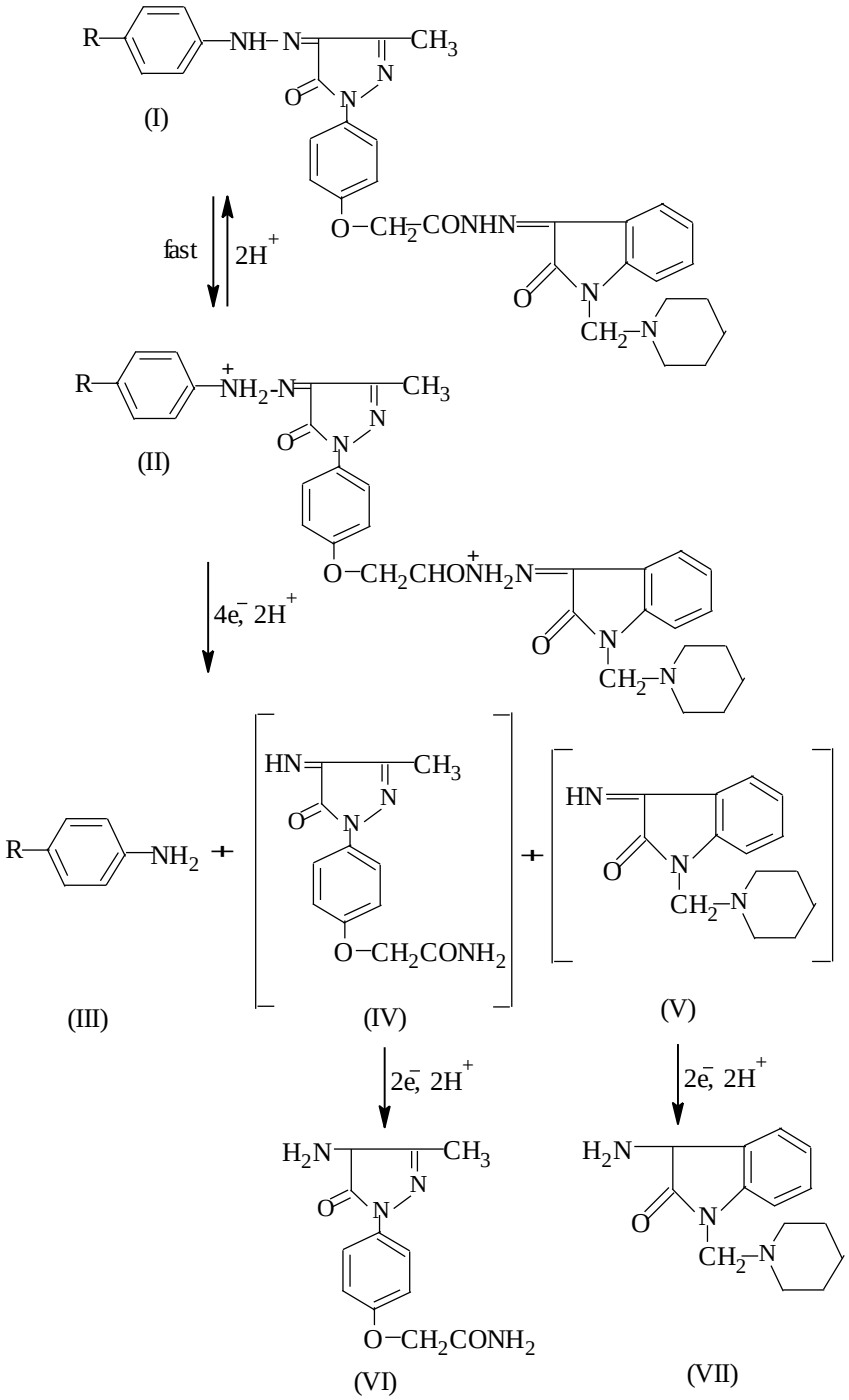


***Scheme 3.*** *Reduction in acidic medium*

*Reduction pattern in alkaline media*

The position of peaks on potential axis in alkaline medium indicates that the first and second peaks were due to two 4-electron reduction processes of azomethine anionic form and third peak was due to reduction of carbonyl group to carbinol. The protons required for the ketone reduction were obtained from aqueous solution (Scheme 4).

*Inverted peaks*

Except in solutions of pH 8.1-10.1 and in 0.1 M NaOH, the compounds of V series exhibit inverted peaks (Figure 11). The inverted peak is a common phenomenon in electrochemical reduction of organic compounds [44-46].

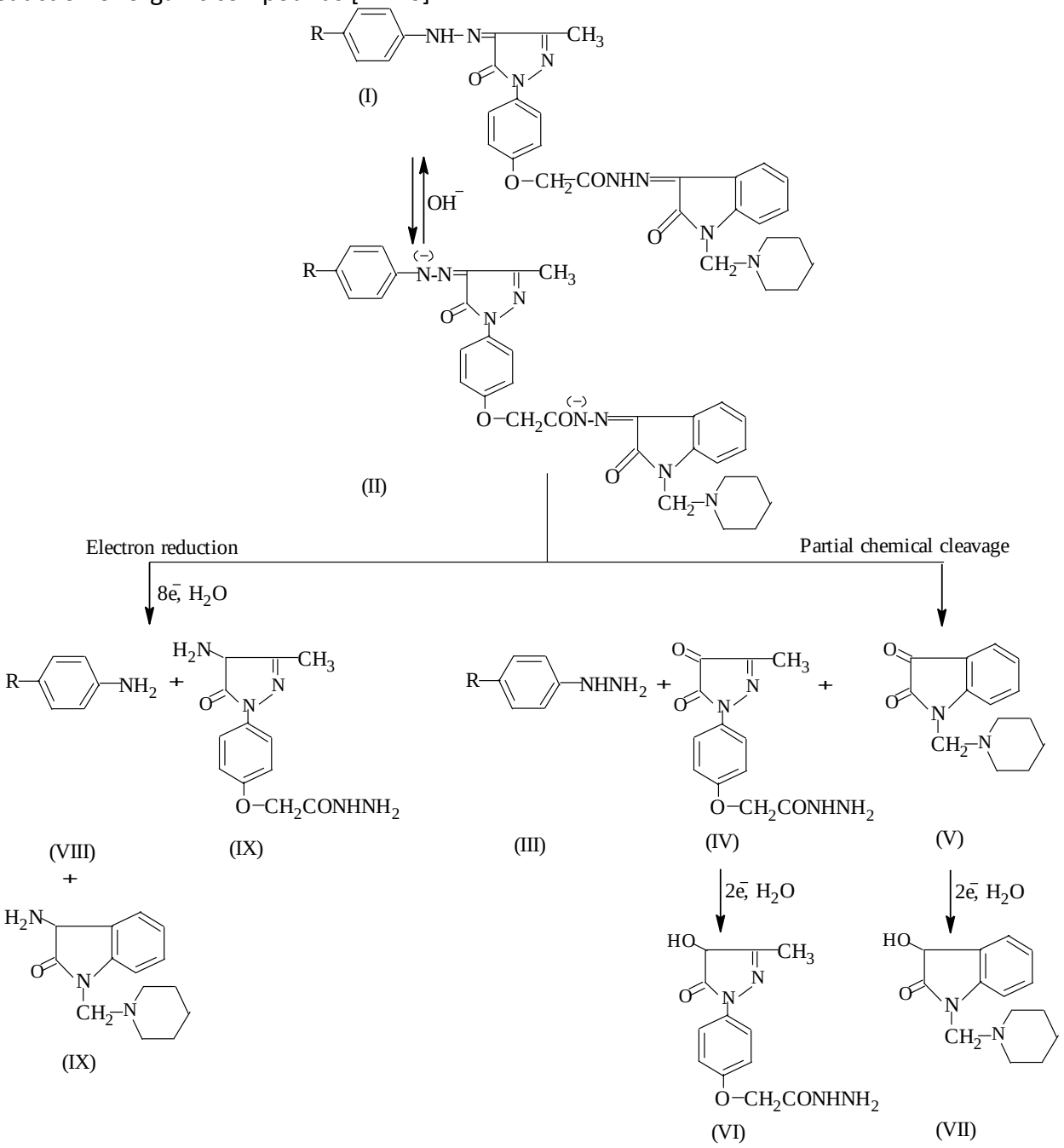


***Scheme 4.*** *Reduction in basic medium*

In present studies, the peak potentials were unaltered at lower sweep rates (10-50 V $s^{-1}$). At higher sweep rates (100-500 V $s^{-1}$), peak current increases with increases in sweep rate. However a cathodic peak during anodic cycle (Inverted peak) was noticed in buffer solutions of pH 2.1-6.10.

Inverted peaks are generally attributed to

- The movement of mercury surface due to uneven drop polarisation. This bears similarity to the explanation of polarographic maximum of the first kind [47-49] or
- the inhibition of electrode reaction as a consequence of coverage of the electrode by a product of the electrode reaction [50-52]

If the peak is attributed to the second possibility, its intensity is expected to increase with decrease in scan rate. Hence the results in the present studies were not attributed to the second possibility. Moreover, a significant polarographic maximum was observed for the compounds under the experimental conditions of study. It is clear therefore that the inverted peak was attributed to the movement of the mercury surface due to uneven drop polarization.

*Effect of substituents on the cyclic voltammetric behaviour of {4-[3- methyl-5-oxo-4(4$^{l}$-substituted phenyl hydrazono)-4,5-dihydro-pyrazol-1-yl]phenoxy}-acetic acid (2-oxo-1-piperidene-1-ylmethyl- 1,2-dihydro indol-3-ylidene)-hydrazide.*

To investigate the influence of the substituent on cathodic peaks corresponding to the azo group reduction, Hammett's linear free energy relations were applied. The plots drawn between the cathodic peak potential and the Hammett's substituent constant were presented in Figure 12. The slope ($\rho$) of the linear plots so obtained was positive and confirms the nucleophilic reduction. The values are presented in Table 12.

***Table 12.*** *Effect of pH on the reaction constant for the reduction of {4-[3-Methyl-5-oxo-4-(4$^{l}$-substituted phenyl hydrazono)-4,5-dihydro-pyrazol-1-yl] phenoxy}-acetic acid (2-oxo-1-piperidine-1-yl methyl)-1.2 di-hydro-indol-3-ylidene)- hydrazide.*

| pH | $\rho$ | |
|---|---|---|
| | I wave | II wave |
| 2.1 | 0.33 | 0.33 |
| 4.1 | 0.25 | 0.25 |
| 6.1 | 0.25 | 0.25 |
| 8.1 | 0.33 | 0.33 |
| 10.1 | 0.33 | 0.33 |

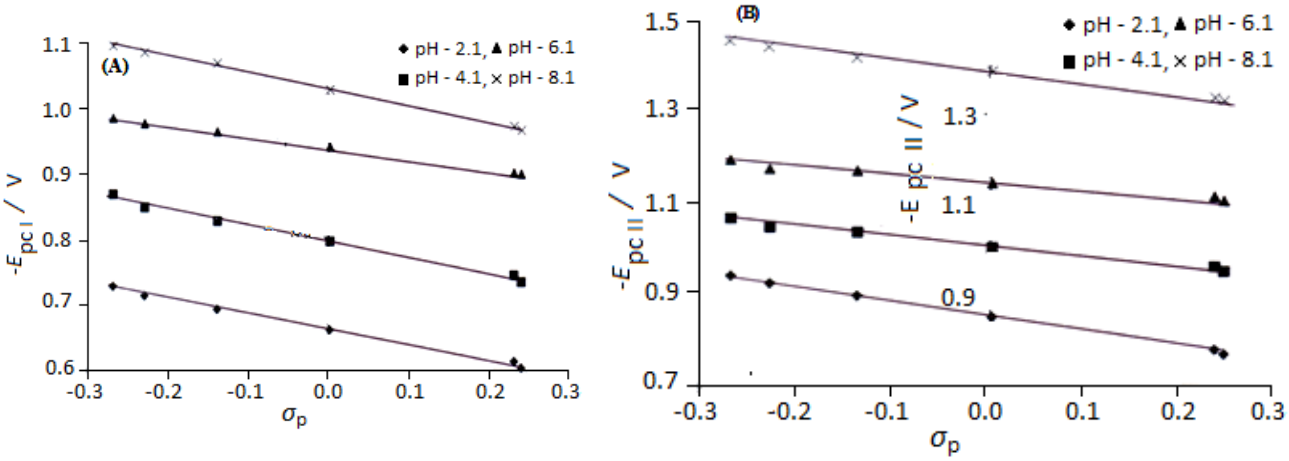


***Figure 12.*** *$-E_{1/2}$–$\sigma_P$ plots of Mannich bases (A: First wave, B: Second wave).* c *= 1 mM; Medium = Dimethylformamide (40% v/v).*

*Cyclic voltammetric studies of {4-[3-methyl-5-oxo-4-(4$^{|}$-substituted phenyl hydrazono)-4,5-dihydro-pyrazol-1-yl]-phenoxy}-acetic acid (2-oxo-1-piperidine-1-ylmethyl-1,2-dihydro–indol-3-ylidene)-hydrazide (Mannich bases V a-f) with a crown–ether modified carbon paste electrode.*

Cyclic voltammetric studies of {4-[3-methyl-5-oxo-4-(4$^{|}$-substituted phenyl hydrazono)-4,5-dihydro-pyrazol-1-yl]-phenoxy}-acetic acid (2-oxo-1-piperidine-1-ylmethyl-1,2-dihydro–indol-3-ylidene)-hydrazide (V a-f) were carried out at modified carbon paste electrode in buffer solutions of pH value 2.1, 4.1, 6.1, 8.1 and 10.1 at different scan rates *i.e.* 10 mV $s^{-1}$, 20 mV $s^{-1}$, and 50 mV $s^{-1}$, 100 mV $s^{-1}$, 200 mV $s^{-1}$, 300 mV $s^{-1}$, 500 mV $s^{-1}$. At all scan rates, the compounds exhibit two well defined cathodic peaks in solutions of pH 2.1-6.1 and three cathodic peaks in alkaline solutions of pH 8.1 - 10.1. An extra anodic peak was noticed in the acidic solutions of pH 2.1 – 6.1.

*Effect of scan rate on peak potential and peak current*

Peak potentials and peak currents change with the change of scan rates. The cathodic peak potentials become more negative and cathodic peak currents increase with increase in scan rate (Tables 2-7 in Supplementary material).

*Effect of pH on peak potentials and peak current*

The cathodic peak potentials were shifted to more negative values with the increase in pH. The peak currents decrease with increase in pH of the medium. The data is given in the Tables 2-7 in Supplementary material.

*Nature of electrode process*

The irreversible nature of electrode process was established by the fact that a plot of $i_{pc}/\upsilon^{1/2}$ versus sweep rate was a straight line parallel to sweep rate axis**.** The irreversible nature of electrode process was confirmed by

- dependence of peak potential on sweep rate,
- the separation of anodic peak and cathodic peak potential ($E_{pa}$–$E_{pc}$ = $\Delta E_p$) was not equal to 60 / *n* mV at 25°C[53], where *n* represents number of electronics involved in the corresponding electrode process.
- the shape of $i_{pc}/\upsilon^{1/2}$ versus $\upsilon$ plot was in accordance with the Nicholson and Shain criteria [43].

The linear plots of $i_{pc}$ versus $\upsilon^{1/2}$ suggest the diffusion controlled nature of the electrode process. This was further supported by the negative shift of peak potential with increase in sweep rate. The plots of $i_{pc}$ *vs* concentration and $i_{pc}$ *vs* $\upsilon^{½}$ fulfil the criteria for the diffusion controlled nature of the electrode process. The plots of Epc *vs* pH were similar to $E_{½}$ *vs.* pH plots and this supports the findings and conclusion drawn from DC polorography.

*Comparison between polarographic studies and cyclic voltammetric studies*

Equal number of polarographic waves and cyclic voltammetric peaks noticed in DC polarographic and cyclic voltammetric studies respectively suggest similar behavior in both the studies. However, an additional anodic peak was noticed in solutions of pH 2.1 – 6.1 may be attributed to oxidation of amine formed in the previous reduction step.

## Conclusions

A series of six novel Mannich bases were synthesized and characterized by IR, $^1$H NMR, mass spectral data and elemental analysis. The compounds under study gave two well defined

polarographic waves in the media pH 1.1-7.1 and three waves in the media pH 8.1-10.1. The results were compared with those obtained in cyclic voltammetry at hanging mercury drop electrode and modified carbon paste electrode. The mechanism for the reduction process in acidic as well as basic medium is proposed.

**References**


[1] H. S. El-Kashef, M. A. Abd-Alla, B. E. Bayoumi, A. A. M. El-Timawy, *J. Chem. Tech. Biotech.* **33** (1983) 294-298.

[2] K. Guckian, M.B. Carter, E. Y. Lin, M. Choi, L. Sun, P. A. Boriack-Sjodin, C. Chuaqui, B. Lane, K. Cheung, L. Ling, W. C. Lee, *Bioorg. Med. Chem. Lett*. **20** (2010) 326-329.

[3] P. Manojkumar, T. K. Ravi, S. Gopalakrishnan, *Eur. J.Med. Chem.* **44** (2009) 4690-4694.

[4] J. P. Raval, A. B. Shah, N. H. Patel, H. V. Patel, P. S. Patel, K. K. Bhatt, K. R. Desai, *Eur. J. Chem* **2** (2011) 238-242.

[5] X. Fan, X. Zhang, L. Zhou, K.A. Keith, E. R. Kernb, P. F. Torrencea, *Bioorg. Med. Chem. Lett.* **16** (2006) 3224-3228.

[6] R. Robinson, *J. Chem. Soc*. **111** (1917) 762-768.

[7] E. J. Corey, R. D. Balanson, *J. Am. Chem. Soc.* **96** (1974) 6516-6517.

[8] S. D. Knight, L .E. Overman, G. Pairaudeau, *J. Am. Chem. Soc.* **115** (1993) 9293-9294.

[9] S. Joshi, A. D. Manikpuri, P. Tiwari, *Bioorg. Med. Chem. Lett.* **17** (2007) 645-648.

[10] S. Joshi, N. Khosla, P. Tiwari, *Bioorg. Med. Chem. Lett.* **12** (2004) 571-576.

[11] B. Shivarama Holla, BS. Sreenivasa, B. Kalluraya, *Boll. Chim. Farm.* **133** (1994) 527-531.

[12] T. B. Shah, A. Gupta, M. R. Patel, V. S. Chaudhari, H. Patel, V. C. Patel, *Ind. J. Chem. B* **48B** (2009) 88-96.

[13] A. Tambo-ong, S. Chopra, B. T. Glasar, K. Matsuyama, T. Tran, P. B. Madrid, *Bioorg. Med. Chem. Lett.* **21** (2011) 5697-5700.

[14] G. Q. Hu, L. L. Hou, S. Q. Xie, W. L. Huang, H. B. Zhang, *Yao Xue Xue Bao* **43** (2008) 926-929.

[15] M. A. La-Scalea, C. M. de Souza Menezes, M. S. da Silva Juliao, M. C. Chung, S. H. Pires Serrano, E. I. Ferreira, *J. Braz. Chem. Soc.* **16** (2005) 774-782.

[16] D. I. Edwards, Comprehensive Medicinal Chemistry. The Rational Design, Mechanistic Study & Therapeutic Application of Chemical Compounds, Pergamon Press, Oxford, 1990, 546-554.

[17] C. Viode, C. De Albuquerque, G. Chauviere, C. Houée-Levin, J. Perie, *New J. Chem.* **21** (1997) 1331-1338.

[18] A. Guissani, Y. Henry, N. Lougmani, B. Hickel, *Free Rad. Biol. Med.* **8** (1990) 173-189.

[19] J. Rozenski, C.J. De Ranter, H. Verplanken, *Quant. Struct-Act. Rel.* **14** (1995) 134-141.

[20] H. Cerecetto, R. Di Maio, M. González, M. Risso, G.Sagrera, G. Seoane, A. Denicola, G. Peluffo, C. Quijano, A. O. M. Stoppani, M. Paulino, C. Olea-Azar, M. A. Basombrio, *Eur. J. Med. Chem*. **35** (2000) 343-350.

[21] K. R. Kumar, A. R. G. Prasad, V. Srilalitha, G. N. Swamy, L.K. Ravindranath, *Sci. Iran. Trans. C* **19** (2012) 605-618.

[22] K. R. Kumar, A. R. G. Prasad, V. Srilalitha, G. N. Swamy, L.K. Ravindranath, *Ovidius University Annals of Chemistry* **23** (2012) 5-20.

[23] L. K. Ravindranath, K. Srikanth, M. Dastagiri Reddy, S. D. Ishrath Begum, *Orient. J. Chem.* 25 (2009) 993-998.

[24] C. S. Marvel, G. S. Heirs, *Organic Synthesis, Vol. I*, John Wiley and Sons, New York, 1941, p. 342.

[25] J.W. Ross, R.D.Demars, I. Shain. *Anal. Chem.* **28** (1956) 1768-1772.

[26] J. Tomes, *Coll. Czech. Chem. Commun*. **9** (1937) 12-18.

[27] W. V. Malik, R. N. Goyal, R. Jain, *J. Electroanal. Chem.* **87** (1978) 129-135.

[28] K. R. Kumar, A. R.G. Prasad, V. Srilalitha, G. N.Swamy, L.K. Ravindranath, *Rev. Colomb. Quim*. **40** (2011) 165-184.
[29] J.J. Lingane, *J. Am. Chem. Soc.* **67** (1945) 1916-1922.
[30] F. Feigl, *Spot Test, Vol. II*, Elsevier, Amsterdam, 1954, 231.
[31] R. N. Adams, Electrochemistry *at Solid Electrodes*, Marce Dekkar Inc., New York, 1969, 332.
[32] R. N. Adams, *Anal. Chem.* **30** (1958) 1576-1576.
[33] Saul Patai, *The chemistry of hydrazo, azo and azoxy* groups (Part – I), John Wiley and Sons, Interscience Publications, London, 1975, 389.
[34] P. Zuman, *Topics in Organic Polarography,* Plenum Press, New York, 1970, 231.
[35] J. Heyrovsky, A polarographic study of the electrokinetic phenomena of adsorption, electro-reduction and overpotential displayed at the dropping mercury cathode, Hermann, Paris, 1934, 448. (Actualités Scientifiques et Industrielles, No. 90: Réunion Internationale de Chimie-Physique, 1933, No. 10)
[36] J. Heyrovsky, *Polarography*, Springer Verlag, Wien, 1941, 239.
[37] T. De Vries, J. L. Kroon*, J. Am. Chem. Soc.* **75** (1953) 2484-2486.
[38] A. R.G. Prasad, V. Seshagiri, L.K. Ravindranath, *Jordan J. Chem.* **6** (2011) 51-64.
[39] L. B. Hammett, *Physical Organic Chemistry*, McGraw-Hill, New York, 1940, 787.
[40] H. H. Jaffe, *Chem. Rev.* **53** (1953) 191-261.
[41] P. Zuman, *Substituent effects in Polarography*, Plenum Press: New York, 1976, 213.
[42] L. K. Ravindranath, S. R. Ramadas, S. Brahmaji Rao, *Electrochim. Acta* **28** (1983) 601-603.
[43] R. S. Nicholson, I. Shain, *Anal. Chem.* **36** (1964) 706-723.
[44] B. J. H. Wang, K .L. Lee. *J. App. Electrochem*. **26** (1996) 153-159.
[45] P. Krtil, L. Kavan, I. Moskovcova, K. Kratochvicova, *J. Appl. Electrochem.* **26** (1996) 523-527.
[46] M. Neol, C. Ravichandran, P. N. Anantharaman, *J. Appl. Electrochem.* **25** (1995) 690-698.
[47] P. Delahay, *New Instrumental Methods in Electrochemistry*, Interscience Publishers Inc., New York, 1966, 389.
[48] M. Pourobaix, *Atlass of Electrochemical Equilibrie in Aqueous Solutions*, Pergamon Press, New York, 1966, 571.
[49] R. S. Nicholson, I. Shain, *Anal. Chem.* **36** (1964) 706-723.
[50] D. A. Tyssee, M.M. Baizer. *J. Electrochem. Soc.* **118** (1971) 1420-1425.
[51] P. Tissot, P. Margaretha, *Electrochim. Acta* **23** (1978) 1049-1052.
[52] K. S. V. Santhanam, A. J. Bard, *J. Am. Chem. Soc.* **88** (1966) 2669-2675.
[53] P. Vanysek, *Electrochim. Acta* **40** (1995) 2841-2847.

*J. Electrochem. Sci. Eng*. **3(2)** (2013) 81-89; doi: **10.5599/jese.2013.0031**

**Open Access : : ISSN 1847-9286**
***www.jESE-online.org***

*Original scientific paper*

# Electrochemical determination of an antitumour platinum(IV) complex: trans-[$PtCl_2(OH)_2$(dimethylamine)(isopropylamine)]. Application to biological samples

CARMEN S. HERNANDEZ DOMÍNGUEZ✉ and PEDRO HERNÁNDEZ

*Departamento de Química Analítica y Análisis Instrumental, Facultad de Ciencias, Universidad Autónoma de Madrid, Cantoblanco, 28029 Madrid, Spain*

✉ Corresponding Author: E-mail: carmen.hernandez.dominguez@gmail.com; Tel: +34 914974988; fax: +34 914974931

Received: November 4, 2012; Revised: February 22, 2013; Published: April 19, 2013

***Abstract***

*A differential pulse voltammetry (DPV) method has been applied for the first time for determination of trans-Pt[$Cl_2(OH)_2$(dimethylamine)(isopropylamine)]. To this end, all chemical and instrumental variables affecting the determination of trans-Pt[$Cl_2(OH)_2$(dimethylamine)(isopropylamine)] were optimized. From studies of the mechanisms governing the electrochemical response of trans-Pt[$Cl_2(OH)_2$(dimethylamine)(isopropylamine)], it was concluded that it is an electrochemically irreversible system with a reduction under diffusion control, with a reduction potential of -425 mV. Under optimal conditions, the variation in the analytical signal ($I_p$) with trans-Pt[$Cl_2(OH)_2$(dimethylamine)(isopropylamine)] concentration is linear in the 0.8 µg $mL^{-1}$ to 20 µg $mL^{-1}$ range, with an LOD of 97 ng $mL^{-1}$ and a LOQ of 323 ng $mL^{-1}$, RSD = 1.58 % and $E_r$ = 0.83 %. The optimized method was applied to the determination of trans-Pt[$Cl_2(OH)_2$(dimethylamine)(isopropylamine)] in biological fluids, human urine and synthetic urine.*

**Keywords**

*trans*-Pt[$Cl_2(OH)_2$(dimethylamine)(isopropylamine)]; differential pulse voltammetry; biological fluids; human urine.

## 1. Introduction

The use of *cis*-diamminedichloroplatinum(II), known as cisplatin or *cis*-DDP, in cancer chemotherapy has made a major impact on the observed response rates of some tumour types, such as testicular or ovarian carcinoma [1]. However, cisplatin has two major drawbacks: 1) severe toxicity that includes nephrotoxicity, neurotoxicity and ototoxicity and 2) the acquisition or presence of resistance to the drug [2]. Because tumour resistance to cisplatin limits its efficacy,

there is an urgent need to discover new platinum complexes capable of overcoming cisplatin resistance.

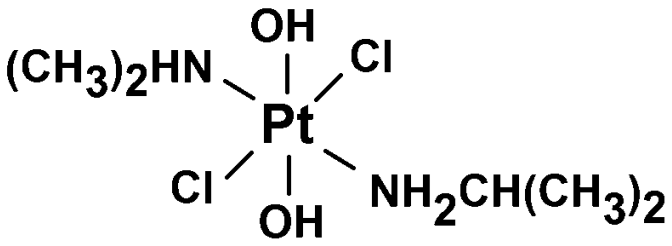


***Figure 1.*** *Structure and molecular weight of the platinum complex, trans-Pt[$Cl_2$($OH)_2$(dimethylamine)(isopropylamine)] (compound 1), used in this article*

Because enhanced removal of cisplatin-DNA adducts has been reported as one of the main causes of cell resistance to cisplatin, there is general consensus that this particular resistance mechanism may be circumvented by platinum complexes that bind to DNA by a different mechanism than cisplatin [3,4]. One platinum compound that possesses DNA-binding properties distinct from those of cisplatin is its *trans* isomer transplatin, *trans*-diamminedichloroplatinum(II), or *trans*-DDP (Fig. 1). In fact, it has been found that *cis*-DDP mainly forms 1,2 intrastrand cross-links on DNA, whereas the main adducts of *trans*-DDP are 1,3 intrastrand cross-links [2]. Unfortunately, early structure-activity relationship studies showed that *trans*-DDP and other *trans*-Pt complexes were inactive as antitumour drugs [5]. However, in 1989, Farrell *et al*. [6] reported the first cytostatic *trans*-Pt(II) complexes. In recent years, several classes of biologically active *trans*-platinum complexes have been reported [7]. Among these unusual classes of platinum drugs, it has recently been found that *trans*-Pt(II)$Cl_2$ complexed with an asymmetric set of aliphatic amines is able to circumvent cisplatin resistance. It is known that resistance to cisplatin is multifactorial and includes three main mechanisms: decreased cellular accumulation of cisplatin, increased cytoplasmatic detoxification (through increased cytoplasmic levels of glutathione and metallothioneins), and increased DNA repair/tolerance of platinum-DNA adducts[8]. It has also been postulated that alterations in the apoptotic cell death pathway may constitute a fourth mechanism of cisplatin resistance[9].

The group of Carmen Navarro-Ranninger [10] has reported that the *trans*-platinum(II) complex with mixed aliphatic amines, *trans*-Pt[$Cl_2$($OH)_2$(dimethylamine)(isopropylamine)] (Fig.1) circumvents cisplatin resistance in cells that overexpress oncogenes. In addition, compound **1** is also able to circumvent resistance to cisplatin in A2780*cis*R ovarian tumour cells, which exhibit resistance through a combination of the three mechanisms mentioned above [11]. Moreover, they observed that circumvention of cisplatin resistance by compound **1** is associated with a higher level of apoptosis induction relative to *cis*-DDP [12,13]. Also of interest was the observation that in A2780*cis*R cells there is a correlation between the DNA interstrand cross-linking efficiency of compound **1** and its ability to induce apoptosis [13].

On these grounds, Navarro-Ranninger *et al*. [10] reported the cytotoxic activity of the *trans*-Pt[$Cl_2$($OH)_2$(Dimethylamine)(isopropylamine)] (TPt complex) (Fig. 1) in pairs of cisplatin-sensitive and-resistant human ovarian tumour cell lines. The resistant cell lines showed acquired resistance to cisplatin and were selected with regard to the three major mechanisms of resistance to the drug. In addition, these cell lines have been used previously to identify novel platinum complexes capable of circumventing cisplatin resistance [14-16]. Because cellular and molecular pharmacology studies are essential to understanding the relationships between structure and

anticancer properties, Navarro-Ranninger *et al.* [10] have compared the cellular accumulation, DNA binding, interstrand cross-linking efficiency, apoptosis induction, and binding to serum albumin and plasma proteins of the *trans*-Pt(IV) complex (compound **1**) with that of its corresponding *trans*-Pt(II) analog. Finally, the in vivo antitumour activity of compound **1** has been evaluated in mice bearing tumour xenografts. In this article, a new electrochemical method to determine TPt complex in biological fluids is developed.

This paper makes a study of the electrochemical behaviour of this compound by differential pulse voltammetry (DPV) aimed at obtaining the optimal conditions for its determination in biological fluids and establishing its formation constants.

The analysis of biological fluids presents a special relevance because small changes in the concentration of its components are thought to be correlated with several neurological or metabolic disorders [14].

## 2. Experimental

**Reagents:** TPt complex [10] was provided by Carmen Navarro-Ranninger. The purity of the analyte was 98 %. This high purity is because the complex of platinum(IV) was a synthetic product, provided by the group of Navarro-Ranninger

Triple distilled mercury was used as working electrode. Buffer solutions prepared with acetic acid, phosphoric acid and borate were adjusted to the desired pH values with sodium hydroxide. Unless otherwise stated, all other reagents were of analytical grade and were used as received. Ultrapure water, obtained from Millipore MilliQ System, was used in the preparation of buffers and solutions and to clean the working electrode of possible substances adsorbed on the gold electrode surface. All solutions were prepared just prior to use, preserved at 4 °C and protected from light.

**Apparatus:** Electrochemical measurements were performed using a Bioanalytical System (BAS) Epsilon Mercury Stand workstation, an Ag/AgCl/KCl 3M reference electrode, and a platinum wire as counter electrode. For pH adjustment, a pH-meter Methrom C831 was employed as well as a circulation ultrathermostat Frigiterm-10 (P-Selecta, Spain) to control the temperature.

**Procedure:** TPt complex stock solution (500 μg $mL^{-1}$) was prepared with ultrapure water and stored at 4±1 °C preserved in aluminium foil covered bottles to avoid photodegradation. Prior to analysis, sample bottles were allowed to equilibrate to room temperature (RT).

**Sample preparation:** The TPt complex dissolved readily and was further diluted to desired concentrations using 0.5 M acetate buffer solution.

The samples used for the implementation of the method described above included a synthetic urine sample prepared in the laboratory and a sample of real human urine.

The composition of the synthetic urine is presented in Table 1 [17].

***Table 1.*** *Synthetic urine composition*

| | NaCl | KCl | $CaCO_3$ | $MgCl_2.6H_2O$ | $H_2SO_4$ (98 %) | HCl (conc) | $NH_4H_2PO_4$ |
|---|---|---|---|---|---|---|---|
| *c* | 5.08 g $L^{-1}$ | 2.86 g $L^{-1}$ | 0.31 g $L^{-1}$ | 0.42 g $L^{-1}$ | 0.67 mL $L^{-1}$ | 8.7 mL $L^{-1}$ | 3.09 g $L^{-1}$ |

Processing of the human urine sample consisted of:

1) doping of the sample with an aliquot of TPt complex (10 μg $mL^{-1}$). This value was chosen because, at this time, there are no published references devoted to the use of these compounds in humans;

2) protein precipitation with 0.1 M $HClO_4^-$;
3) digestion of the precipitate for a weekend (48 hours);
4) filtering of the sample. The filters used in the development of this process were cellulose membrane filters with a pore size of 0.45 μm and
5) adjust the pH of the sample to the appropriate value.

## 3. Results and discussion

The electrochemical study of the TPt complex was performed by DPV and square wave voltammetry in order to determine the best conditions for its analysis.

### *3. 1. Influence of pH and ionic strength.*

In order to select the optimum pH, a pH range between pH 2 and pH 12 was employed. The buffers used were phosphate buffer for pH 2, 3, 6, 7, 8, 10, 11 and 12; acetic acid buffer for pH 4 and 5; and borate buffer for pH 9. The concentration of all the buffers was 0.5 M.

In Figure 2 the variation in peak intensity with respect to pH (Fig. 2a) and the variation in peak potential versus pH (Fig. 2b) are represented. This figure shows that the greatest intensity was reached at pH 4 (Fig. 2a). By representing the variation in peak potential with respect to pH (Fig 2b) three straight segments with clear variations in slope are apparent, indicating that the compound under study has two dissociation constants, which correspond to the values of $K_1 = 10^{-4.2}$, $K_2 = 10^{-7.7}$. This fact can be corroborated by observing the slopes in the $E_p$ *vs.* pH graph (Fig. 2b)

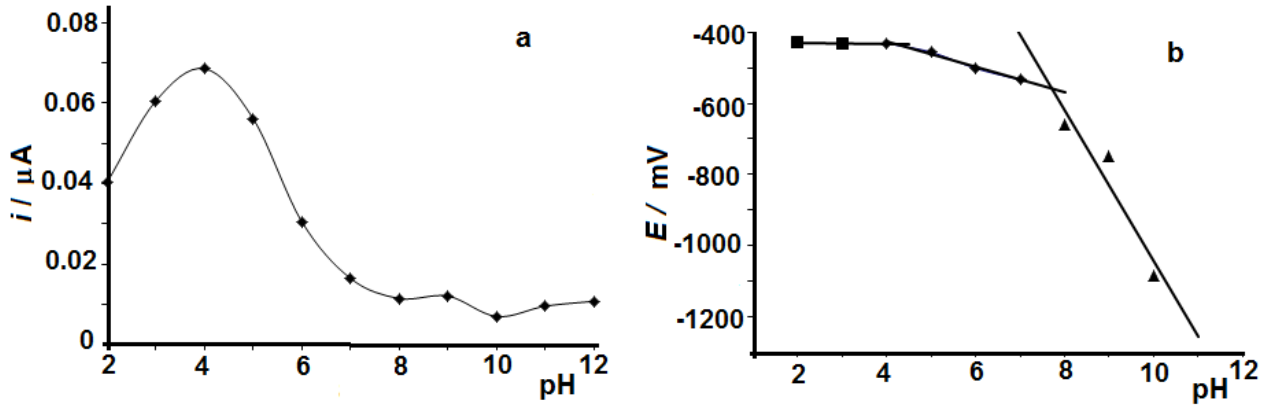


***Figure 2.*** *a) Variation in DPV peak intensity at different pH values. b) Variation in peak potentials. Dissociation constants were calculated from the variations in the slopes. Measurement conditions: ionic strength = 0.05 M; TPt complex concentration = 5 μg mL$^{-1}$; pulse amplitude = 50 mV; scan rate = 10 mV s$^{-1}$*

$E_p$ = -2pH - 426; $r^2$ = 1 (1)

$E_p$ = -35.2 pH - 287.4; $r^2$ = 0.995 (2)

$E_p$ = -211.5 pH + 1072.5; $r^2$ = 0.992 (3)

From the standpoint of electrochemistry, pH 4 was chosen for further study because it is the value that provided the greater intensity.

The ionic strength necessary to achieve the greatest possible sensitivity in the electrochemical reaction was also studied. For this study we used solutions of acetic acid-acetate buffer (pH 4) in the concentration range between $5\times10^{-2}$ and 2.0 M, and reached a maximum intensity at $5\times10^{-2}$ M. This concentration was used for further studies.

*3. 2. Instrumental variables*

Once the study of the chemical variables was completed, we proceeded to the optimization of instrumental variables, both by DPV and square wave voltammetry (SWV). In both techniques the values of pH 4 and ionic strength $5\times10^{-2}$ M, determined above, and the analyte concentration of 10 µg $mL^{-1}$ were kept constant.

3. 2. 1. Influence of pulse amplitude

By changing this variable using differential pulse voltammetry, it appeared that the peak current increased linearly according to the equation:

$$i = 0.0015\ \Delta E + 0.0003 \quad (4)$$

using a scan rate of 10 mV $s^{-1}$ throughout the study.

However, at the same time, the width of the half peak increased, so it was necessary to compromise between sensitivity and selectivity. This occurred at a value of pulse amplitude 50 mV.

The peak potential was modified according to the equation:

$$E_p = 0.4338\ \Delta E - 466.88 \quad (5)$$

To calculate the number of electrons exchanged during the reduction a DC voltammetry was carried out, and compared with the findings obtained with DPV (Figure 3).

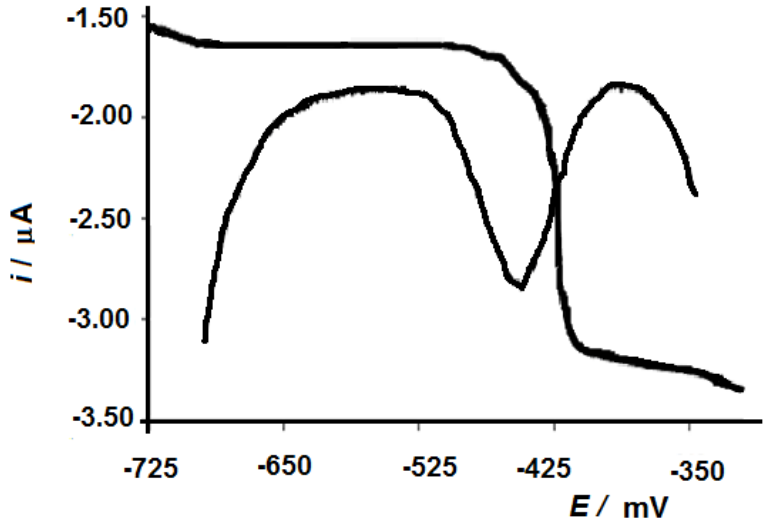


***Figure 3.*** *Comparison of DC and DP polarograms. Measurement conditions: pH 4; ionic strength = 0.05 M; TPt complex concentration = 5 µg $mL^{-1}$; scan rate = 10 mV $s^{-1}$*

The number of electrons exchanged was found to be two using the following equation [18]:

$$E_p = E_{1/2} \pm \Delta E/ne \quad (6)$$

where $E_p$ is the peak potential calculated at pH 4 in DPV, $E_{1/2}$ is the potential calculated from DC voltammetry and $\Delta E$ is the pulse applied, at a peak potential of -426 mV and -409 mV half-wave.

Therefore, the reduction process can be written as:

$$Pt(IV) + 2e^- \Leftrightarrow Pt(II) \quad (7)$$

The square-wave behaviour is similar to that observed with DPV, the peak current increasing linearly with pulse amplitude according to the equation:

$$I = 0.0035\ \Delta E + 0.32 \quad (8)$$

at a frequency of 25 Hz and a step of 2 mV, which promotes an effective scan rate of 50 mV $s^{-1}$.

When performing these studies by using square wave voltammetry it is presented the same situation of commitment that in differential pulse voltammetry, in other words, by increasing the amplitude of pulses produces a substantial increase in the half-peak width

The variation in peak potential follows the equation

$$E_p = 0.85\ \Delta E - 457.02 \quad (9)$$

3. 2. 2. Influence of scan rate

As in previous studies, the pH, ionic strength and analyte concentration (10 µg $mL^{-1}$) were held constant.

When the scan rate was modified at DPV and the pulse amplitude remained constant ($\Delta E$ = 50 mV), the variation in peak current was linear with scan rate according the equation:

$$i = 0.0058\ v^{0.5} + 0.32 \quad (10)$$

However, the peak potential does not remain constant, indicating that the electrochemical reduction is an irreversible process controlled by diffusion.

A study of this variable in SWV was carried out by changing the frequency and step, but at a constant pulse amplitude ($\Delta E$ = 50 mV). The results were that in modifying the frequency and the step, the peak intensity followed a linear trend fitting the square root of each of the two variables. In addition, the peak potential shifts as well, indicating that the reduction process is irreversible and under diffusion control.

As in previous studies, half-peak width increases, selecting as the most appropriate conditions a frequency of 50 Hz and 2 mV step, representing a scan rate of 100 mV $s^{-1}$.

The results obtained (Fig. 4) are consistent with those found earlier; the peak intensity fits linearly to the square root of the scan rate by:

$$i = 0.012\ v^{0.5} + 0.12 \quad (11)$$

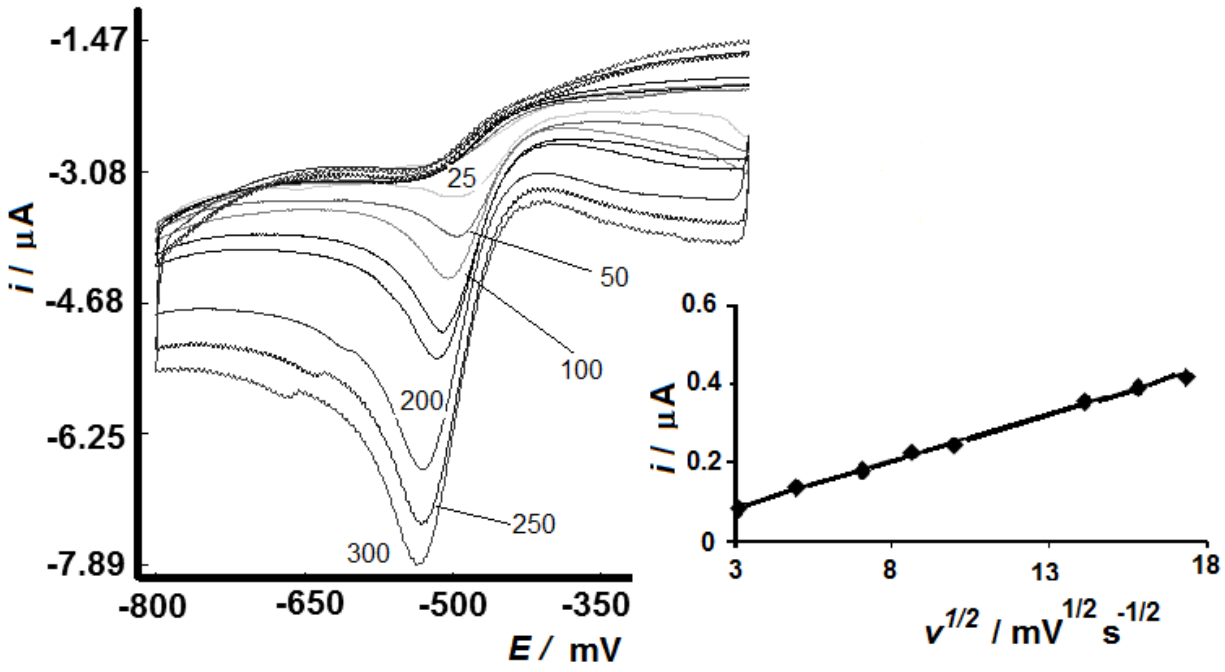


***Figure 4.*** *Cyclic voltammograms obtained at different scan rates. Measurement conditions: pH 4; ionic strength = 0.05 M; TPt complex concentration = 5 µg $mL^{-1}$ pulse amplitude = 50 mV*

and the peak potential also changes linearly as:

$$E_p = -2.06\ \Delta E - 487.78 \quad (12)$$

This confirms the irreversibility of the process controlled by diffusion.

The reduction process was also studied by cyclic voltammetry in order to contrast the results obtained in earlier techniques. The voltammograms obtained clearly demonstrate that the process is irreversible and under diffusion control.

3. 2. 3. Calibration curve and limit of detection

After choosing the most appropriate measurement conditions for determining the compound under study, the influence of the analyte concentration was studied using the following conditions (Table 2)

***Table 2.*** *Conditions for calibration curve*

| | pH | $\Delta E$ / mV | $v$ / mV $s^{-1}$ | Ionic strength, M |
|---|---|---|---|---|
| Differential pulse polarography | 4 | 50 | 10 | 0.05 |
| Square wave polarography | 4 | 50 | 100* | 0.05 |

**Frequency = 50 Hz, Scan increment = 2 mV*

The analytical performance of DPV method developed for TPt complex determination was evaluated. From the voltammograms recorded for increasing amounts of TPt complex using the optimized parameters described above, it was observed that the peak current increased with the analyte concentration over a large range (0.8 μg $mL^{-1}$ to 20 μg $mL^{-1}$) with good linearity according to $i = 0.015\ c - 0.0053$; $r^2 = 0.998$ with an $E_r = 0.83$ % and an RSD of 1.58 % ($n = 10$ at the 10 μg $mL^{-1}$ level). The minimum detectable amount was 97 ng $mL^{-1}$, while a concentration of 323 ng $mL^{-1}$ was calculated as the detection limit (Fig. 5).

We proceeded in the same manner when SWV was carried out. In this case, square-wave voltammograms were recorded for increasing amounts of TPt complex under the optimal conditions found for its determination. A linear response was found in the 0.1 μg $mL^{-1}$ to 20 μg $mL^{-1}$ range according to $i = 0.63c - 0.0158$; $r^2$=0.9962. The sensitivity of the method was inferred from the $LOD_{(3\sigma)}$=105 ng $mL^{-1}$ and $LOQ_{(10\ \sigma)}$=393 ng $mL^{-1}$ values. On the other hand, the RSD and $E_r$ values of 2.10 % and 1.72 %, respectively ($n$=10 at the 18 μg $mL^{-1}$ level) indicated the accuracy and reproducibility of the proposed method.

*3. 3. Analytical application*

Prior to using the method for determinations of TPt complex in urine, we conducted a study of the inorganic salts present in a synthetic urine prepared in the laboratory with the composition detailed in Table 1 and doped with 10 μg $L^{-1}$ TPt [17].

To perform this experiment the standard addition method was used, obtaining the equation**,** $i = 0.0012c - 0.023$ with a correlation coefficient of $r^2 = 0.993$.

Given the suitability of the results, we proceeded to determine the TPt complex in human urine samples. The following procedure was used in pretreating the sample and the DPV.

The sample was doped with an aliquot of 10 μg $mL^{-1}$ TPt complex, then proteins were precipitated with 1 M $HClO_4$. The precipitate was digested for 48 hours, filtered and the filtrate

was then brought to pH 4 with a 0.05 M buffer solution and standard measurement by DPV was performed.

Figure 5 shows the voltammograms obtained; the inset shows the reciprocal plot of *I* versus [TPt complex], showing the excellent fit of the experimental data to the equation $i = 0.21c + 1.98$, with a correlation coefficient of $r^2$=0.997.

When the data obtained were extrapolated into the equation of the calibration curve, the concentration of TPt complex obtained was 9.80±0.05 μg $mL^{-1}$

The procedure followed in the electrochemical study of the synthetic urine sample was the same as in human urine. The equation obtained when the standard addition was carried out was $i = 0.0034c + 0.0023$, with a correlation coefficient of $r^2$=0.9903. By extrapolating the obtained data, the concentration of the TPt complex was 9.75 ±0.05 μg $mL^{-1}$.

The difference between the obtained data for human urine and synthetic urine could be because the matrix of the human urine sample is much more complex than the synthetic urine matrix.

Just as in the calibration section, the differences between the slopes are due to the determination conditions, being that determination of the TPt complex was performed using DPV and SWV, and each of these electrochemical techniques has optimum conditions.

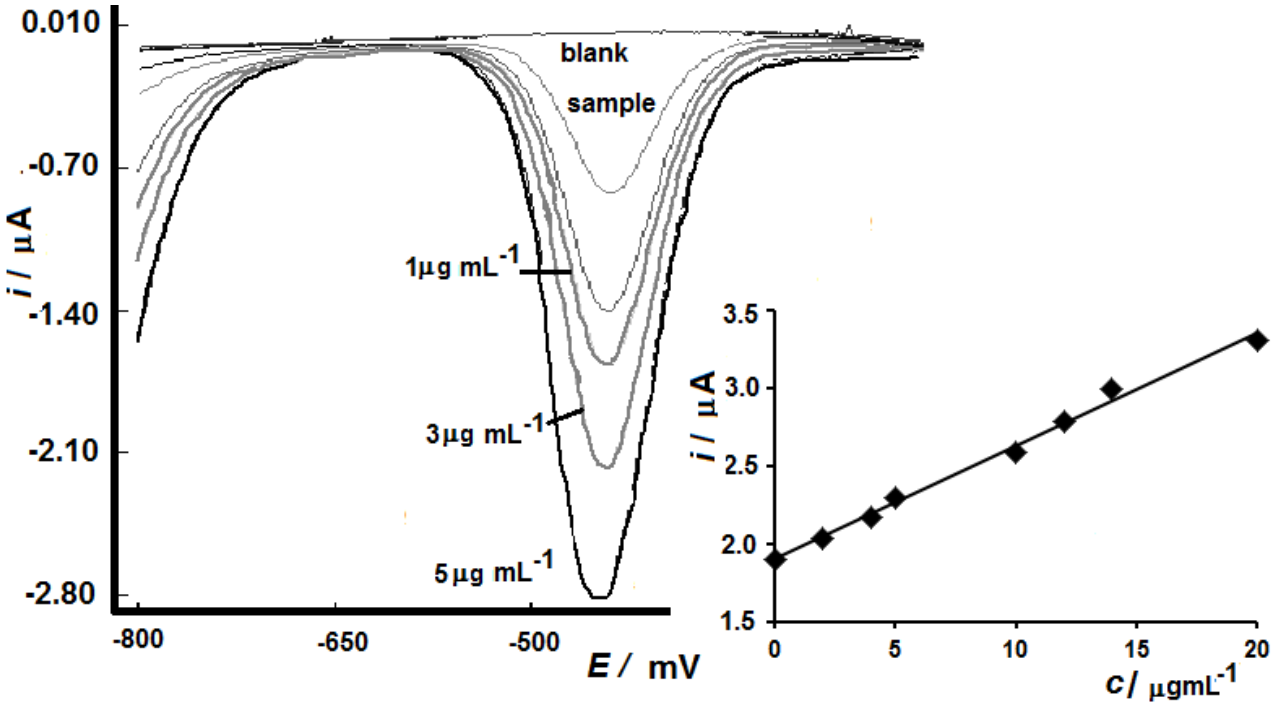


***Figure 5.*** *Calibration curve for DPV in human urine. Measurement conditions: pH 4; ionic strength = 0.05 M; pulse amplitude = 50 mV; scan rate = 10 $mVs^{-1}$*

## 4. Conclusions

A sensitive differential pulse voltammetry (DPV) method to analyse TPt complex has been applied and the mechanisms governing the electrochemical response have been elucidated. The proposed method can be applied to the determination of the studied Pt(IV)-complex in biological fluids, with the inherent advantages of electrochemical techniques*, i.e.*, greater economy and easy instrumentation with high accuracy and reproducibility, as shown from the obtained results.

***Acknowledgements**: The authors thank Carmen Navarro for providing the platinum complex and MICINN for their economic support.*

**References**

[1] E. Wong, C.M. Giandomenido, *Chem. Rev.* **99** (1999) 2451-2466.
[2] S.M. Cohen, S.J. Lippard, *Prog. Nucleic Acid Re.* **67** (2001) 93-103
[3] N. Farrell, *Cancer Invest.* **11** (1993) 578-589.
[4] Z.Z. Zdraveski, J.A. Mello, C.K. Farinelli, J.M. Essigmann, M.G. Marinus. *J. Biol. Chem.* **277** (2002) 1255-1260.
[5] T.A. Connors, M.J. Cleare, K.R. Harra, *Cancer Treat. Rep.* **63** (1979) 1499-1502.
[6] N. Farrell, T.T.B. Ha, J.P. Souchard, F.L. Wimmer, S. Cros, N.P. Johnson, *J. Med. Chem.* **32** (1989) 2240-2241.
[7] G. Natile, M. Coluccia, *Coordin. Chem. Rev.* **216** (2001) 383-410.
[8] R.P. Perez. *Eur. J. Cancer* **34** (1998) 1535-1542.
[9] V.M. González, M.A. Fuertes, C. Alonso, J.M. Perez, *Mol. Pharmacol.* **59** (2001) 657-663.
[10] J.M. Perez, L.R. Kelland, E.I. Montero, F.E. Boxal, M.A. Fuertes, C. Alonso, C. Navarro-Ranninger, *Mol. Pharmacol.* **63** (2003) 933-944.
[11] J.M. Perez, E.I. Montero, A.G. Quiroga, M.A. Fuertes, C. Alonso, C. Navarro-Ranninger. *Metal Based Drugs,* **8** (2001) 29-37.
[12] J.M. Perez, E.I. Montero, A.M. González, A. Alvarez-Valdés, C. Alonso, C. Navarro-Ranninger, *J. Inorg. Biochem.* **77** (1999) 37-42.
[13] E.I. Montero, J.M. Perez, A. Schwartz, M.A. Fuertes, J.M. Maligne, C. Alonso, M. Leng, C. Navarro-Ranninger, *ChemBioChem* **3** (2002) 61-67.
[14] L.R. Kelland, G. Abel, M.J. McKeage, M. Jones, P.M. Goddard, M. Valenti, B.A. Murrer, K.R. Harrap. *Cancer Res.* **53** (1993) 2581-2586.
[15] L.R. Kelland, C.F.J Barnard, K.J Mellish, M. Jones, P.M. Goddard, M. Valenti, A. Bryant, B.A. Murrer, K.R. Harrap. *Cancer Res.* **54** (1994) 5618-5622.
[16] L.R. Kelland, C.F.J. Barnard, I.G. Evans B.A. Murrer, B.R.C. Theobald, S.B. Wyer, P.M. Goddard, M. Jones, M. Valenti, *J. Med. Chem.* **38** (1995) 3016-3024.
[17] B.J. Stevens. Clinical Analysis by Atomic Absorption. Department of Pathology. The Royal Children's Hospital. Melbourne, Australia. 1970. Varian Techtron.
[18] J.M. Pingarrón, P. Sánchez Batanero *Química Electroanalítica: Fundamentos y Aplicaciones*, Editorial Síntesis, Madrid, 2003.

*J. Electrochem. Sci. Eng.* **3(2)** (2013) S1-S8; doi: **10.5599/jese.2013.0030**

**Open Access : : ISSN 1847-9286**

***www.jESE-online.org***

**SUPPLEMENTARY MATERIAL TO**

# Novel Mannich bases bearing pyrazolone moiety Synthesis, characterization and electrochemical studies

KRISHNA NAIK✉, ALURU RAGHAVENDRA GURU PRASAD*, YADATI NARASIMHA SPOORTHY and LAKSHMANA RAO KRISHNA RAO RAVINDRANATH

*Sri Krishnadevaraya University, Anantapur, A.P., India.*

*J. Electrochem. Sci. Eng.* **3(2)** (2013) 57-79; doi: **10.5599/jese.2011.0030**

***Table 1.*** *Polarographic characteristics and kinetic parameters of{4-[3-methyl-5-oxo-4-(4$^{l}$-substituted phenyl hydrazono)-4,5-dihydro-pyrazol-1-yl]-phenoxy}-acetic acid (2-oxo-1-piperidine-1-ylmethyl-1,2-dihydro–indol-3-ylidene)- hydrazide (1 mM) at pH 4.1 in various treatments, Medium : Aqueous dimethyl formamide (40% V/V) (I W = First wave II W = Second wave III W = Third wave)*

| # | pH | ($\Delta E_{1/2}$/$\Delta$pH)/ mV | | $\alpha_{na}$ | | | No. of protons p | | $D \times 10^{-6}$ / cm sec$^{-1}$ | | | $i \times 10^{3}$/ µA | | | $K^{0}_{fh}$/ cm sec$^{-1}$ | | | $\Delta G^{*}$ / kJ mol$^{-1}$ | | |
|---|---|---|---|---|---|---|---|---|---|---|---|---|---|---|---|---|---|---|---|---|
| | | I W | II W | I W | II W | III W | I W | II W | I W | II W | III W | I W | II W | III W | I W | II W | III W | I W | II W | III W |
| Va | 2.10 | 0.06 | 0.09 | 0.47 | 0.43 | - | 0.476 | 0.654 | 7.50 | 6.10 | - | 3.33 | 3.00 | - | 3.085 | 1.333 | - | 11.682 | 12.083 | - |
| | 4.10 | 0.06 | 0.09 | 0.47 | 0.43 | - | 0.476 | 0.654 | 6.10 | 4.79 | - | 3.00 | 2.66 | - | 2.579 | 1.134 | - | 11.765 | 12.159 | - |
| | 6.10 | 0.06 | 0.09 | 0.45 | 0.39 | - | 0.456 | 0.593 | 2.68 | 1.87 | - | 2.00 | 1.66 | - | 2.264 | 1.060 | - | 11.828 | 12.188 | - |
| | 8.10 | 0.06 | 0.09 | 0.41 | 0.36 | 0.42 | 0.415 | 0.547 | 1.51 | 0.92 | 5.85 | 1.50 | 1.16 | 2.94 | 0.704 | 1.050 | 0.032 | 12.388 | 12.196 | 11.401 |
| | 10.10 | 0.06 | 0.09 | 0.41 | 0.36 | 0.42 | 0.415 | 0.547 | 1.51 | 0.92 | 5.85 | 1.50 | 1.16 | 2.94 | 0.704 | 1.050 | -0.032 | 12.388 | 12.196 | 11.401 |
| Vb | 2.10 | 0.09 | 0.08 | 0.52 | 0.48 | - | 0.791 | 0.649 | 8.82 | 7.02 | - | 3.61 | 3.22 | - | 3.001 | 3.758 | - | 11.694 | 11.585 | - |
| | 4.10 | 0.09 | 0.08 | 0.52 | 0.48 | - | 0.791 | 0.649 | 7.23 | 5.61 | - | 3.27 | 2.88 | - | 2.787 | 3.144 | - | 11.728 | 11.673 | - |
| | 6.10 | 0.09 | 0.08 | 0.50 | 0.44 | - | 0.760 | 0.595 | 3.84 | 2.13 | - | 2.38 | 1.77 | - | 2.660 | 1.416 | - | 11.753 | 12.054 | - |
| | 8.10 | 0.09 | 0.08 | 0.46 | 0.41 | .0.43 | 0.699 | 0.554 | 1.98 | 1.10 | 6.76 | 1.72 | 1.27 | 3.16 | 1.055 | 1.395 | 3.145 | 12.192 | 12.062 | 11.012 |
| | 10.10 | 0.09 | 0.08 | 0.46 | 0.41 | 0.43 | 0.699 | 0.554 | 1.98 | 1.10 | 6.76 | 1.72 | 1.27 | 3.16 | 1.055 | 1.395 | 3.145 | 12.192 | 12.062 | 11.012 |
| Vc | 2.10 | 0.11 | 0.09 | 0.58 | 0.52 | - | 1.078 | 0.791 | 8.29 | 7.23 | - | 3.50 | 3.27 | - | 1.898 | 1.597 | - | 11.912 | 11.996 | - |
| | 4.10 | 0.11 | 0.09 | 0.58 | 0.52 | - | 1.078 | 0.791 | 6.76 | 5.85 | - | 3.16 | 2.94 | - | 1.562 | 1.366 | - | 12.008 | 12.071 | - |
| | 6.10 | 0.11 | 0.09 | 0.56 | 0.48 | - | 1.041 | 0.730 | 3.16 | 2.28 | - | 2.16 | 1.83 | - | 1.523 | 1.008 | - | 12.016 | 12.217 | - |
| | 8.10 | 0.11 | 0.09 | 0.52 | 0.45 | 0.47 | 0.967 | 0.684 | 1.87 | 1.20 | 6.56 | 1.66 | 1.33 | 3.11 | 1.281 | 0.991 | 1.025 | 12.100 | 12.226 | 11.377 |
| | 10.10 | 0.11 | 0.09 | 0.52 | 0.45 | 0.47 | 0.967 | 0.684 | 1.87 | 1.20 | 6.56 | 1.66 | 1.33 | 3.11 | 1.281 | 0.991 | 1.025 | 12.100 | 12.226 | 11.377 |
| Vd | 2.10 | 0.11 | 0.09 | 0.55 | 0.49 | - | 1.022 | 0.745 | 8.05 | 6.80 | - | 3.44 | 3.16 | - | 1.549 | 6.679 | - | 12.012 | 11.314 | - |
| | 4.10 | 0.11 | 0.09 | 0.55 | 0.49 | - | 1.022 | 0.745 | 6.56 | 5.66 | - | 3.11 | 2.88 | - | 1.480 | 1.115 | - | 12.033 | 12.167 | - |
| | 6.10 | 0.11 | 0.09 | 0.53 | 0.45 | - | 0.985 | 0.684 | 3.02 | 2.14 | - | 2.11 | 1.77 | - | 0.808 | 0.744 | - | 12.322 | 12.343 | - |
| | 8.10 | 0.11 | 0.09 | 0.51 | 0.42 | 0.49 | 0.948 | 0.639 | 1.76 | 1.10 | 7.04 | 1.61 | 1.27 | 3.22 | 0.706 | 0.698 | 0.145 | 12.385 | 12.393 | 12.121 |
| | 10.10 | 0.11 | 0.09 | 0.51 | 0.42 | 0.49 | 0.948 | 0.639 | 1.76 | 1.10 | 7.04 | 1.61 | 1.27 | 3.22 | 0.706 | 0.698 | 0.145 | 12.385 | 12.393 | 12.121 |
| Ve | 2.10 | 0.06 | 0.08 | 0.56 | 0.58 | - | 0.568 | 0.784 | 8.84 | 7.28 | - | 3.61 | 3.27 | - | 12.462 | 5.753 | - | 11.012 | 11.385 | - |
| | 4.10 | 0.06 | 0.08 | 0.56 | 0.58 | - | 0.568 | 0.784 | 7.53 | 5.88 | - | 3.33 | 2.94 | - | 3.025 | 4.511 | - | 11.690 | 11.498 | - |
| | 6.10 | 0.06 | 0.08 | 0.53 | 0.52 | - | 0.537 | 0.703 | 3.52 | 2.14 | - | 2.27 | 1.77 | - | 1.117 | 3.239 | - | 12.167 | 11.657 | - |
| | 8.10 | 0.06 | 0.08 | 0.48 | 0.44 | 0.41 | 0.486 | 0.595 | 2.14 | 1.10 | 6.56 | 1.77 | 1.27 | 3.11 | 0.982 | 2.350 | 0.374 | 12.229 | 11.811 | 11.016 |
| | 10.10 | 0.06 | 0.08 | 0.48 | 0.44 | 0.41 | 0.486 | 0.595 | 2.14 | 1.10 | 6.56 | 1.77 | 1.27 | 3.11 | 0.982 | 2.350 | 0.374 | 12.229 | 11.811 | 11.016 |
| Vf | 2.10 | 0.08 | 0.09 | 0.58 | 0.60 | - | 0.784 | 0.912 | 8.57 | 7.04 | - | 3.55 | 3.22 | -- | 1.687 | 1.579 | - | 11.970 | 11.999 | - |
| | 4.10 | 0.08 | 0.09 | 0.58 | 0.60 | - | 0.784 | 0.912 | 7.04 | 5.66 | - | 3.22 | 2.88 | - | 1.276 | 1.325 | - | 12.104 | 12.083 | - |
| | 6.10 | 0.08 | 0.09 | 0.55 | 0.54 | -- | 0.743 | 0.821 | 3.35 | 2.14 | - | 2.22 | 1.77 | - | 1.238 | 1.116 | - | 12.117 | 12.167 | - |
| | 8.10 | 0.08 | 0.09 | 0.50 | 0.49 | 0.43 | 0.676 | 0.745 | 2.01 | 1.10 | 6.80 | 1.72 | 1.27 | 3.16 | 1.146 | 1.113 | 0.215 | 12.555 | 12.167 | 11.447 |
| | 10.10 | 0.08 | 0.09 | 0.50 | 0.49 | 0.43 | 0.676 | 0.745 | 2.01 | 1.10 | 6.80 | 1.72 | 1.27 | 3.16 | 1.146 | 1.113 | 0215 | 12.555 | 12.167 | 11.447 |

***Table 2.*** *Cyclic voltammetric results of {4-[3-methyl-5-oxo-4-(phenyl hydrazono)-4,5-dihydro-pyrazol-1-yl]-phenoxy}-acetic acid (2-oxo-1-piperidine-1-ylmethyl-1,2-dihydro–indol-3-ylidene)- hydrazide (1 mM), Medium: Aqueous dimethylformamide (40% V/V)*

| pH | Scan rate, V $s^{-1}$ | Hanging mercury drop electrode | | | | | | | | Crown–ether modified carbon paste electrode | | | | | | | |
|---|---|---|---|---|---|---|---|---|---|---|---|---|---|---|---|---|---|
| | | $-E_{PCI}$ / V | $-E_{PCI\,I}$ / V | $-E_{PC\,III}$ / V | $-E_{PC}$ inv, V | $i_{PCI}$ / µA | $i_{PCII}$/ µA | $i_{PCIII}$/ µA | $i_{PC}$ inv/ µA | $E_{pcI}$ / V | $E_{pcII}$ / V | $E_{pcIII}$ / V | $E_{pa}$ / V | $i_{pcI}$ / µA | $i_{pcII}$ / µA | $E_{pcIII,}$ / V | $i_{pa,}$/ µA |
| 2.1 | 0.010 | 0.54 | 0.74 | | 0.64 | 1.3 | 1.1 | | 1.0 | 0.44 | 0.64 | | 0.86 | 1.9 | 1.7 | | 1.2 |
| | 0.020 | 0.58 | 0.78 | | 0.68 | 1.8 | 1.6 | | 1.4 | 0.48 | 0.68 | | 0.90 | 2.6 | 2.3 | | 1.6 |
| | 0.050 | 0.62 | 0.82 | | 0.72 | 2.9 | 2.4 | | 2.2 | 0.52 | 0.72 | | 0.94 | 4.8 | 3.7 | | 2.6 |
| | 0.100 | 0.66 | 0.86 | | 0.76 | 4.1 | 3.5 | | 3.1 | 0.56 | 0.76 | | 0.98 | 6.0 | 5.3 | | 3.7 |
| | 0.200 | 0.70 | 0.90 | | 0.80 | 5.8 | 4.9 | | 4.7 | 0.60 | 0.80 | | 10.2 | 8.4 | 7.5 | | 5.3 |
| | 0.300 | 0.76 | 0.96 | | 0.86 | 7.2 | 6.0 | | 5.4 | 0.66 | 0.86 | | 1.08 | 10.3 | 9.2 | | 6.5 |
| | 0.500 | 0.82 | 1.02 | | 0.92 | 9.1 | 7.8 | | 7.1 | 0.72 | 0.92 | | 1.14 | 13.4 | 12.0 | | 8.4 |
| 4.1 | 0.010 | 0.67 | 0.88 | | 0.77 | 0.9 | 0.8 | | 0.7 | 0.57 | 0.78 | | 1.00 | 1.6 | 1.5 | | 1.1 |
| | 0.020 | 0.71 | 0.92 | | 0.81 | 1.2 | 1.2 | | 1.0 | 0.61 | 0.82 | | 1.04 | 2.2 | 2.1 | | 1.5 |
| | 0.050 | 0.75 | 0.96 | | 0.85 | 1.9 | 1.7 | | 1.5 | 0.65 | 0.86 | | 1.08 | 3.5 | 3.3 | | 2.4 |
| | 0.100 | 0.79 | 1.00 | | 0.79 | 2.8 | 2.5 | | 2.2 | 0.69 | 0.90 | | 1.12 | 5.0 | 4.7 | | 3.4 |
| | 0.200 | 0.83 | 1.04 | | 0.83 | 4.0 | 3.5 | | 3.3 | 0.73 | 0.94 | | 1.16 | 7.1 | 6.7 | | 4.9 |
| | 0.300 | 0.89 | 1.10 | | 0.89 | 5.0 | 4.3 | | 3.8 | 0.79 | 1.00 | | 1.22 | 8.7 | 8.2 | | 6.0 |
| | 0.500 | 0.95 | 1.16 | | 0.95 | 6.3 | 5.6 | | 4.9 | 0.85 | 1.06 | | 1.28 | 11.3 | 10.6 | | 7.8 |
| 6.1 | 0.010 | 0.80 | 1.06 | | 0.90 | 0.6 | 0.5 | | 0.4 | 0.70 | 0.96 | | 1.18 | 1.3 | 1.2 | | 1.0 |
| | 0.020 | 0.84 | 1.10 | | 0.94 | 0.8 | 0.7 | | 0.6 | 0.74 | 1.00 | | 1.22 | 1.8 | 1.6 | | 1.4 |
| | 0.050 | 0.88 | 1.14 | | 0.98 | 1.3 | 1.1 | | 0.9 | 0.78 | 1.04 | | 1.26 | 2.9 | 2.6 | | 2.2 |
| | 0.100 | 0.92 | 1.18 | | 1.02 | 1.8 | 1.5 | | 1.3 | 0.82 | 1.08 | | 1.30 | 4.1 | 3.7 | | 3.1 |
| | 0.200 | 0.96 | 1.22 | | 1.06 | 2.6 | 2.3 | | 1.8 | 0.86 | 1.12 | | 1.34 | 5.8 | 5.3 | | 4.4 |
| | 0.300 | 1.02 | 1.26 | | 1.12 | 3.2 | 2.7 | | 2.3 | 0.92 | 1.18 | | 1.40 | 7.1 | 6.5 | | 5.4 |
| | 0.500 | 1.08 | 1.32 | | 1.16 | 4.2 | 3.5 | | 2.8 | 0.98 | 1.24 | | 1.46 | 9.1 | 8.4 | | 7.1 |
| 8.1 | 0.010 | 0.90 | 1.26 | 1.61 | | 0.5 | 0.3 | 0.8 | | 0.80 | 1.18 | 1.51 | | 1.0 | 0.8 | 1.1 | |
| | 0.020 | 0.94 | 1.30 | 1.65 | | 0.7 | 0.4 | 1.2 | | 0.84 | 1.22 | 1.55 | | 1.4 | 1.2 | 1.5 | |
| | 0.050 | 0.98 | 1.34 | 1.69 | | 1.1 | 0.7 | 1.7 | | 0.88 | 1.26 | 1.59 | | 2.2 | 1.7 | 2.4 | |
| | 0.100 | 1.02 | 1.38 | 1.73 | | 1.5 | 0.9 | 2.5 | | 0.92 | 1.30 | 1.63 | | 3.1 | 2.5 | 3.4 | |
| | 0.200 | 1.06 | 1.42 | 1.77 | | 2.3 | 1.5 | 3.5 | | 0.96 | 1.34 | 1.67 | | 4.4 | 3.6 | 4.9 | |
| | 0.300 | 1.12 | 1.48 | 1.83 | | 2.7 | 1.6 | 4.3 | | 1.02 | 1.40 | 1.73 | | 5.4 | 4.3 | 6.0 | |
| | 0.500 | 1.18 | 1.54 | 1.89 | | 3.5 | 2.2 | 5.6 | | 1.08 | 1.46 | 1.79 | | 7.1 | 5.6 | 7.8 | |
| 10.1 | 0.010 | 0.90 | 1.26 | 1.61 | | 0.5 | 0.3 | 0.8 | | 0.80 | 1.18 | 1.51 | | 1.0 | 0.8 | 1.1 | |
| | 0.020 | 0.94 | 1.30 | 1.65 | | 0.7 | 0.4 | 1.2 | | 0.84 | 1.22 | 1.55 | | 1.4 | 1.2 | 1.5 | |
| | 0.050 | 0.98 | 1.34 | 1.69 | | 1.1 | 0.7 | 1.7 | | 0.88 | 1.26 | 1.59 | | 2.2 | 1.7 | 2.4 | |
| | 0.100 | 1.02 | 1.38 | 1.73 | | 1.5 | 0.9 | 2.5 | | 0.92 | 1.30 | 1.63 | | 3.1 | 2.5 | 3.4 | |
| | 0.200 | 1.06 | 1.42 | 1.77 | | 2.3 | 1.5 | 3.5 | | 0.96 | 1.34 | 1.67 | | 4.4 | 3.6 | 4.9 | |
| | 0.300 | 1.12 | 1.48 | 1.83 | | 2.7 | 1.6 | 4.3 | | 1.02 | 1.40 | 1.73 | | 5.4 | 4.3 | 6.0 | |
| | 0.500 | 1.18 | 1.54 | 1.89 | | 3.5 | 2.2 | 5.6 | | 1.08 | 1.46 | 1.79 | | 7.1 | 5.6 | 7.8 | |

***Table 3.*** *Cyclic voltammetric results of {4-[3-methyl-5-oxo-4-(4$^{l}$-methyl phenyl hydrazono)-4,5-dihydro-pyrazol-1-yl]-phenoxy}-acetic acid (2-oxo-1-piperidine-1-ylmethyl-1,2-dihydro–indol-3-ylidene)- hydrazide (1 mM), Medium: Aqueous dimethylformamide (40% V/V)*

| pH | Scan rate, V $s^{-1}$ | Hanging mercury drop electrode | | | | | | | | Crown–ether modified carbon paste electrode | | | | | | | |
|---|---|---|---|---|---|---|---|---|---|---|---|---|---|---|---|---|---|
| | | $-E_{PCI}$ / V | $-E_{PCI\ I}$ / V | $-E_{PC\ III}$ / V | $-E_{PC}$ inv, V | $i_{PCI}$ / µA | $i_{PCII}$/ µA | $i_{PCIII}$/ µA | $i_{PC}$ inv/ µA | $E_{pcI}$ / V | $E_{pcII}$ / V | $E_{pcIII}$ / V | $E_{pa}$ / V | $i_{pcI}$ / µA | $i_{pcII}$ / µA | $E_{pcIII,}$ / V | $i_{pa,}$/ µA |
| 2.1 | 0.010 | 0.64 | 0.77 | | 0.67 | 1.1 | 1.0 | | 0.9 | 0.54 | 0.67 | | 0.88 | 1.6 | 1.2 | | 1.1 |
| | 0.020 | 0.68 | 0.83 | | 0.73 | 1.6 | 1.4 | | 1.2 | 0.58 | 0.71 | | 0.92 | 2.2 | 1.6 | | 1.5 |
| | 0.050 | 0.72 | 0.87 | | 0.77 | 2.4 | 2.2 | | 1.9 | 0.62 | 0.75 | | 0.96 | 3.5 | 2.6 | | 2.4 |
| | 0.100 | 0.76 | 0.91 | | 0.81 | 3.5 | 3.1 | | 2.8 | 0.66 | 0.79 | | 1.00 | 5.0 | 3.7 | | 3.4 |
| | 0.200 | 0.80 | 0.95 | | 0.85 | 4.9 | 4.7 | | 4.0 | 0.70 | 0.83 | | 1.04 | 7.1 | 5.3 | | 4.9 |
| | 0.300 | 0.86 | 1.01 | | 0.91 | 6.0 | 5.4 | | 5.0 | 0.76 | 0.89 | | 1.10 | 8.7 | 6.5 | | 6.0 |
| | 0.500 | 0.92 | 1.07 | | 0.97 | 7.8 | 7.1 | | 6.3 | 0.82 | 0.95 | | 1.16 | 11.3 | 8.4 | | 7.8 |
| 4.1 | 0.010 | 0.54 | 1.02 | | 0.92 | 1.0 | 0.9 | | 0.7 | 0.88 | 0.92 | | 1.13 | 1.3 | 1.0 | | 1.0 |
| | 0.020 | 0.58 | 1.06 | | 0.96 | 1.4 | 1.2 | | 1.0 | 0.92 | 0.96 | | 1.17 | 1.8 | 1.4 | | 1.4 |
| | 0.050 | 0.62 | 1.10 | | 1.00 | 2.2 | 1.9 | | 1.5 | 0.96 | 1.00 | | 1.21 | 2.9 | 2.2 | | 2.2 |
| | 0.100 | 0.66 | 1.14 | | 1.04 | 3.1 | 2.8 | | 2.2 | 1.0 | 1.04 | | 1.25 | 4.1 | 3.1 | | 3.1 |
| | 0.200 | 0.70 | 1.18 | | 1.08 | 4.7 | 4.0 | | 3.3 | 1.04 | 1.08 | | 1.29 | 5.8 | 4.4 | | 4.4 |
| | 0.300 | 0.76 | 1.24 | | 1.14 | 5.4 | 5.0 | | 3.8 | 1.10 | 1.14 | | 1.35 | 7.1 | 5.4 | | 5.4 |
| | 0.500 | 0.82 | 1.30 | | 1.20 | 7.1 | 6.3 | | 4.9 | 1.16 | 1.20 | | 1.41 | 9.1 | 7.1 | | 7.1 |
| 6.1 | 0.010 | 1.11 | 1.10 | | 1.00 | 0.8 | 0.6 | | 0.5 | 1.01 | 1.00 | | 1.21 | 1.1 | 0.8 | | 0.6 |
| | 0.020 | 1.15 | 1.14 | | 1.04 | 1.2 | 0.8 | | 0.7 | 1.05 | 1.04 | | 1.25 | 1.5 | 1.2 | | 0.9 |
| | 0.050 | 1.19 | 1.18 | | 1.08 | 1.7 | 1.3 | | 1.1 | 1.09 | 1.08 | | 1.29 | 2.4 | 1.7 | | 1.3 |
| | 0.100 | 1.23 | 1.22 | | 1.12 | 2.5 | 1.8 | | 1.5 | 1.13 | 1.12 | | 1.33 | 3.4 | 2.5 | | 1.9 |
| | 0.200 | 1.27 | 1.26 | | 1.16 | 3.5 | 2.6 | | 2.3 | 1.17 | 1.16 | | 1.37 | 4.9 | 3.6 | | 2.7 |
| | 0.300 | 1.33 | 1.32 | | 1.22 | 4.3 | 3.2 | | 2.3 | 1.23 | 1.22 | | 1.43 | 6.0 | 4.3 | | 3.2 |
| | 0.500 | 1.39 | 1.38 | | 1.28 | 5.6 | 4.2 | | 3.5 | 1.29 | 1.28 | | 1.49 | 7.8 | 5.6 | | 4.3 |
| 8.1 | 0.010 | 1.21 | 1.28 | 1.58 | | 0.6 | 0.4 | 1.0 | | 1.11 | 1.18 | 1.48 | | 0.9 | 0.6 | 1.0 | |
| | 0.020 | 1.25 | 1.32 | 1.62 | | 0.8 | 0.6 | 1.4 | | 1.15 | 1.22 | 1.52 | | 1.2 | 0.9 | 1.4 | |
| | 0.050 | 1.29 | 1.36 | 1.66 | | 1.3 | 0.9 | 2.2 | | 1.19 | 1.26 | 1.56 | | 1.9 | 1.3 | 2.2 | |
| | 0.100 | 1.33 | 1.40 | 1.70 | | 1.8 | 1.3 | 3.1 | | 1.23 | 1.30 | 1.60 | | 2.8 | 1.9 | 3.1 | |
| | 0.200 | 1.37 | 1.44 | 1.74 | | 2.6 | 1.8 | 4.7 | | 1.27 | 1.34 | 1.64 | | 4.1 | 2.7 | 4.4 | |
| | 0.300 | 1.43 | 1.50 | 1.80 | | 3.2 | 2.3 | 5.4 | | 1.33 | 1.40 | 1.70 | | 5.0 | 3.2 | 5.4 | |
| | 0.500 | 1.49 | 1.56 | 1.86 | | 4.2 | 2.8 | 7.1 | | 1.39 | 1.46 | 1.76 | | 6.3 | 4.3 | 7.1 | |
| 10.1 | 0.010 | 1.21 | 1.28 | 1.58 | | 0.6 | 0.4 | 1.0 | | 1.11 | 1.18 | 1.48 | | 0.9 | 0.6 | 1.0 | |
| | 0.020 | 1.25 | 1.32 | 1.62 | | 0.8 | 0.6 | 1.4 | | 1.15 | 1.22 | 1.52 | | 1.2 | 0.9 | 1.4 | |
| | 0.050 | 1.29 | 1.36 | 1.66 | | 1.3 | 0.9 | 2.2 | | 1.19 | 1.26 | 1.56 | | 1.9 | 1.3 | 2.2 | |
| | 0.100 | 1.33 | 1.40 | 1.70 | | 1.8 | 1.3 | 3.1 | | 1.23 | 1.30 | 1.60 | | 2.8 | 1.9 | 3.1 | |
| | 0.200 | 1.37 | 1.44 | 1.74 | | 2.6 | 1.8 | 4.7 | | 1.27 | 1.34 | 1.64 | | 4.1 | 2.7 | 4.4 | |
| | 0.300 | 1.43 | 1.50 | 1.80 | | 3.2 | 2.3 | 5.4 | | 1.33 | 1.40 | 1.70 | | 5.0 | 3.2 | 5.4 | |
| | 0.500 | 1.49 | 1.56 | 1.86 | | 4.2 | 2.8 | 7.1 | | 1.39 | 1.46 | 1.76 | | 6.3 | 4.3 | 7.1 | |

***Table 4.*** *Cyclic voltammetric results of {4-[3-methyl-5-oxo-4-(4$^{I}$-methoxy phenyl hydrazono)-4,5-dihydro-pyrazol-1-yl]-phenoxy}-acetic acid (2-oxo-1-piperidine-1-ylmethyl-1,2-dihydro–indol-3-ylidene)- hydrazide (1 mM), Medium: Aqueous dimethylformamide (40% V/V)*

| pH | Scan rate, V $s^{-1}$ | Hanging mercury drop electrode | | | | | | | | Crown–ether modified carbon paste electrode | | | | | | | |
|---|---|---|---|---|---|---|---|---|---|---|---|---|---|---|---|---|---|
| | | $-E_{PCI}$ / V | $-E_{PCI\,I}$ / V | $-E_{PC\,III\,/}$ V | $-E_{PC}$ inv, V | $i_{PCI}$ / µA | $i_{PCII}$/ µA | $i_{PCIII}$/ µA | $i_{PC}$ inv/ µA | $E_{pcI}$ / V | $E_{pcII}$ / V | $E_{pcIII}$ / V | $E_{pa}$ / V | $i_{pcI\,/}$ µA | $i_{pcII}$ / µA | $E_{pcIII,}$ / V | $i_{pa,}$/ µA |
| 2.1 | 0.010 | 0.73 | 0.78 | | 0.68 | 1.1 | 1.0 | | 0.8 | 0.63 | 0.68 | | 0.89 | 2.1 | 2.3 | | 1.9 |
| | 0.020 | 0.77 | 0.82 | | 0.72 | 1.6 | 1.4 | | 1.2 | 0.67 | 0.72 | | 0.93 | 2.9 | 3.2 | | 2.6 |
| | 0.050 | 0.81 | 0.86 | | 0.76 | 2.4 | 2.2 | | 1.7 | 0.71 | 0.76 | | 0.97 | 4.6 | 5.0 | | 4.8 |
| | 0.100 | 0.85 | 0.90 | | 0.80 | 3.5 | 3.1 | | 2.5 | 0.75 | 0.80 | | 1.01 | 6.6 | 7.2 | | 6.0 |
| | 0.200 | 0.89 | 0.94 | | 0.84 | 4.9 | 4.7 | | 3.6 | 0.79 | 0.84 | | 1.05 | 9.3 | 10.2 | | 8.4 |
| | 0.300 | 0.95 | 1.00 | | 0.90 | 6.0 | 5.4 | | 4.3 | 0.85 | 0.90 | | 1.11 | 11.4 | 12.5 | | 10.3 |
| | 0.500 | 1.01 | 1.06 | | 0.96 | 7.8 | 7.1 | | 5.6 | 0.91 | 0.96 | | 1.17 | 14.8 | 16.2 | | 13.4 |
| 4.1 | 0.010 | 0.98 | 1.05 | | 0.90 | 1.0 | 0.9 | | 0.7 | 0.90 | 0.94 | | 1.15 | 2.0 | 2.1 | | 1.7 |
| | 0.020 | 1.02 | 1.09 | | 0.94 | 1.4 | 1.3 | | 0.9 | 0.94 | 0.98 | | 1.19 | 2.8 | 2.9 | | 2.3 |
| | 0.050 | 1.06 | 1.13 | | 0.98 | 2.2 | 1.9 | | 1.5 | 0.98 | 1.02 | | 1.23 | 4.4 | 4.6 | | 3.7 |
| | 0.100 | 1.10 | 1.17 | | 1.02 | 3.1 | 2.8 | | 2.3 | 1.02 | 1.06 | | 1.27 | 6.3 | 6.6 | | 5.3 |
| | 0.200 | 1.14 | 1.21 | | 1.06 | 4.7 | 4.1 | | 3.2 | 1.06 | 1.10 | | 1.31 | 8.9 | 9.3 | | 7.5 |
| | 0.300 | 1.20 | 1.27 | | 1.12 | 5.4 | 4.9 | | 3.9 | 1.12 | 1.16 | | 1.37 | 10.9 | 11.4 | | 9.2 |
| | 0.500 | 1.26 | 1.33 | | 1.18 | 7.1 | 6.4 | | 4.9 | 1.18 | 1.22 | | 1.43 | 14.1 | 14.8 | | 12.0 |
| 6.1 | 0.010 | 1.26 | 1.18 | | 1.08 | 0.7 | 0.6 | | 0.6 | 1.08 | 1.16 | | 1.37 | 1.7 | 1.8 | | 1.5 |
| | 0.020 | 1.30 | 1.22 | | 1.12 | 0.9 | 0.9 | | 0.9 | 1.12 | 1.20 | | 1.41 | 2.1 | 2.5 | | 2.1 |
| | 0.050 | 1.34 | 1.26 | | 1.16 | 1.5 | 1.3 | | 1.3 | 1.16 | 1.24 | | 1.45 | 3.3 | 3.9 | | 3.3 |
| | 0.100 | 1.38 | 1.30 | | 1.20 | 2.3 | 1.9 | | 1.9 | 1.20 | 1.28 | | 1.49 | 4.7 | 5.6 | | 4.7 |
| | 0.200 | 1.42 | 1.34 | | 1.24 | 3.2 | 2.7 | | 2.7 | 1.24 | 1.32 | | 1.53 | 6.7 | 8.0 | | 6.7 |
| | 0.300 | 1.48 | 1.40 | | 1.30 | 3.9 | 3.2 | | 3.2 | 1.30 | 1.38 | | 1.59 | 8.2 | 9.8 | | 8.2 |
| | 0.500 | 1.54 | 1.46 | | 1.36 | 4.9 | 4.3 | | 4.3 | 1.36 | 1.44 | | 1.65 | 10.6 | 12.7 | | 10.6 |
| 8.1 | 0.010 | 1.43 | 1.33 | 1.64 | | 0.5 | 0.4 | 0.9 | | 1.23 | 1.33 | 1.54 | | 1.2 | 1.4 | 1.6 | |
| | 0.020 | 1.47 | 1.37 | 1.68 | | 0.7 | 0.6 | 1.3 | | 1.27 | 1.37 | 1.58 | | 1.6 | 1.9 | 2.2 | |
| | 0.050 | 1.51 | 1.41 | 1.72 | | 1.1 | 0.9 | 1.9 | | 1.31 | 1.41 | 1.62 | | 2.6 | 3.0 | 3.5 | |
| | 0.100 | 1.55 | 1.45 | 1.76 | | 1.5 | 1.3 | 2.8 | | 1.35 | 1.45 | 1.66 | | 3.7 | 4.4 | 5.0 | |
| | 0.200 | 1.39 | 1.49 | 1.80 | | 2.3 | 1.8 | 4.1 | | 1.39 | 1.49 | 1.70 | | 5.3 | 6.2 | 7.1 | |
| | 0.300 | 1.65 | 1.55 | 1.86 | | 2.8 | 2.3 | 4.9 | | 1.45 | 1.55 | 1.76 | | 6.6 | 7.6 | 8.7 | |
| | 0.500 | 1.71 | 1.61 | 1.92 | | 3.5 | 2.8 | 6.4 | | 1.51 | 1.61 | 1.82 | | 8.4 | 9.8 | 11.3 | |
| 10.1 | 0.010 | 1.43 | 1.33 | 1.64 | | 0.5 | 0.4 | 0.9 | | 1.23 | 1.33 | 1.54 | | 1.2 | 1.4 | 1.6 | |
| | 0.020 | 1.47 | 1.37 | 1.68 | | 0.7 | 0.6 | 1.3 | | 1.27 | 1.37 | 1.58 | | 1.6 | 1.9 | 2.2 | |
| | 0.050 | 1.51 | 1.41 | 1.72 | | 1.1 | 0.9 | 1.9 | | 1.31 | 1.41 | 1.62 | | 2.6 | 3.0 | 3.5 | |
| | 0.100 | 1.55 | 1.45 | 1.76 | | 1.5 | 1.3 | 2.8 | | 1.35 | 1.45 | 1.66 | | 3.7 | 4.4 | 5.0 | |
| | 0.200 | 1.59 | 1.49 | 1.80 | | 2.3 | 1.8 | 4.1 | | 1.39 | 1.49 | 1.70 | | 5.3 | 6.2 | 7.1 | |
| | 0.300 | 1.65 | 1.55 | 1.86 | | 2.8 | 2.3 | 4.9 | | 1.45 | 1.55 | 1.76 | | 6.6 | 7.6 | 8.7 | |
| | 0.500 | 1.71 | 1.61 | 1.92 | | 3.5 | 2.8 | 6.4 | | 1.51 | 1.61 | 1.82 | | 8.4 | 9.8 | 11.3 | |

***Table 5.*** *Cyclic voltammetric results of {4-[3-methyl-5-oxo-4-(4$^{l}$-ethoxy phenyl hydrazono)-4,5-dihydro-pyrazol-1-yl]-phenoxy}-acetic acid (2-oxo-1-piperidine-1-ylmethyl-1,2-dihydro–indol-3-ylidene)- hydrazide (1 mM), Medium: Aqueous dimethylformamide (40 % V/V)*

| pH | Scan rate, V $s^{-1}$ | Hanging mercury drop electrode | | | | | | | | Crown–ether modified carbon paste electrode | | | | | | | |
|---|---|---|---|---|---|---|---|---|---|---|---|---|---|---|---|---|---|
| | | $-E_{PCI}$ / V | $-E_{PCI\,I}$ / V | $-E_{PC\,III}$ / V | $-E_{PC}$ inv, V | $i_{PCI}$ / µA | $i_{PCII}$/ µA | $i_{PCIII}$/ µA | $i_{PC}$ inv/ µA | $E_{pcI}$ / V | $E_{pcII}$ / V | $E_{pcIII}$ / V | $E_{pa}$ / V | $i_{pcI}$ / µA | $i_{pcII}$ / µA | $E_{pcIII,}$ / V | $i_{pa,}$/ µA |
| 2.1 | 0.010 | 0.76 | 0.73 | | 0.63 | 1.2 | 1.0 | | 0.9 | 0.75 | 0.78 | | 0.99 | 1.9 | 1.7 | | 1.5 |
| | 0.020 | 0.80 | 0.77 | | 0.67 | 1.7 | 1.4 | | 1.3 | 0.79 | 0.82 | | 1.03 | 2.6 | 2.3 | | 2.1 |
| | 0.050 | 0.84 | 0.81 | | 0.71 | 2.6 | 2.2 | | 1.9 | 0.83 | 0.86 | | 1.07 | 4.8 | 3.7 | | 3.3 |
| | 0.100 | 0.88 | 0.85 | | 0.75 | 3.7 | 3.1 | | 2.8 | 0.87 | 0.90 | | 1.11 | 6.0 | 5.3 | | 4.7 |
| | 0.200 | 0.92 | 0.89 | | 0.79 | 5.3 | 4.4 | | 4.1 | 0.91 | 0.94 | | 1.15 | 8.4 | 7.5 | | 6.7 |
| | 0.300 | 1.06 | 0.95 | | 0.85 | 6.6 | 5.4 | | 5.0 | 0.97 | 1.00 | | 1.21 | 10.3 | 9.2 | | 8.2 |
| | 0.500 | 1.12 | 1.01 | | 0.91 | 8.5 | 7.1 | | 6.4 | 1.03 | 1.06 | | 1.27 | 13.4 | 12.0 | | 10.6 |
| 4.1 | 0.010 | 1.08 | 0.94 | | 0.84 | 1.0 | 0.9 | | 0.7 | 0.96 | 1.1 | | 1.31 | 1.6 | 1.4 | | 1.3 |
| | 0.020 | 1.12 | 0.98 | | 0.88 | 1.4 | 1.3 | | 1.0 | 1.00 | 1.14 | | 1.35 | 2.2 | 1.9 | | 1.8 |
| | 0.050 | 1.16 | 1.02 | | 0.92 | 2.2 | 1.9 | | 1.5 | 1.04 | 1.18 | | 1.39 | 3.5 | 3.0 | | 2.9 |
| | 0.100 | 1.20 | 1.06 | | 0.96 | 3.1 | 2.8 | | 2.2 | 1.08 | 1.22 | | 1.43 | 5.0 | 4.4 | | 4.1 |
| | 0.200 | 1.24 | 1.10 | | 1.00 | 4.4 | 4.1 | | 3.3 | 1.12 | 1.26 | | 1.47 | 7.1 | 6.2 | | 5.8 |
| | 0.300 | 1.30 | 1.16 | | 1.06 | 5.4 | 5.0 | | 3.8 | 1.18 | 1.32 | | 1.53 | 8.7 | 7.6 | | 7.1 |
| | 0.500 | 1.36 | 1.22 | | 1.12 | 7.1 | 6.4 | | 4.9 | 1.24 | 1.38 | | 1.59 | 11.3 | 9.8 | | 9.1 |
| 6.1 | 0.010 | 1.23 | 1.12 | | 1.02 | 0.8 | 0.7 | | 0.6 | 1.14 | 1.25 | | 1.46 | 1.2 | 1.1 | | 1.0 |
| | 0.020 | 1.27 | 1.16 | | 1.06 | 1.2 | 1.0 | | 0.9 | 1.18 | 1.29 | | 1.50 | 1.6 | 1.6 | | 1.4 |
| | 0.050 | 1.31 | 1.20 | | 1.10 | 1.8 | 1.5 | | 1.3 | 1.22 | 1.33 | | 1.54 | 2.6 | 2.4 | | 2.2 |
| | 0.100 | 1.35 | 1.24 | | 1.14 | 2.5 | 2.2 | | 1.9 | 1.26 | 1.37 | | 1.58 | 3.7 | 3.4 | | 3.1 |
| | 0.200 | 1.39 | 1.28 | | 1.18 | 3.6 | 3.3 | | 2.7 | 1.30 | 1.41 | | 1.62 | 5.3 | 4.9 | | 4.4 |
| | 0.300 | 1.45 | 1.34 | | 1.24 | 4.3 | 3.8 | | 3.2 | 1.36 | 1.47 | | 1.68 | 6.6 | 6.0 | | 5.4 |
| | 0.500 | 1.51 | 1.40 | | 1.30 | 5.6 | 4.9 | | 4.3 | 1.42 | 1.53 | | 1.74 | 8.4 | 7.8 | | 7.1 |
| 8.1 | 0.010 | 1.49 | 1.30 | 1.59 | | 0.6 | 0.5 | 1.0 | | 1.32 | 1.51 | 1.61 | | 0.9 | 0.7 | 1.2 | |
| | 0.020 | 1.53 | 1.34 | 1.63 | | 0.9 | 0.7 | 1.4 | | 1.36 | 1.55 | 1.65 | | 1.2 | 1.0 | 1.6 | |
| | 0.050 | 1.57 | 1.38 | 1.67 | | 1.3 | 1.1 | 2.2 | | 1.40 | 1.59 | 1.69 | | 1.9 | 1.5 | 2.6 | |
| | 0.100 | 1.61 | 1.42 | 1.71 | | 1.9 | 1.5 | 3.1 | | 1.44 | 1.63 | 1.73 | | 2.8 | 2.2 | 3.7 | |
| | 0.200 | 1.65 | 1.46 | 1.75 | | 2.7 | 2.3 | 4.4 | | 1.48 | 1.67 | 1.77 | | 4.0 | 3.3 | 5.3 | |
| | 0.300 | 1.71 | 1.52 | 1.81 | | 3.2 | 2.8 | 5.4 | | 1.54 | 1.73 | 1.83 | | 4.9 | 3.8 | 6.6 | |
| | 0.500 | 1.77 | 1.58 | 1.87 | | 4.3 | 3.5 | 7.1 | | 1.60 | 1.79 | 1.89 | | 6.3 | 4.9 | 8.4 | |
| 10.1 | 0.010 | 1.49 | 1.30 | 1.59 | | 0.6 | 0.5 | 1.0 | | 1.32 | 1.51 | 1.61 | | 0.9 | 0.7 | 1.2 | |
| | 0.020 | 1.53 | 1.34 | 1.63 | | 0.9 | 0.7 | 1.4 | | 1.36 | 1.55 | 1.65 | | 1.2 | 1.0 | 1.6 | |
| | 0.050 | 1.57 | 1.38 | 1.67 | | 1.3 | 1.1 | 2.2 | | 1.40 | 1.59 | 1.69 | | 1.9 | 1.5 | 2.6 | |
| | 0.100 | 1.61 | 1.42 | 1.71 | | 1.9 | 1.5 | 3.1 | | 1.44 | 1.63 | 1.73 | | 2.8 | 2.2 | 3.7 | |
| | 0.200 | 1.65 | 1.46 | 1.75 | | 2.7 | 2.3 | 4.4 | | 1.48 | 1.67 | 1.77 | | 4.0 | 3.3 | 5.3 | |
| | 0.300 | 1.71 | 1.52 | 1.81 | | 3.2 | 2.8 | 5.4 | | 1.54 | 1.73 | 1.83 | | 4.9 | 3.8 | 6.6 | |
| | 0.500 | 1.77 | 1.58 | 1.87 | | 4.3 | 3.5 | 7.1 | | 1.60 | 1.79 | 1.89 | | 6.3 | 4.9 | 8.4 | |

***Table 6.*** *Cyclic voltammetric results of {4-[3-methyl-5-oxo-4-(4$^{l}$-chloro phenyl hydrazono)-4,5-dihydro-pyrazol-1-yl]-phenoxy}-acetic acid (2-oxo-1-piperidine-1-ylmethyl-1,2-dihydro–indol-3-ylidene)- hydrazide (1 mM), Medium : Aqueous dimethylformamide (40% V/V)*

| pH | Scan rate, V $s^{-1}$ | Hanging mercury drop electrode | | | | | | | | Crown–ether modified carbon paste electrode | | | | | | | |
|---|---|---|---|---|---|---|---|---|---|---|---|---|---|---|---|---|---|
| | | $-E_{PCI}$ / V | $-E_{PCI\ I}$ / V | $-E_{PC\ III}$ / V | $-E_{PC}$ inv, V | $i_{PCI}$ / µA | $i_{PCII}$/ µA | $i_{PCIII}$/ µA | $i_{PC}$ inv/ µA | $E_{pcI}$ / V | $E_{pcII}$ / V | $E_{pcIII}$ / V | $E_{pa}$ / V | $i_{pcI}$ / µA | $i_{pcII}$ / µA | $E_{pcIII,}$ / V | $i_{pa,}$/ µA |
| 2.1 | 0.010 | 0.34 | 0.78 | | 0.68 | 1.3 | 1.1 | | 1.0 | 0.24 | 0.70 | | 0.91 | 1.7 | 1.4 | | 1.2 |
| | 0.020 | 0.38 | 0.82 | | 0.72 | 1.8 | 1.6 | | 1.4 | 0.28 | 0.74 | | 0.95 | 2.3 | 1.9 | | 1.6 |
| | 0.050 | 0.42 | 0.86 | | 0.76 | 2.9 | 2.4 | | 2.2 | 0.32 | 0.78 | | 0.99 | 3.7 | 3.0 | | 2.6 |
| | 0.100 | 0.46 | 0.90 | | 0.80 | 4.1 | 3.4 | | 3.1 | 0.36 | 0.82 | | 1.03 | 5.3 | 4.4 | | 3.7 |
| | 0.200 | 0.50 | 0.94 | | 0.84 | 5.8 | 4.9 | | 4.4 | 0.40 | 0.86 | | 1.07 | 7.5 | 6.2 | | 5.3 |
| | 0.300 | 0.56 | 1.00 | | 0.90 | 7.2 | 6.0 | | 5.4 | 0.46 | 0.92 | | 1.13 | 9.2 | 7.6 | | 6.6 |
| | 0.500 | 0.62 | 1.06 | | 0.96 | 9.1 | 7.8 | | 7.1 | 0.52 | 0.98 | | 1.19 | 12.0 | 9.8 | | 8.4 |
| 4.1 | 0.010 | 0.51 | 0.99 | | 0.89 | 1.1 | 0.9 | | 0.8 | 0.40 | 0.89 | | 1.1 | 1.5 | 1.2 | | 1.0 |
| | 0.020 | 0.55 | 1.03 | | 0.93 | 1.6 | 1.2 | | 1.2 | 0.44 | 0.93 | | 1.14 | 2.1 | 1.6 | | 1.4 |
| | 0.050 | 0.59 | 1.07 | | 0.97 | 2.4 | 1.9 | | 1.7 | 0.48 | 0.97 | | 1.18 | 3.3 | 2.6 | | 2.2 |
| | 0.100 | 0.63 | 1.11 | | 1.01 | 3.4 | 2.8 | | 2.5 | 0.52 | 1.01 | | 1.22 | 4.7 | 3.7 | | 3.1 |
| | 0.200 | 0.67 | 1.15 | | 1.05 | 4.9 | 4.1 | | 3.6 | 0.56 | 1.05 | | 1.26 | 6.7 | 5.3 | | 4.4 |
| | 0.300 | 0.73 | 1.21 | | 1.11 | 6.0 | 5.0 | | 4.3 | 0.62 | 1.11 | | 1.32 | 8.2 | 6.6 | | 5.4 |
| | 0.500 | 0.79 | 1.27 | | 1.17 | 7.8 | 6.3 | | 5.6 | 0.68 | 1.17 | | 1.38 | 10.6 | 8.4 | | 7.1 |
| 6.1 | 0.010 | 0.66 | 1.17 | | 1.07 | 0.9 | 0.7 | | 0.6 | 0.56 | 1.07 | | 1.28 | 1.2 | 1.0 | | 0.7 |
| | 0.020 | 0.70 | 1.21 | | 1.11 | 1.2 | 1.0 | | 0.9 | 0.60 | 1.11 | | 1.32 | 1.6 | 1.4 | | 1.0 |
| | 0.050 | 0.74 | 1.25 | | 1.15 | 1.9 | 1.5 | | 1.3 | 0.64 | 1.15 | | 1.36 | 2.6 | 2.2 | | 1.5 |
| | 0.100 | 0.78 | 1.29 | | 1.19 | 2.8 | 2.2 | | 1.9 | 0.68 | 1.19 | | 1.40 | 3.7 | 3.1 | | 2.2 |
| | 0.200 | 0.82 | 1.33 | | 1.23 | 4.1 | 3.3 | | 2.7 | 0.72 | 1.23 | | 1.44 | 5.3 | 4.4 | | 3.3 |
| | 0.300 | 0.88 | 1.39 | | 1.29 | 5.0 | 3.8 | | 3.2 | 0.78 | 1.29 | | 1.50 | 6.6 | 5.4 | | 3.8 |
| | 0.500 | 0.94 | 1.45 | | 1.35 | 6.3 | 4.9 | | 4.3 | 0.84 | 1.35 | | 1.56 | 8.4 | 7.1 | | 4.9 |
| 8.1 | 0.010 | 0.81 | 1.32 | 1.63 | | 0.6 | 0.5 | 1.0 | | 0.71 | 1.23 | 1.53 | | 0.8 | 0.6 | 1.0 | |
| | 0.020 | 0.85 | 1.36 | 1.67 | | 0.9 | 0.7 | 1.4 | | 0.75 | 1.27 | 1.57 | | 1.2 | 0.9 | 1.4 | |
| | 0.050 | 0.89 | 1.40 | 1.71 | | 1.3 | 1.1 | 2.2 | | 0.79 | 1.31 | 1.61 | | 1.7 | 1.3 | 2.2 | |
| | 0.100 | 0.93 | 1.44 | 1.75 | | 1.9 | 1.5 | 3.1 | | 0.83 | 1.35 | 1.65 | | 2.7 | 1.9 | 3.1 | |
| | 0.200 | 0.97 | 1.48 | 1.79 | | 2.7 | 2.3 | 4.4 | | 0.87 | 1.39 | 1.69 | | 3.6 | 2.7 | 4.4 | |
| | 0.300 | 1.03 | 1.54 | 1.85 | | 3.2 | 2.8 | 5.4 | | 0.93 | 1.45 | 1.75 | | 4.3 | 3.2 | 5.4 | |
| | 0.500 | 1.09 | 1.60 | 1.91 | | 4.3 | 3.5 | 7.1 | | 0.99 | 1.51 | 1.81 | | 5.6 | 4.3 | 7.1 | |
| 10.1 | 0.010 | 0.81 | 1.32 | 1.63 | | 0.6 | 0.5 | 1.0 | | 0.71 | 1.23 | 1.53 | | 0.8 | 0.6 | 1.0 | |
| | 0.020 | 0.85 | 1.36 | 1.67 | | 0.9 | 0.7 | 1.4 | | 0.75 | 1.27 | 1.57 | | 1.2 | 0.9 | 1.4 | |
| | 0.050 | 0.89 | 1.40 | 1.71 | | 1.3 | 1.1 | 2.2 | | 0.79 | 1.31 | 1.61 | | 1.7 | 1.3 | 2.2 | |
| | 0.100 | 0.93 | 1.44 | 1.75 | | 1.9 | 1.5 | 3.1 | | 0.83 | 1.35 | 1.65 | | 2.7 | 1.9 | 3.1 | |
| | 0.200 | 0.97 | 1.48 | 1.79 | | 2.7 | 2.3 | 4.4 | | 0.87 | 1.39 | 1.69 | | 3.6 | 2.7 | 4.4 | |
| | 0.300 | 1.03 | 1.54 | 1.85 | | 3.2 | 2.8 | 5.4 | | 0.93 | 1.45 | 1.75 | | 4.3 | 3.2 | 5.4 | |
| | 0.500 | 1.09 | 1.60 | 1.91 | | 4.3 | 3.5 | 7.1 | | 0.99 | 1.51 | 1.81 | | 5.6 | 4.3 | 7.1 | |

***Table 7.*** *Cyclic voltammetric results of {4-[3-methyl-5-oxo-4-(4$^{l}$-bromo phenyl hydrazono)-4,5-dihydro-pyrazol-1-yl]-phenoxy}-acetic acid (2-oxo-1-piperidine-1-ylmethyl-1,2-dihydro–indol-3-ylidene)- hydrazide (1 mM), Medium: Aqueous dimethylformamide (40% V/V)*

| pH | Scan rate, V $s^{-1}$ | Hanging mercury drop electrode | | | | | | | | Crown–ether modified carbon paste electrode | | | | | | | |
|---|---|---|---|---|---|---|---|---|---|---|---|---|---|---|---|---|---|
| | | $-E_{PCI}$ / V | $-E_{PCI\,I}$ / V | $-E_{PC\,III}$ / V | $-E_{PC}$ inv, V | $i_{PCI}$ / µA | $i_{PCII}$/ µA | $i_{PCIII}$/ µA | $i_{PC}$ inv/ µA | $E_{pcI}$ / V | $E_{pcII}$ / V | $E_{pcIII}$ / V | $E_{pa}$ / V | $i_{pcI}$ / µA | $i_{pcII}$ / µA | $E_{pcIII,}$ / V | $i_{pa,}$/ µA |
| 2.1 | 0.010 | 0.43 | 0.82 | | 0.72 | 1.6 | 1.4 | | 1.1 | 0.33 | 0.72 | | 0.93 | 2.0 | 1.8 | | 1.4 |
| | 0.020 | 0.47 | 0.86 | | 0.76 | 2.2 | 2.0 | | 1.6 | 0.37 | 0.76 | | 0.97 | 2.8 | 2.5 | | 1.9 |
| | 0.050 | 0.51 | 0.90 | | 0.80 | 3.5 | 3.0 | | 2.4 | 0.41 | 0.80 | | 1.01 | 4.4 | 3.9 | | 3.0 |
| | 0.100 | 0.55 | 0.94 | | 0.84 | 5.1 | 4.4 | | 3.4 | 0.45 | 0.84 | | 1.05 | 6.3 | 5.6 | | 4.4 |
| | 0.200 | 0.59 | 0.98 | | 0.88 | 7.2 | 6.2 | | 4.9 | 0.49 | 0.88 | | 1.09 | 8.9 | 8.0 | | 6.2 |
| | 0.300 | 0.65 | 1.04 | | 0.94 | 8.7 | 7.6 | | 6.0 | 0.55 | 0.94 | | 1.15 | 10.9 | 9.8 | | 7.6 |
| | 0.500 | 0.71 | 1.10 | | 1.00 | 11.3 | 9.9 | | 7.8 | 0.61 | 1.00 | | 1.21 | 14.1 | 12.7 | | 9.8 |
| 4.1 | 0.010 | 0.54 | 1.02 | | 0.92 | 1.3 | 1.1 | | 0.9 | 0.44 | 0.92 | | 1.13 | 1.7 | 1.5 | | 1.1 |
| | 0.020 | 0.58 | 1.06 | | 0.96 | 1.8 | 1.6 | | 1.2 | 0.48 | 0.96 | | 1.17 | 2.3 | 2.1 | | 1.6 |
| | 0.050 | 0.62 | 1.10 | | 1.00 | 2.9 | 2.4 | | 1.9 | 0.52 | 1.00 | | 1.21 | 3.7 | 3.3 | | 2.4 |
| | 0.100 | 0.66 | 1.14 | | 1.04 | 4.1 | 3.4 | | 2.8 | 0.56 | 1.04 | | 1.25 | 5.3 | 4.7 | | 3.4 |
| | 0.200 | 0.70 | 1.18 | | 1.08 | 5.8 | 4.9 | | 4.1 | 0.60 | 1.08 | | 1.29 | 7.5 | 6.7 | | 4.9 |
| | 0.300 | 0.76 | 1.24 | | 1.14 | 7.2 | 6.0 | | 5.0 | 0.66 | 1.14 | | 1.35 | 9.2 | 8.2 | | 6.0 |
| | 0.500 | 0.82 | 1.30 | | 1.20 | 9.1 | 7.8 | | 6.3 | 0.72 | 1.20 | | 1.41 | 12.0 | 10.6 | | 7.8 |
| 6.1 | 0.010 | 0.75 | 1.19 | | 1.09 | 1.1 | 0.9 | | 0.7 | 0.65 | 1.09 | | 1.30 | 1.2 | 1.1 | | 0.9 |
| | 0.020 | 0.79 | 1.23 | | 1.13 | 1.6 | 1.2 | | 1.0 | 0.69 | 1.13 | | 1.34 | 1.6 | 1.5 | | 1.2 |
| | 0.050 | 0.83 | 1.27 | | 1.17 | 2.4 | 1.9 | | 1.5 | 0.73 | 1.17 | | 1.38 | 2.6 | 2.4 | | 1.9 |
| | 0.100 | 0.87 | 1.31 | | 1.21 | 3.4 | 2.8 | | 2.2 | 0.77 | 1.21 | | 1.42 | 3.7 | 3.4 | | 2.8 |
| | 0.200 | 0.91 | 1.35 | | 1.25 | 4.9 | 4.1 | | 3.3 | 0.81 | 1.25 | | 1.46 | 5.3 | 4.9 | | 4.0 |
| | 0.300 | 0.97 | 1.41 | | 1.31 | 6.0 | 5.0 | | 3.8 | 0.87 | 1.31 | | 1.52 | 6.6 | 6.0 | | 4.9 |
| | 0.500 | 1.03 | 1.47 | | 1.37 | 7.8 | 6.3 | | 4.9 | 0.93 | 1.37 | | 1.58 | 8.4 | 7.8 | | 6.3 |
| 8.1 | 0.010 | 0.90 | 1.38 | 1.64 | | 0.8 | 0.6 | 1.0 | | 0.80 | 1.28 | 1.54 | | 1.0 | 0.6 | 0.9 | |
| | 0.020 | 0.94 | 1.42 | 1.68 | | 1.2 | 0.9 | 1.4 | | 0.84 | 1.32 | 1.58 | | 1.4 | 0.9 | 1.2 | |
| | 0.050 | 0.98 | 1.46 | 1.72 | | 1.7 | 1.3 | 2.2 | | 0.88 | 1.36 | 1.62 | | 2.2 | 1.3 | 1.9 | |
| | 0.100 | 1.02 | 1.50 | 1.76 | | 2.5 | 1.9 | 3.1 | | 0.92 | 1.40 | 1.66 | | 3.1 | 1.9 | 2.8 | |
| | 0.200 | 1.06 | 1.54 | 1.80 | | 3.6 | 2.7 | 4.4 | | 0.96 | 1.44 | 1.70 | | 4.4 | 2.7 | 4.0 | |
| | 0.300 | 1.12 | 1.60 | 1.86 | | 4.3 | 3.2 | 5.4 | | 1.02 | 1.50 | 1.76 | | 5.4 | 3.2 | 4.9 | |
| | 0.500 | 1.18 | 1.66 | 1.92 | | 5.6 | 4.3 | 7.1 | | 1.08 | 1.56 | 1.82 | | 7.1 | 4.3 | 6.3 | |
| 10.1 | 0.010 | 0.90 | 1.38 | 1.64 | | 0.8 | 0.6 | 1.0 | | 0.80 | 1.28 | 1.54 | | 1.0 | 0.6 | 0.9 | |
| | 0.020 | 0.94 | 1.42 | 1.68 | | 1.2 | 0.9 | 1.4 | | 0.84 | 1.32 | 1.58 | | 1.4 | 0.9 | 1.2 | |
| | 0.050 | 0.98 | 1.46 | 1.72 | | 1.7 | 1.3 | 2.2 | | 0.88 | 1.36 | 1.62 | | 2.2 | 1.3 | 1.9 | |
| | 0.100 | 1.02 | 1.50 | 1.76 | | 2.5 | 1.9 | 3.1 | | 0.92 | 1.40 | 1.66 | | 3.1 | 1.9 | 2.8 | |
| | 0.200 | 1.06 | 1.54 | 1.80 | | 3.6 | 2.7 | 4.4 | | 0.96 | 1.44 | 1.70 | | 4.4 | 2.7 | 4.0 | |
| | 0.300 | 1.12 | 1.60 | 1.86 | | 4.3 | 3.2 | 5.4 | | 1.02 | 1.50 | 1.76 | | 5.4 | 3.2 | 4.9 | |
| | 0.500 | 1.18 | 1.66 | 1.92 | | 5.6 | 4.3 | 7.1 | | 1.08 | 1.56 | 1.82 | | 7.1 | 4.3 | 6.3 | |